

HD-A138 467

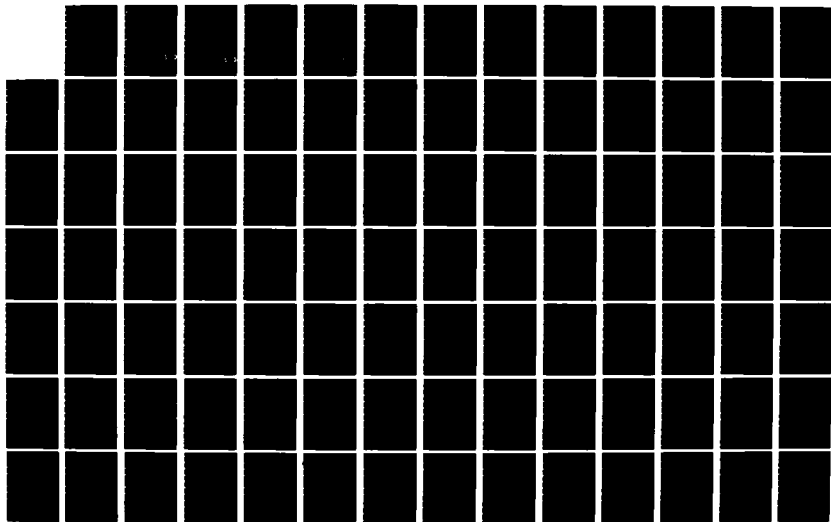
CLUTTER CANCELLATION TECHNIQUES FOR USE IN A
SPACE-BASED RADAR SYSTEM(U) AIR FORCE INST OF TECH
WRIGHT-PATTERSON AFB OH SCHOOL OF ENGINEERING
J DEVENUTO DEC 83 AFIT/GE/EE/83D-18

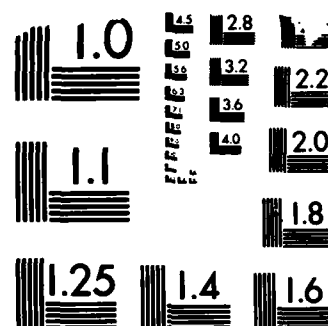
1/3

UNCLASSIFIED

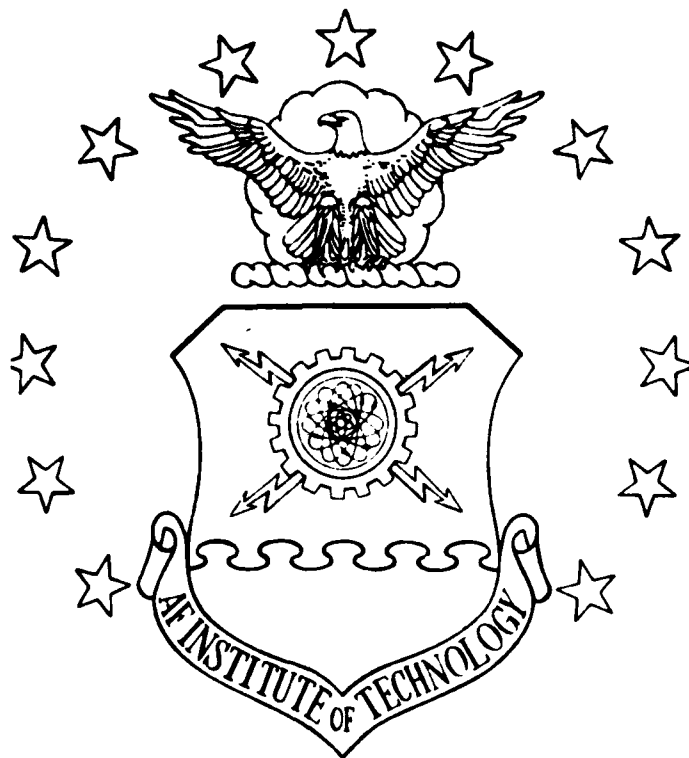
F/G 77/9

NL





AD A138467



CLUTTER CANCELLATION TECHNIQUES
FOR USE IN A
SPACE-BASED RADAR SYSTEM

Thesis

AFIT/GE/EE/83D-18

Joseph DeVenuto
1 LT USAF

DISTRIBUTION STATEMENT A

Approved for public release
Distribution Unlimited

DTIC
ELECTE
S MAR 1 1984 **D**
B

DEPARTMENT OF THE AIR FORCE
AIR UNIVERSITY (ATC)

AIR FORCE INSTITUTE OF TECHNOLOGY

Wright-Patterson Air Force Base, Ohio

84 02 20 048

DTIC FILE COPY

AFIT/GE/EE/83D-18

CLUTTER CANCELLATION TECHNIQUES
FOR USE IN A
SPACE-BASED RADAR SYSTEM

Thesis

AFIT/GE/EE/83D-18

Joseph DeVenuto
1 LT USAF

DTIC
ELECTE
S MAR 1 1984 D
B

Approved for public release; distribution unlimited

AFIT/GE/EE/83D-18

CLUTTER CANCELLATION TECHNIQUES

FOR USE IN A
SPACE-BASED RADAR SYSTEM

THESIS

Presented to the Faculty of the School of Engineering
of the Air Force Institute of Technology
Air University
in Partial Fulfillment of the
Requirements for the Degree of
Master of Science

by

Joseph DeVenuto, BS

1 Lt

USAF

Graduate Electrical Engineering

December 1983

Approved for public release; distribution unlimited

Acknowledgements

I want to express my sincere appreciation and gratitude to Major Ken Castor, my thesis advisor, for his help and direction throughout this thesis. I would also like to thank Dr. Vic Syed and Major Larry Kizer, members of my thesis committee, for their assistance and constructive comments on my work, Colonel Garry Schnelzer, of Space Division, for sponsoring this thesis, and Jim Kluck, also from Space Division, for his assistance in understanding the clutter cancellation problem and the necessary clutter computer modeling.

I especially want to thank my wife, Denise, for proofreading the entire text. I also wish to thank Denise and our two children, Lisa and Lorraine, for their patience, understanding and encouragement, which allowed me to complete this thesis.

Joseph DeVenuto

RE: Classified Reference, Distribution
Unlimited
No Change per Major K. Castro, AFIT/EN



Accession For	
NTIS GRA&I	<input checked="checked" type="checkbox"/>
DTIC TAB	<input type="checkbox"/>
Unannounced	<input type="checkbox"/>
Justification	
PER CALL JC	
By	
Distribution/	
Availability Codes	
Dist	Avail and/or Special
A-1	

Preface

For one unfamiliar with radar, it is often very difficult to gain a complete and thorough understanding of a particular aspect of radar engineering because of the multitude of disciplines and variety of backgrounds and viewpoints of the individuals explaining radar engineering. A large percentage of radar literature deals with the analysis of specific aspects of radar engineering as opposed to synthesis. I have found this to be especially true in understanding the signal processing that is needed to cancel the clutter present in airborne or spaceborne radar returns so as to obtain target range and velocity information. There appears to be two reasons for this inadequacy: 1) to adequately model and describe the clutter problem a varied and extensive mathematical background is needed and 2) much of the literature that relates to the clutter cancellation problem either broadly treats the subject or concentrates on a specific feature or aspect and causes one to lose perspective of the interrelationship between the specific topic and the clutter cancellation problem. It is thus my objective to present a concise and succinct system explanation of the signal processing needed to perform clutter cancellation by blending mathematical theory and modeling of signal analysis techniques with a heuristic description of the physical problem.

To understand the clutter cancellation problem it is

important that one maintain a proper perspective between the reality of the physical situation and the occasional abstraction of mathematical modeling. Mathematical models allow one to describe and handle the clutter problem manageably. These models are idealizations or approximations of the actual physical phenomena involved; yet to be useful they must convey the essential features of the situation. The balancing of the complexity of reality against the simplicity of the math models of that reality is one of the central issues that I wish to explore. While it is important to understand the theory and proof of various mathematical principles, because many insights into the natural order of events can be brought to light, I do not wish to get bogged down in elaborate abstraction and precision of various particular branches of mathematics. I hope to build upon the mathematical proofs and combine physical reality to give one a full appreciation and grasp of the problem.

Based upon these somewhat philosophical thoughts, I will proceed in the next several chapters explaining the math fundamentals that 1) justify signal representation and analysis and 2) provide a way of modeling clutter. These mathematical ideas will then be applied in developing the signal processing techniques that minimize and even eliminate clutter from a radar return. Hopefully, after reading this text, one will have a fairly substantial understanding of the clutter cancellation problem and can then effectively channel one's efforts into specialized research of a particular aspect

of the clutter cancellation problem.

Joseph DeVenuto

Contents

	Page
Acknowledgements.....	ii
Preface.....	iii
List of Figures.....	viii
List of Tables.....	x
Abstract.....	xi
I. Introduction.....	1
Motivation.....	1
Problem Statement.....	2
Scope.....	3
Assumptions.....	4
Evaluation Standards.....	4
Approach.....	5
Summary of Current Knowledge.....	7
II. Theoretical Considerations.....	8
Introduction.....	8
Signal Representation.....	8
Signal Analysis.....	26
Matched Filter Development.....	32
Detection Processor Development.....	41
Digital Signal Processing.....	47
Ambiguity Function Development.....	60
III. Clutter Models and Cancellation Techniques.....	69
Introduction.....	69
Elements of Clutter.....	70
Typical Radar Receiver.....	86
Cancellation Techniques.....	88
IV. Computer Models.....	107
Approach.....	107
Clutter PSD Calculation.....	108
Clutter Cancellation Simulator.....	116
Improvement Factor Calculation.....	117
V. Results and Analysis.....	119
Test Case.....	119
Clutter Comparisons.....	121

Cancellation Scheme Comparisons.....	128
VI. Conclusions and Recommendations.....	143
Conclusions.....	143
Recommendations.....	146
Bibliography.....	149
Appendix A: Problem Parameters.....	A-1
Appendix B: Clutter Area Calculations.....	B-1
Appendix C: Useful Formulas.....	C-1
Appendix D: Program Listings.....	D-1
Vita.....	213

List of Figures

<u>Figure</u>	<u>Page</u>
II-1 Real and Complex Signal Magnitude Spectrum.....	14
II-2 Noise Autocorrelation and Spectral Characteristics..	26
II-3 Impulse Sampling and its Fourier Transform.....	49
III-1 Frequency Spectra of various types of fixed targets.	80
III-2 Clutter Spectrum.....	82
III-3 Spaceborne Radar Clutter Spectrum.....	85
III-4 Block Diagram of a MTI Radar Receiver.....	87
III-5 Pulse Doppler MTI System.....	90
III-6 Single Delay Line Canceler.....	94
III-7 Delay Line Frequency Response.....	96
III-8 Transversal Filter.....	98
III-9 Block Diagram / Typical Response.....	102
III-10 DPCA MTI Canceler.....	103
IV-1 Flowchart for CLUTCAN Program.....	109
IV-2 Situation Geometry.....	111
IV-3 Generation of Constant Doppler Contours.....	112
IV-4 Isodop and Isorange Points.....	113
IV-5 Range-Doppler Clutter Cell.....	114
V-1 Ground Clutter PSD for 35° Boresight Depression Angle.....	121
V-2 Ground Clutter PSD for 45° Boresight Depression Angle	122
V-3 Ground Clutter PSD for 55° Boresight Depression	

	Angle.....	122
V-4	Ground Clutter PSD for 65° Boresight Depression	
	Angle.....	123
V-5	Ground Clutter PSD for 75° Boresight Depression	
	Angle.....	123
V-6	Sea Clutter PSD for 45° Boresight Azimuth angle....	124
V-7	Snow/Ice Clutter PSD for 45° Boresight Azimuth	
	Angle.....	124
V-8	Transversal Filter with Butterworth Weights.....	130
V-9	Transversal Filter with Bartlett Weights.....	131
V-10	Transversal Filter with Hanning Weights.....	131
V-11	Transversal Filter with Hamming Weights.....	132
V-12	Transversal Filter with Blackman Weights.....	132
V-13	Transversal Filter with Binomial Weights.....	133
V-14	Transversal Filter with Uniform Weights.....	133
V-15	Transversal Filter with Bartlett Weights.....	134
V-16	Transversal Filter with Hanning Weights.....	134
V-17	Transversal Filter with Binomial Weights.....	135
V-18	Transversal Filter with Uniform Weights.....	135
V-19	Butterworth Weighted Filter (Even number of Taps)..	136
V-20	Hanning Weighted Filter (Even number of Taps).....	136
V-21	Butterworth Weighted Filter (Odd number of Taps)...	137
V-22	Hanning Weighted Filter (Odd number of Taps).....	137
V-23	Binomial Weighted Filter with Different Number of	
	Taps.....	138

List of Tables

<u>Table</u>	<u>Page</u>
II-1 Tapering Methods.....	58
III-1 Characteristics of Clutter Spectra.....	84
V-1 Depression Angle Influence on Clutter Spread.....	125
V-2 Depression Angle Influence on Received Clutter Power.....	126
V-3 Comparison of Ground / Sea Clutter Power.....	127
V-4 Comparison of Ground / Snow-Ice Clutter Power.....	127
V-5 Clutter Attenuation Factor for Different Cancellation Schemes.....	141
V-6 Clutter Attenuation Factor for Different Viewing Geometries.....	142

Abstract

The ability of a space-based radar surveillance system to obtain target information from a clutter corrupted radar echo signal is dependent upon the clutter cancellation technique employed. To thoroughly understand the nature of clutter so as to efficiently and effectively design and develop clutter cancellation techniques, fundamental mathematical relationships dealing with radar signal representation, probability theory, detection and estimation theory and signal comparison techniques were established and defined. Since the implementation of the mathematical expressions which describe clutter and clutter cancellation techniques is accomplished digitally, digital signal representation and digital filter characterization via FFT's were also established and defined. Drawing upon the established mathematical principals, as well as temporal probability models, spectral models and average backscatter coefficient models, clutter was described. Capitalizing on the different spectral characteristics between clutter and targets, three representative doppler cancellation schemes were developed. The three schemes were delay line cancelers, doppler filter banks and multiple look systems.

Using the models developed for clutter and clutter cancellation schemes, an interactive simulation was developed, and used to analyze the clutter cancellation ability of various cancellation methods against different backgrounds.

I. Introduction

Motivation

Joint United States - Canadian Air Defense Policy states that Canada and the U.S. will jointly maintain an air defense system that can 1) provide tactical warning and attack characterization so as to limit damage to strategic and retaliatory forces and command, control and communication (C)³ nodes and 2) exercise control of peace-time access to continental airspace (Ref 4:1). A viable air defense system is predicated on a surveillance system that will provide timely, reliable and unambiguous warning at a level sufficient to support survival of strategic forces located in North America.

In October 1981, in support of the North American Tactical Warning (ATW) Mission, Air Force Space Division proposed a constellation of space-based radar sensor systems to provide indication and warning of an impending air attack on North America. Performance of the surveillance system is based upon the sensor's ability to detect, track and provide intercept vectors of potential hostile aircraft. The radar system aboard each space platform is judged by its ability to extract range and velocity information describing a target (aircraft) from a returning radar signal.

The extraction of target range and velocity information would be fairly straightforward if it were not for the fact that the return signal is corrupted by energy returns from

unwanted scatters. This unwanted energy limits the radar system performance. The limitation to target detection and target estimation by unwanted energy returns can be so severe that at times the target is completely masked. To eliminate the masking of targets, techniques must be employed which reject or cancel out the unwanted energy returns.

Problem Statement

The return from unwanted targets is defined as clutter. Clutter is the return, or group of returns of reflected radar energy which results from scattering points of background targets such as buildings, birds, insects, weather, land and/or sea. The magnitude of the clutter returns is a function of not only the orientation of the radar antenna energy pattern with respect to the background targets, but also the amount of surface area illuminated. The radar antenna energy pattern describes the magnitude of energy the antenna radiates as a function of direction. The pattern is characterized by a main lobe, or main beam, and sidelobes. Generally the greatest amount of clutter energy returns result from the illumination of background targets with the mainlobe, but since the surface area which the sidelobes illuminate is so large, the sidelobe clutter return cannot be ignored.

Because a radar based on a space platform illuminates a large surface area, the return signal, or echo signal is dominated by ground, sea, and weather clutter. The distribution of the power magnitude versus frequency is called

a power spectral density (PSD). The echo signal which results from clutter is generally described by a PSD curve. Current clutter cancellation techniques employed on mobile radar platforms, such as aircraft, ships, or trucks, use filtering schemes or clutter cancellation techniques to filter out the power spectrum which corresponds to stationary and unwanted background returns. This allows for detection of targets of interest such as aircraft or missiles.

Scope

This study analyzes the clutter cancellation capability of various techniques available that could be used in Air Force Space Division's space-based radar (SBR) system to cancel ground and sea clutter. This study compares the various cancellation techniques presently employed on mobile radar systems in a space-based radar system, and is not a study intended to be an exhaustive effort to collect all methods available to cancel clutter. Clutter cancellation techniques can be broadly divided into doppler and nondoppler processing techniques. This study concentrates on the doppler processing techniques that are described in Chapter III.

Assumptions

Although this effort was motivated by Air Force Space Division's space-based radar design development, the satellite and radar parameters are generic. The radar aboard the spacecraft is a pulse doppler phased array radar. The radar

antenna size, radiated power, orientation, and transmitted waveform are described in Appendix A.

There is still some disagreement as to the exact statistics of earth and sea clutter, therefore the clutter model defined in Space Division's Space-based Radar System Specification was used. This model is detailed in Appendix A.

Evaluation Standards

The clutter attenuation factor, CA, will be used to evaluate the performance of the various clutter cancellation techniques that could be employed on the space-based radar system. The clutter attenuation factor is the ratio of the received clutter power normalized by the output clutter power of a clutter cancellation technique, or $CA = C_{in} / C_{out}$.

This criterion was selected because it clearly shows the capability of a cancellation technique to remove clutter energy. (Clutter attenuation factor has the added advantage of having a universal definition throughout literature.) The detectability of signal energy is the end product we wish to achieve, thus for this study the cancellation technique which yields the largest CA is considered as the optimal cancellation technique. Obviously, other factors such as cost, weight, space qualification and complexity could have been considered in choosing an optimal technique, but due to a wide variety of components available to implement a specific technique, cost and complexity as well as the other factors were not discussed so as to limit the size of the study.

Approach

Several steps were necessary to analyze the various clutter cancellation techniques:

1. Various fundamental mathematical relationships dealing with radar signal representation, probability theory, signal comparison techniques, i.e. correlation, spectral analysis, etc., detection and estimation theory, and digital design needed to all be established.
2. Since typically clutter cancelers filter or mask out the power spectral components which correspond to clutter, the design and implementation of filters had to be understood from both the time and frequency domain viewpoint. The frequency and time domain viewpoints allow one to comprehend exactly what the filter is doing to the voltage signal that represents clutter.
3. A complete and thorough understanding of the characteristics, parameters and models which describe land, sea, and atmospheric clutter as seen from a space-based radar, had to be gained. Clutter power intensity as a function of background had to be understood. The clutter power spectral density had to be thoroughly comprehended. An understanding of clutter was essential because clutter cancellation methods could not be effectively developed to cancel an unknown quantity.

4. Once clutter and filter were understood, clutter cancellation algorithms and techniques could be synthesized.
5. The clutter and the filters which make up the clutter cancellation techniques, were computer modeled to more fully understand the cancelling problem and to test the feasibility of various cancellation techniques.
6. The attenuation factor for the selected cancellation techniques were then computed and compared to determine the optimal technique.

These six steps will be used to answer the question of what is the optimal clutter cancellation technique to be employed on a space-based radar system.

Summary of Current Knowledge

General information on airborne doppler radar, pulse doppler, pulse doppler clutter, and clutter cancellation techniques can be found in Merrill Skolnik's books Introduction to Radar Systems (Ref 56) and Radar Handbook (Ref 57) and also David Barton's Radar System Analysis (Ref 6). Specific clutter descriptions and clutter models can also be found in Barton's Radar Clutter, Volume 5. This book contains a compendium of articles describing clutter and clutter modeling. Clutter cancellation techniques and clutter rejection circuitry can be found in Barton's CW and Doppler Radar, Volume 7 and D. Curtis Schleher's MTI Radar. Both of these books are compendiums of articles which deal with

clutter cancellation. These references as well as other support material, were used to develop the foundation of knowledge that is presented in the next three chapters.

Chapter II Theoretical Background

Introduction

Before developing and analyzing return clutter waveforms and the receiver/processors to eliminate clutter, it is necessary to establish some fundamental concepts. In this chapter I develop 1) appropriate time and frequency signal representation for both deterministic and random signals; 2) signal analysis techniques; 3) matched filters and their usage; and 4) detection and estimation criteria. Since signal analysis in radar is usually accomplished with a special purpose digital computer, digital domain signal representation and digital analysis of signals and systems will be presented. It is not my intent to present a complete and thorough development of all these digital concepts, as has been elegantly accomplished in the various references cited, but rather to highlight their important and salient features and show their application to the clutter cancellation problem. With an understanding of signal representation and analysis, prudent waveform design through the use of ambiguity functions can be explained.

Signal Representation

Signal representation is probably the most important and fundamental concept needed to understand both the analysis and the design of radar engineering. Information about the presence, cross section, range, velocity, etc. of a target is

all determined from the received reflection of the transmitted signal. More efficient signal analysis and design can occur with proper waveform representation. For the clutter cancellation problem a way of representing 1) the transmitted and reflected target energy 2) the reflected clutter energy and 3) noise energy is needed.

The energy transmitted from the radar antenna and received from a reflected target can be represented by a deterministic signal in either the time domain or in the frequency domain. The time domain representation can either take a real or complex form with the frequency domain expressions being transforms of one of the time domain forms. The most straightforward representation of a radar signal is as a real-valued time function consisting of a high frequency carrier modulated in amplitude and/or phase by functions that are generally narrowband (i.e. $B/f \leq .1$ where B is the signal bandwidth and f is the carrier frequency). The radar signal, denoted $s(t)$, can therefore be written as

$$s(t) = A(t) \cos[2\pi f t + \theta(t) + \phi] \quad (\text{II-1})$$

where $A(t)$ is the amplitude modulation function, $\theta(t)$ is the phase modulation function, f is the carrier frequency in hertz, and ϕ is the initial phase angle. Throughout the rest of this section I assume $\phi = 0$ with no loss in generality.

Making use of the trigonometric identities listed in Appendix C, equation II-1 can be presented in quadrature form

as

$$s(t) = x(t) \cos 2\pi f_o t - y(t) \sin 2\pi f_o t \quad (\text{II-2})$$

where

$$\begin{aligned} x(t) &= A(t) \cos \theta \\ y(t) &= A(t) \sin \theta \end{aligned} \quad (\text{II-3})$$

In the development so far we have simply represented the signal in a different form, i.e. as quadrature components, however a similar quadrature component formation is used in the development of the clutter cancellation techniques. We will see that the formation of quadrature components, similar to those described by equation II-3, enhances the radar processor's ability to recover information that would otherwise be lost. Quadrature components are also used to enhance the detection process.

From the quadrature component representation, the complex exponential representation, $u(t)$, is formed from the two real low pass signals $x(t)$ and $y(t)$ as

$$u(t) = x(t) + j y(t) = A(t) e^{j\theta(t)} \quad (\text{II-4})$$

where

$$\begin{aligned} A^2(t) &= x^2(t) + y^2(t) \\ \theta(t) &= \tan^{-1} [y(t)/x(t)] \end{aligned} \quad (\text{II-5})$$

In equation II-4, $u(t)$ is the complex envelope of the signal

$s(t)$. Using appropriate trigonometric identities it is easy to show that the radar signal described in equation II-1 can be rewritten as

$$s(t) = .5 [u(t) \exp[j2\pi f_c t] + u^*(t) \exp[-j2\pi f_c t]] \quad (a)$$

(II-6)

$$= \text{Re} [u(t) \exp[j2\pi f_c t]] \quad (b)$$

where Re means "real part of." Equation II-6b provides a form where only the complex envelope of the signal need be utilized in calculations, thus eliminating the need for any manipulations of the carrier frequency.

A different complex representation of the radar signal described in equation II-1 can be obtained by application of the Hilbert transformation. Given the signal $s(t)$, we form the analytic signal $s_a(t)$ by

$$s_a(t) = s(t) + j \hat{s}(t). \quad (II-7)$$

The function $\hat{s}(t)$ is the Hilbert transform given by

$$\hat{s}(t) = (1/2\pi) \int s(\sigma)/(t - \sigma) d\sigma \quad (II-8)$$

where " \int " denotes the Cauchy principle value of the integral. (Note: Integrals without labeled limits are defined to have infinite limits.) From equations II-6b and II-7 we see that

$$s_a(t) = \text{Re} [s_a(t)] = \text{Re} [u(t) \exp[j2\pi f_o t]] \quad (\text{II-9})$$

therefore the analytic signal is related to the complex exponential representation by

$$s_a(t) = u(t) \exp[j2\pi f_o t] \quad (\text{II-10})$$

Thus for analysis of radar signal we can use the complex exponential signal form and assume it is the same as the Hilbert transform representation (Ref 20:20).

When using the complex envelope representation, attention must be focused on the relationship between the energy, E , of the signal and the energy of the complex envelope. From Parseval's theorem the energy of a signal is

$$\begin{aligned} E_s &= \int |s(t)|^2 dt = \int A^2(t) \cos^2 [2\pi f_o t + \theta(t) + \phi_o] dt \\ &= \int A^2(t) / 2 dt \end{aligned} \quad (\text{II-11})$$

The energy in the complex envelope is

$$\begin{aligned} E_c &= \int |u(t)|^2 dt = \int A(t) e^{j\theta(t)} A^*(t) e^{-j\theta(t)} dt \\ &= \int A^2(t) dt \end{aligned} \quad (\text{II-12})$$

Therefore we see that the energy in the complex envelope contains twice the energy of the signal it represents.

As mentioned before, the radar signal can also be described by its frequency content. The frequency spectrum, $S(f)$, is the Fourier transform of the time domain function $s(t)$

$$S(f) = \int s(t) e^{-j2\pi ft} dt \quad (\text{II-13})$$

The inverse transform is thus written as

$$s(t) = \int S(f) e^{j2\pi ft} df \quad (\text{II-14})$$

There are many Fourier transform properties which aid in the radar analysis and design. (See Appendix C page C-2 for a list, Ref 45: Chapter 3 or Ref 46: Chapter 2) Two particularly useful properties are the symmetry relation and the frequency shifting theorem. If $s(t)$ is a real-valued function the symmetry relation is

$$S(f) = S^*(-f) \quad (\text{II-15})$$

where $S^*(f)$ is the complex conjugate of $S(f)$. The shifting theorem is defined as

$$g(t) \exp[j2\pi f_0 t] \leftrightarrow G(f - f_0) \quad (\text{II-16})$$

Applying equations II-15 and II-16 to the radar signal, equation II-1 can be written as

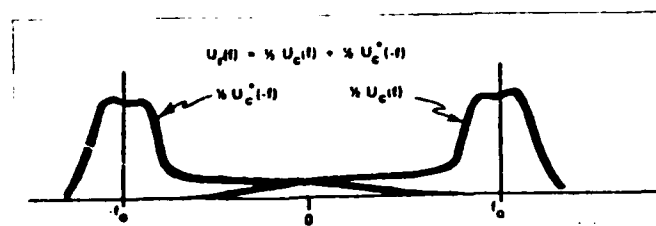
$$S(f) = .5 [U(f - f_o) + U(f + f_o)] \quad (II-17)$$

where $U(f - f_o)$ is the Fourier transform of $u(t)$, defined in equation II-4.

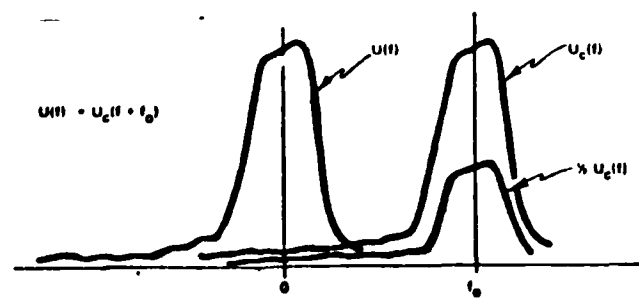
Taking the Fourier transform of the complex signal form, described in equation II-6a, we get

$$S(f) = .5[U(f - f_o) + U^*(f - f_o)] = U(f - f_o) \quad (II-18)$$

From equation II-18 we see that the amplitude frequency spectrum of the complex form is twice the amplitude of the first component of the signal amplitude spectrum. Figure II-1 illustrates the spectrum magnitude for the real and complex signals and their interrelationship.



(a) Real Signal Magnitude Spectrum



(b) Complex Signal Magnitude Spectrum

Fig. II-1 Real and Complex Signal Magnitude Spectrum

Up to this point when describing the radar signal frequency spectrum we have only been concerned with the amplitude spectrum. Two other useful spectral quantities are the energy spectral density (ESD) and the power spectral density (PSD), defined as

$$\text{ESD of } s(t) = |S(f)|^2 \quad (\text{II-19})$$

$$\text{PSD of } s(t) = \lim_{T \rightarrow \infty} |S(f)|^2 / T \quad (\text{II-20})$$

where T is the observation time. The signal energy and average power can thus be calculated by integrating over the signal bandwidth. The signal energy is thus

$$E = \int |S(f)|^2 df \quad (\text{Joules/Hz}) \quad (\text{II-21})$$

and the average power is

$$P_{\text{ave}} = \lim_{T \rightarrow \infty} \int |S(f)|^2 / T df \quad (\text{Watts/Hz}) \quad (\text{II-22})$$

The signal average power and the power spectral density provide a convenient, and most useful, way of describing clutter and noise and thereby a method of analyzing the various clutter cancellation schemes. This will become evident in the next chapter.

Because of the randomness in amplitude and phase of clutter scatterers and the random nature of noise, clutter and noise cannot be described by a deterministic signal, but rather by a stochastic process. A stochastic process is

defined as a collection of time functions, $x(t, \underline{c})$, that are the outcomes from a repeated experiment. The outcomes from each experiment repetition, one for each c_i , form a family, or ensemble, of functions. If only discrete values of time are considered, then $x(t, \underline{c})$ is a discrete stochastic process, otherwise $x(t, \underline{c})$ is a continuous stochastic process. (For notational convenience the "c" in $x(t, \underline{c})$ will be suppressed in future discussions when it is clear that stochastic processes are the issue.)

The probability theory notation to be used will be described before discussing the representation of noise and clutter as stochastic processes. While the notation and statistical properties presented assume continuous random variables, the theory applies to discrete random variables. To obtain the discrete form simply replace the integrals with summations. Given two events, defined by the random variables X and Y that belong to a sample space, the following probability properties are defined:

- 1) The probability of event X occurring, or the relative frequency, is $P(X) = \lim_{n \rightarrow \infty} n_X / n$.
- 2) The joint probability of both events X and Y occurring is $P(X, Y)$.
- 3) The events X and Y are independent if $P(X, Y) = P(X)P(Y)$.
- 4) The conditional probability of event X occurring given that event Y has occurred is $P(X/Y)$.
- 5) Conditional probability can be written as $P(X, Y) =$

$$P(X/Y)P(Y) = P(Y/X)P(X).$$

The distribution of a function of the random variable X is defined

$$P(x) = P[X \leq x] \quad (\text{II-23})$$

defined for $-\infty \leq x \leq \infty$ (Ref 44:88). The probability density function (pdf) of X is the derivative of the distribution function.

$$p(x) = d P(x)/dx \quad (\text{II-24})$$

where

- 1) $p(x)$ is the probability that the value of x lies between x and $x + dx$.
- 2) $p(x) \geq 0$ for all values of x .
- 3) $\int p(x) dx = 1$.
- 4) The derivative of $P(x)$ is assumed to exist.

From equations II-23 and II-24 we see that .

$$P(x) = \int_{-\infty}^x p(x) dx \quad (\text{II-25})$$

$$P[a \leq X \leq b] = P(b) - P(a) = \int_a^b p(x) dx \quad (\text{II-26})$$

where $P(b) > P(a)$. On page C-3 of Appendix C is a list of the pdf's commonly used in this study.

The expected value (mean) of a random variable with a pdf $p(x)$ is

$$E[x] = m_x = \int x p(x) dx \quad (\text{II-27})$$

where "E" is the expectation operator. The expectation of a function $f(x)$ is defined as

$$E[f(x)] = \int f(x) p(x) dx \quad (\text{II-28})$$

where if $f(x) = x^n$, the function $E[x^n]$ is called the n^{th} moment. Note the first moment of $p(x)$ is the mean of $p(x)$. The second moment about the mean, or second central moment, is the variance defined as

$$\begin{aligned} \sigma_x^2 &= E[(X - m_x)^2] = \int (X - m_x)^2 p(x) dx \\ &= E[X^2] - m_x^2 \end{aligned} \quad (\text{II-29})$$

The square root of the variance is called the standard deviation. The third central moment is a measure of the asymmetry of $p(x)$ about m_x and is called the skewness of the distribution.

The statistical properties developed for a single random variable can be extended to multiple random variables. We can think of multiple random variables as being components of a random point in a multiple dimension space. The point is called a vector random variable or random vector. This concept will be exploited in detection theory when detection is based upon multiple signal returns. Random vector

statistics is also utilized when a continuous signal is discretized. We will limit the discussion of multiple random variables to two variables X and Y with no loss in generality.

If X and Y are two jointly distributed random variables, with joint pdf $p(x,y)$, the following properties hold:

$$1) P(x,y) = P[X \leq x, Y \leq y]$$

$$2) 0 \leq P(x,y) \leq 1 \quad \text{for all } x,y$$

$$3) p(x,y) = \frac{\partial^2 P(x,y)}{\partial x \partial y}$$

$$4) P(x,y) = \int_{-\infty}^x \int_{-\infty}^y p(x,y) dx dy$$

$$5) P[a \leq X \leq b, c \leq Y \leq d] = \int_a^b \int_c^d p(x,y) dx dy$$

$$6) \iint p(x,y) dx dy = 1$$

7) The marginal densities of X and Y are:

$$p(x) = \int p(x,y) dy = \int p(x/y) p(y) dy$$

$$p(y) = \int p(x,y) dx = \int p(y/x) p(x) dx$$

8) The mean of X and Y is:

$$E[X] = m_x = \iint x p(x,y) dx dy = \int x p(x) dx$$

$$E[Y] = m_y = \iint y p(x,y) dx dy = \int y p(y) dy$$

9) The $(n + k)^{th}$ order joint moment, or cross moment of X and Y is:

$$E[X^n Y^k] = \iint x^n y^k p(x,y) dx dy$$

10) The first joint central moment, the covariance, is:

$$\sigma_{xy} = E[(X - m_x)(Y - m_y)] = \iiint (X - m_x)(Y - m_y)p(x,y)dx dy$$

11) The normalized covariance of X and Y, or correlation coefficient, is:

$$\rho_{xy} = \frac{E[(X - m_x)(Y - m_y)]}{\sqrt{[E[(X - m_x)^2] E[(Y - m_y)^2]]^{.5}}} = \frac{\sigma_{xy}}{\sigma_x \sigma_y}$$

where $|\rho_{xy}| \leq 1$.

12) The random variables are uncorrelated if $E[XY] = E[X]E[Y]$. If the random variables are uncorrelated then the correlation coefficient is zero. If the two random variables are independent then they are uncorrelated.

13) The random variables are orthogonal if $E[XY] = 0$.

A final statistical operation that needs to be explained is a method of obtaining the statistics of a random variables defined indirectly as a function of another random variable. This occurs for example when the quadrature components of the received voltage is known and the pdf of the magnitude and phase of the received voltage are needed. Given a N - dimensional space X with joint pdf $p(x_1 \dots x_N)$, let the new N variables be defined on a space Y be defined by the N functions

$$y_k = g_k(x_1 \dots x_N); \quad k = 1, \dots, N \quad (\text{II-30})$$

The inverse functions are defined as

$$x_k = h(y_{k-1} \dots y_N); \quad k = 1, \dots, N \quad (\text{II-31})$$

The new joint pdf is given by

$$p(y_1 \dots y_N) = p[x_k = h(y_{k-1} \dots y_N); k=1 \dots N] |J| \quad (\text{II-32})$$

where $|J|$ is the Jacobian of the transformation defined as

$$|J| = \begin{vmatrix} \partial h / \partial y_{1-1} & \dots & \partial h / \partial y_{1-N} \\ \vdots & & \vdots \\ \partial h / \partial y_{N-1} & \dots & \partial h / \partial y_{N-N} \end{vmatrix} \quad (\text{II-33})$$

(For a more complete discussion of the probability properties presented consult Ref 44:Chapters 1-8 and Ref 45:Chapter 4.)

The statistical properties just discussed for random variables also apply to stochastic processes. (For a complete explanation of stochastic properties consult Ref 44:Chapters 10 and 11 or Ref 20:34-39.) In the clutter cancellation discussions that ensue, we will assume that the noise and clutter processes are wide-sense stationary, that is the statistical properties of the ensemble do not change under a shift in the time origin, but are a function of time difference τ (Ref 66:30) and that the ensemble average is a

constant.

For a random process we define an ensemble moments and time moments. If the ensemble moments and the time moments are equal then we say the process is ergodic and we only need analyze one set of moments, usually the ensemble moments. The ensemble first moment, or average, is defined

$$E[x(t)] = \int x(t_1, q) p(q, t_1) dq = \int x p(x, t_1) dx \quad (\text{II-34})$$

where t_1 is a fixed time. The time average is defined as

$$\langle x(t) \rangle = \lim_{T \rightarrow \infty} [1/2T] \int_{-T}^T x(t) dt \quad (\text{II-35})$$

where $\langle \rangle$ denotes the time average.

One of the most important relationships of stochastic processes is that of correlation. Correlation is a measure of interdependence or association between signal values (Ref 60:233). Again we have both an ensemble and time correlation function. The ensemble autocorrelation function, the correlation between a function and a delay version of itself, is

$$R_x(\tau) = E[x(t)x^*(t + \tau)] = \iint x(t_1)x^*(t_2)p[x(t_1)x^*(t_2)] dx(t_1)dx(t_2) \quad (\text{II-36})$$

where $t_1 = t$ and $t_2 = t + \tau$. The ensemble cross-correlation between two processes $x(t)$ and $y(t)$ is defined as

$$R_{xy}(\tau) = E[x(t)y^*(t + \tau)] = \iint x(t_1)y^*(t_2)p[x(t_1)y^*(t_2)] dx(t_1)dy(t_2) \quad (II-37)$$

$$R_{yx}(\tau) = E[y(t)x^*(t + \tau)] = \iint y(t_1)x^*(t_2)p[y(t_1)x^*(t_2)] dy(t_1)dx(t_2) \quad (II-38)$$

The time autocorrelation function is defined as

$$R_x(\tau) = \langle x(t)x^*(t + \tau) \rangle = \lim_{T \rightarrow \infty} [1/2T] \int x(t)x^*(t + \tau) dt \quad (II-39)$$

If the process $x(t)$ is ergodic then $R_x(\tau) = R(\tau)$. For the clutter problem we assume that the noise and clutter processes are ergodic.

The correlation function has several properties that are useful in the design and analysis of clutter and of cancellation techniques.

$$\begin{aligned} 1) \text{ For complex processes: } R_{xy}(-\tau) &= R_{yx}^*(\tau) \\ R_{xy}(\tau) &= R_{yx}^*(\tau) \end{aligned}$$

$$\begin{aligned} 2) \text{ For real processes: } R_{xx}(\tau) &= R_{xx}(-\tau) \\ R_{xy}(\tau) &= R_{yx}(-\tau) \end{aligned}$$

$$3) |R_x(\tau)| \leq R_x(0)$$

$$|R_x(\tau)| \leq [R_x(0) R_y(0)]^{.5} \leq .5[R_x(0) + R_y(0)]$$

$$4) R_x(0) = E[x(t)x^*(t)] = \sigma_x^2$$

$$5) R_x(\tau) = x(t) * x^*(-t) = \int x(\tau) x^*(t-\tau) d\tau$$

$$6) R_{xy}(\tau) = x^*(-t) * y(t) = \int x^*(t-\tau) y(\tau) d\tau$$

Analogous to narrowband deterministic signals, a random process is said to be narrowband if its spectral density is zero except for a narrow frequency region around a high carrier frequency (Ref 66:75). If $n(t)$ is a real narrowband WSS random process with zero mean, it may be expressed as

$$n(t) = x(t) \cos 2\pi f_o t - y(t) \sin 2\pi f_o t \quad (\text{II-40})$$

where the quadrature components $x(t)$ and $y(t)$ are low pass, zero mean, WSS processes. The correlation properties listed above also apply to narrowband processes (Ref 66:75-78).

The last, extensively used correlation property to be discussed, is the Wiener - Khinchine theorem. This theorem states that the power spectral density of a WSS process $x(t)$, with autocorrelation $R_x(\tau)$, is defined as the Fourier transform of $R_x(\tau)$. Therefore

$$S_x(f) = \int_{-\infty}^{\infty} R_x(\tau) e^{-j2\pi f\tau} d\tau \quad (\text{II-41})$$

and it follows that

$$R_x(\tau) = \int_{-\infty}^{\infty} S_x(f) e^{j2\pi f\tau} df \quad (\text{II-42})$$

The average power is thus

$$R_x(0) = \int_{-\infty}^{\infty} S_x(f) df = E[|x(t)|^2] \quad (\text{II-43})$$

For the two real, jointly, WSS random processes $x(t)$ and $y(t)$ with a cross correlation function $R_{xy}(\tau)$, the cross power spectral density is

$$S_{xy}(f) = \int_{-\infty}^{\infty} R_{xy}(\tau) e^{-j2\pi f\tau} d\tau \quad (\text{II-44})$$

and the inverse transformation is

$$R_{xy}(\tau) = \int_{-\infty}^{\infty} S_{xy}(f) e^{j2\pi f\tau} df \quad (\text{II-45})$$

From correlation property (1) we obtain

$$S_{xy}(f) = S_{yx}(-f) ; \text{ Real process} \quad (\text{II-46})$$

$$\star$$

$$S_{xy}(f) = S_{xy}(f) ; \text{ Complex process}$$

As will become evident in the next several sections and then in Chapter III, the power spectral density of a deterministic signal or a random process provides a useful way

of describing not only a waveform, but also a way to describe and develop signal analysis techniques that exploit the different power spectral characteristics of signal so as to distinguish target information from clutter and noise.

Before proceeding on to the development of signal analysis techniques, we first need to provide a descriptor for white noise. We will delay discussion of colored noise, i.e. clutter, because it will be covered in Chapter III. In the clutter problem we are dealing with bandpass signals, therefore white noise can be described by the bandpass signal defined in equation II-45, where $x(t)$ and $y(t)$ are lowpass, zero mean, WSS Gaussian processes. We define noise to have an impulse autocorrelation function and an unit spectral response. For this study we characterize white noise as show in Figure II-2.

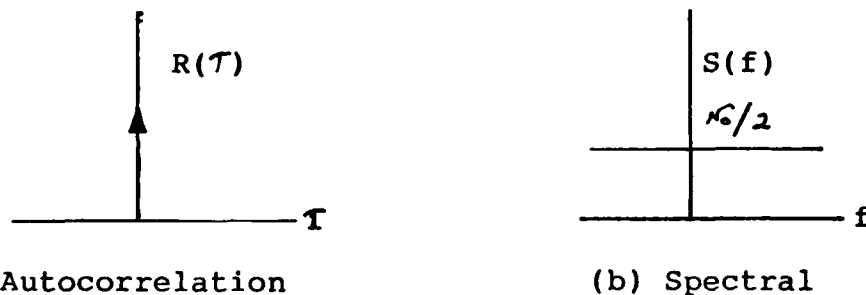


Fig. II-2 Noise Autocorrelation and Spectral Characteristics

Signal Analysis

As would be expected, since deterministic and random signals are decribed in both the time and frequency domain, signal analysis is also performed in both domains. The signal

analysis techniques used to cancel clutter and obtain target information from a reflected radar signal, are based in one form or another on the correlation principle. Correlation is the process of determining the mutual relationship which exists between two signals in bandwidth, time duration, shape and energy distribution, etc. (Ref 13:92). As shown in the last section, correlation applies to both deterministic and random functions, therefore the correlation concepts will be described assuming a deterministic signal. In the cases where $s(t)$ is a random signal, i.e. clutter or noise, then moment calculations must be applied. Target information such as range and range rate is related to various signal parameters, i.e. delay and frequency shift. Given the target information desired, the appropriate signal parameter from the reflected radar signal is compared, or correlated, with the transmitted signal. The level of comparison provides an indication of the value of the signal parameter and thus the desired target information.

From the time domain perspective, correlation is accomplished via the concept of convolution between a linear, time invariant system and a signal. From the previous section we saw that convolution is related to correlation by

$$R_s(t) = s(t) * s(-t) \quad (II_47)$$

If $s(t)$ is real and symmetric, then convolution is correlation. Given a signal $s(t)$, a linear system, or filter,

can be derived such that a prescribed response occurs for perfect correlation. Any deviation from the desired response indicates other than perfect correlation. The response of the linear filter to any signal is given by the convolution integral

$$y(t) = \int s(\tau) h(t - \tau) d\tau \quad (\text{II-48})$$

The convolution between the signal and the filter is denoted $s(t)*h(t)$. To obtain specific target information, a filter is designed to provide a measure of correlation of the appropriate signal parameter between the transmitted and reflected radar signal. The filter, operating in the presence of noise and clutter, exploits the characteristic differences between the signal and clutter and noise. A convenient way of designing the filter to perform the desired correlation on either random or deterministic signals is accomplished via frequency domain analysis.

Frequency domain analysis can be approached from two points of view. The first perspective looks at frequency domain analysis as transforming a signal into a new domain and then observing the amplitude, energy, or power distribution over the frequency spectrum for certain distribution characteristics. Unwanted characteristics are removed through selective nulling, or filtering. This perspective is useful when dealing with both random and deterministic signals. The second frequency domain perspective views frequency analysis

as a tool to conveniently design the appropriate correlation filters that are suggested in the time domain. Applying the Fourier transform, equation II-13, to the convolution integral, the frequency domain representation is

$$Y(f) = \int e^{-j2\pi ft} dt \int s(\tau) h(t-\tau) d\tau \quad (\text{II-49})$$

Letting $p = t - \tau$, equation II-48 can be rewritten as

$$Y(f) = \int s(\tau) e^{-j2\pi f(p+\tau)} dp \int s(\tau) h(p) d\tau \quad (\text{II-49a})$$

Rearranging we see

$$\begin{aligned} Y(f) &= \int s(\tau) e^{-j2\pi f\tau} d\tau \int h(p) e^{-j2\pi fp} dp \\ &= S(f) H(f) \end{aligned} \quad (\text{II-50})$$

that the time domain convolution of two functions is simply the multiplication of the Fourier transform of each deterministic signals. The response of a filter to a random signal is described in terms of the power spectrum. Driving a deterministic filter, with transfer function $H(f)$, with a random signal $x(t)$, having a PSD of $S_x(f)$, the filter output PSD is

$$S_y(f) = S_x(f) |H(f)|^2 \quad (\text{II-51})$$

(Ref 45:347). Equation II-50 also illustrates the fact that in the frequency domain the necessary filter is the ratio of the desired frequency response divided by the signal frequency. Both perspectives on frequency analysis will be utilized throughout this study. Spectral characteristics will be used in describing the signal, noise and clutter, while frequency domain synthesis techniques (Refs 29, 44, 46) will be used to design the necessary filters.

Since the signal can conveniently be described in the frequency domain, and analysis, design, and synthesis of filters tend to be easier in the frequency domain, spectral analysis will be heavily utilized in describing and analyzing the clutter cancellation problem. Estimation of the power spectral density of a signal is traditionally calculated by one of three methods (Ref 7:250): 1) Bandpass filtering - the signal is passed through a bank of filters, or a comb filter, the response is then squared and scaled by the observation time. The filter bank can either be implemented with lumped constants or digitally. Digital filtering will be discussed in an upcoming section. 2) Indirect method - the signal autocorrelation function is estimated, usually by

$$R_s(m) = [1/(N-m)] \sum_{n=0}^{N-m-1} s(nT + mT) s^*(nT) \quad (\text{II-52})$$

where n is the sample number and m is the frequency index. The PSD is calculated by taking the Fourier transform of the correlation function usually via a fast Fourier transform

(FFT) operation such as the one suggested by Blackman and Tukey

$$S_{BT}(f) = \Delta t \sum_{m=-M}^M R_s(m) \exp[-j2\pi f m \Delta t] \quad (II-53)$$

(Ref 34:1383). 3) Direct method - the Fourier transform of the signal is calculated, squared, and scaled, usually through a FFT algorithm. FFT algorithm usage will be discussed in the digital filtering section. The direct method can also be implemented by one of several modern estimation methods, the majority of which are based on the rational model approach. In the rational model method the PSD of a time series is assumed to be modeled as a rational function

$$S(e^{jw}) = \left| \frac{b_0 + b_1 e^{-jw} + \dots + b_n e^{-jwn}}{a_0 + a_1 e^{-jw} + \dots + a_m e^{-jwm}} \right|^2 \quad (II-54)$$

where $m > n$ (Ref 34:1387). The PSD is determined through the selection of the coefficients. The use of nontraditional spectral estimation techniques for clutter and target estimation will not be considered within this study.

Having established the fundamental radar signal analysis techniques, we can now look at specific filters that maximize the signal to interference and allow for detection.

Matched Filter Development

In the last section we showed that target information is obtained by correlating, or convolving, the received signal with a linear filter. Proceeding from that framework, effective extraction of range and velocity information from the echo signal can be accomplished by maximizing the signal to interference ratio, S/I . Interference is defined as the energy from white noise as well as from unwanted scattering elements (clutter or colored noise). It can be shown that the signal-to-noise ratio is indirectly related to radar performance measures such as probability of detection, probability of false alarm, and range and doppler estimation accuracy (Ref 22:143).

A radar signal processor is nothing more than a composition of various filters. Before developing the filter that maximizes the S/I ratio, let's first philosophically look at the role of the processor to aid in the filter development and to provide insight into the detection and estimation problem. The function of the radar signal processor is to determine whether a target is present or absent, at what range and at what velocity. Detection criteria is normally based on the concept of direct probability. Direct probability is the probability which describes the chance of an event happening before the event occurs. If the event actually happened, then the best estimate, or hypothesis, as to the cause of the event illustrates the concept of inverse probability (Ref 56:377). Detection criteria based on inverse probability is particular-

ly useful in statistical detection and statistical parameter estimation. To illustrate the above ideas, take for example the event of the radar receiver output voltage. It is of interest to determine whether the output was caused by noise or by a target in the presence of noise. The probability that the cause of the event was noise or signal-plus-noise before the event occurs is labeled the "a priori probability," while the probability that the receiver output voltage was caused by noise or signal-plus-noise after the event occurred is called the "a posteriori probability." The "a posteriori" probability represents the state of information obtained as a result of observing the output. The method of inverse probability uses the "a priori probabilities" associated with each of the possible hypothesis (i.e. whether the receiver output was caused by noise or signal-plus-noise) to explain the cause of the event. The "a priori probabilities", along with a knowledge of the event, are used to compute the "a posteriori probabilities." A separate probability is computed for each hypothesis and the largest "a posteriori probability" is selected as the most likely cause of the event (Ref 56:377).

The best any receiver can do is to form the "a posteriori probability" distribution (Ref 67:31). To illustrate the idea of inverse probability, the "a posteriori probability" of the delay, τ , of the transmitted waveform will be formed. As stated before, these signal parameters provide information on the target's range. The probability distribution information, most conveniently handled in logarithmic

form, is called the information function. The information function for the time delay distribution is

$$Q(\tau) = \ln [P(Y/\tau)] \quad (\text{II-55})$$

where Y is the received signal voltage with a time delay associated with it, and $P(Y/\tau)$ is the probability density for the received signal given a delay τ (Ref 67:31).

In the case where the echo return of the waveform has a time delay of τ the received signal is

$$Y(t) = s(t - \tau) + n(t) \quad (\text{II-56})$$

where $s(t)$ is the transmitted signal and $n(t)$ is the added white Gaussian noise with probability distribution proportional to

$$k \exp\left[-\frac{1}{N} \int_0^T [n(t)]^2 dt\right] \quad (\text{II-57})$$

where N is the mean noise per unit bandwidth and T defines the observation period (Ref 67:31). The noise function can be rewritten as $n(t) = Y(t) - s(t-\tau)$. Substituting into equation II-57, we obtain

$$k \exp\left[-\frac{1}{N} \int_0^T [Y(t) - s(t-\tau)]^2 dt\right] \quad (\text{II-58})$$

Equation II-58 is proportional to the probability density of

the noise waveform hypothesised on the echo signal being delayed τ . The information function concerning range is thus

$$Q(\tau) = -k/N \int_0^T [Y(t) - s(t-\tau)]^2 dt \quad (\text{II-59})$$

The actual time delay is obtained by maximizing the information function. This is done by varying τ to obtain the value that gives the least mean square departure from the received signal.

Expanding the integral in equation II-59, we get

$$\int_0^T [Y(t)]^2 dt - 2 \int_0^T Y(t)s(t-\tau) dt + \int_0^T [s(t-\tau)]^2 dt \quad (\text{II-60})$$

Upon reception, $Y(t)$ is known and can be absorbed by the constant k . Integrating over one period makes $s(t-\tau)$ independent of time delay and therefore is known and can also be absorbed by the constant k . Thus equation II-60 becomes

$$Q(\tau) = 2k/N \int_0^T [Y(t) s(t-\tau)] dt \quad (\text{II-61})$$

Equation II-61 is the information function which in logarithmic form gives the "a posteriori probability" distribution of the values of τ . From this function we obtain the probability that the received signal is from a target with a time delay of τ . A similar development for determining the "a posteriori" distribution for the received waveform's frequency shift can also be performed.

The information function, equation II-61, is simply the output from a linear filter, which apart from the scaling factor $2k/N$, is the convolution of the input $Y(t)$ and the impulse response $h(t) = s(-t)$. The filter is the unique linear filter which gives the maximum peak signal to noise ratio. The filter has the same frequency response, which in magnitude has the same shape as the amplitude of complex envelope of the transmitted signal $s(t)$, but in phase is equal in magnitude and opposite in sign (Ref 67:32). The filter described in Woodward's information function (equation II-61) is commonly called the matched filter.

While the matched filter can be developed in the time domain (Ref 22:144-149), it is more easily shown in the frequency domain by applying the Schwartz inequality (Ref 46:159-162).

In general the received signal is the sum of the transmitted waveform $s(t)$ and noise $n(t)$

$$y(t) = s(t) + n(t) \quad (\text{II-62})$$

where $n(t)$ can either be white or colored noise. The signal $y(t)$ is applied to the receiver filter with a transfer function $H(f)$. The signal component at the filter output is

$$s_o(t) = \int S(f) H(f) e^{j2\pi ft} df \quad (\text{II-63})$$

where $S(f)$ is the Fourier amplitude spectrum of $s(t)$. If t_o

is the time that the output signal is maximum, then the peak signal power, P , is

$$P = |s(t)|^2 = \left| \int_0 S(f) H(f) \exp[j2\pi ft] df \right|^2 \quad (\text{II-64})$$

The average filter output noise power is

$$N_o = \int_0 S_N(f) |H(f)|^2 df \quad (\text{II-65})$$

where $S_N(f)$ is the receiver input noise density spectrum. The signal to noise power to be maximized is

$$\frac{S_o}{N_o} = \frac{\left| \int_0 S(f) H(f) \exp[j2\pi ft] df \right|^2}{\int_0 S_N(f) |H(f)|^2 df} \quad (\text{II-66})$$

To maximize equation II-70, the Schwarz inequality is applied. If $A(f)$ and $B(f)$ are general complex functions of the real variable f , the inequality is

$$\left| \int A(f) B(f) df \right|^2 \leq \int |A(f)|^2 df \int |B(f)|^2 df \quad (\text{II-67})$$

where the equality holds only when $B(f)$ is proportional to $A(f)$. Making the substitutions

$$A(f) = \sqrt{S_N(f)} H(f)$$

$$B(f) = S(f) \exp[2\pi j f t] / (2\sqrt{S_N(f)})$$

into equation II-66 the signal to noise ratio becomes

$$S_o / N_o \leq \int |S(f)|^2 / S_N(f) df \quad (\text{II-68})$$

The maximum occurs when the equality holds. The optimal transfer function, or matched filter, is therefore

$$H_{\text{opt}}(f) = k \frac{S^*(f) \exp[-2\pi j f t]}{S_N(f)} \quad (\text{II-69})$$

The key feature of equation II-69 is that the optimal filter is proportional to the ratio of the complex conjugate of the signal spectrum to the noise power spectrum.

If the noise is white, the matched filter becomes

$$H_{\text{opt}}(f) = k S^*(f) \exp[2\pi j f t] \quad (\text{II-70})$$

Taking the inverse Fourier transform, the impulse response is

$$h_{\text{opt}}(t) = k s^*(t - t_o) \quad (\text{II-71})$$

If the noise spectrum is composed of white and colored noise then

$$S_N(f) = N_0/2 + \frac{2\alpha\beta}{\alpha^2 + (2\pi f)^2} \quad (\text{II-72})$$

where α and β are the coefficients of the colored noise autocorrelation function $R_N(\tau) = \alpha \exp[-\beta|\tau|]$. The matched filter is thus

$$H_{\text{opt}}(f) = \frac{2k [(2\pi f)^2 + \beta^2] S_N^*(f) \exp[-j2\pi f t_0]}{N_0 [(2\pi f)^2 + u]} \quad (\text{II-73})$$

where $u = \beta^2 + 4\alpha\beta/N_0$ (Ref 22:194).

If the causality delay, t_0 , is set to zero, the convolution between $s(t)$ and its matched filter is simply the $s(t)$ autocorrelation function

$$s(t)*h(t) = k \int s(\tau) s^*(\tau-t) d\tau = R_s(-t) \quad (\text{II-74})$$

and the crosscorrelation between $s(t)$ and its matched filter is simply $s(t)$ convolved with itself

$$R(\tau) = s(t)*h^*(-t) = k \int s(\tau) s(t-\tau) d\tau \quad (\text{II-75})$$

We thus see that the matched filter response provides the correlation measure necessary to obtain an indication of the desired target information.

The majority of the filters in the radar receiver/signal

processor are essentially matched filters of one form or another. The matched filter is used so frequently that the processor is often labeled a matched filter receiver. The matched filter is principally used in the pulse compression filter, the bank of doppler filters and the target detection and estimation circuits. From equation II-69 we see that the optimal filter can be designed so as to maximize the signal to noise ratio given a specific PSD for the interference, i.e. clutter or noise. This shows the importance of knowing the clutter statistics. Often the clutter spectrum is difficult to obtain. A reasonable approximation to the clutter PSD is

$$S_N(f) = p |S(f)|^2 \quad (\text{II-76})$$

where $S(f)$ is the Fourier transform of the signal and p is a proportionality factor that relates the number of overlapping echoes (Ref 22:171). Thus a matched filter using the approximation is

$$H_{\text{opt}} = (k / S(f)) \exp[-j2\pi f t_o] \quad (\text{II-77})$$

If the noise spectrum is composed of both noise and clutter,

$$S_N(f) = N_o / 2 + p |S(f)|^2 \quad (\text{II-78})$$

then the matched filter approximation becomes

$$H_{opt}(f) = \frac{k S^*(f) \exp[-j2\pi f t_0]}{N_0/2 + p|S(f)|^2} \quad (II-79)$$

By applying the shifting theorem, equation II-16, to any of the matched filter transfer functions we can see how the matched filter can be used to construct the filter banks that maximize S/I ratio and allow for doppler detection. The matched filter usage in the detection concepts will be shown in the next section.

Detection Processor Development

In the previous section the idea of inverse probability was utilized in looking at the radar signal processor's function. The role of the processor is essentially reduced to computing the "a posteriori probabilities" via a matched filter. It was then shown that this filter maximized the signal to interference ratio. Since radar performance measures are directly proportional to the signal-to-interference ratio, maximization of this ratio is beneficial. The ability of a radar to detect and estimate target parameters is a widely used performance measure. Before proceeding with the detection processor development, the interrelationship between signal analysis and the use of matched filters to maximize signal to interference ratio needs to be clarified.

The term receiver/processor is used to indicate mathema-

tical operation(s) performed on a signal corrupted by interference to obtain, or format to obtain, specific information (Ref 66:155). The "processor" referred to in the last section, dealt with the mathematical operations that are used to cancel clutter from the echo waveform and then prepare the echo, still corrupted by noise, to be analyzed in either the time or frequency domain. It will be seen in the next chapter that this type of processing merely segments the reflected radar signal into range and doppler bins, discards those bins that contain clutter and then passes the signal to be processed so as to extract target information. Extraction of target information can be divided into detection and estimation. Detection is the determination of a target's presence, while estimation is the process of obtaining target range and velocity. Once a target is detected, the echo signal can then be processed more efficiently to estimate range and velocity. Since this study is limited to only doppler cancellation techniques, it will be assumed that range and velocity estimation is obtained as a result of target declaration in a specific doppler-range bin. For this reason target estimation techniques will not be discussed and the reader is referred to Ref 66: Chapter 10 for more information on estimation theory. The remainder of this section will deal with the detection process.

Since it is assumed that detection processing occurs after clutter has been cancelled, only the detection processor in the presence of white noise need be discussed. The optimal

detection processor is that processor that best satisfies given probability of detection and probability of false alarm criteria under a given set of detection assumptions (Ref 66:155). For the radar detection problem, the detector, utilizing the concept of inverse probability previously developed, computes the likelihood ratio for the observed voltage

$$l(\underline{v}) = \frac{p(\underline{v}/H_1)}{p(\underline{v}/H_0)} \quad (\text{II-80})$$

where $p(\underline{v}/H_1)$ is the "a posteriori probability" that the voltage output from the previous processing was caused by the reflection from a target and $p(\underline{v}/H_0)$ is the "a posteriori probability" that the output voltage was caused by noise alone. The likelihood ratio is then compared with a given threshold, K,

$$l(\underline{v}) = \frac{p(\underline{v}/H_1)}{p(\underline{v}/H_0)} \begin{matrix} H_1 \\ > K \\ H_0 \end{matrix} \quad (\text{II-81})$$

to determine if a target is present. The threshold value for the radar problem is determined by applying the Neyman Pearson criteria. This criteria maximizes the probability of detection for a given false alarm probability. From equation II-81 we see that if the likelihood ratio exceeds the threshold value K then hypothesis H_1 is assumed true and a target's

presence is declared, likewise if the ratio value is less than the threshold then hypothesis H_0 is assumed true implying that the voltage was the result of noise. Knowledge of the likelihood ratio thus permits specification of the test statistic which describes the structure of the optimal detection processor. The performance of the processor can also be evaluated by analyzing the statistical properties of the test statistic (Ref 22:291).

The likelihood expression for a single pulse, with known signal amplitude and phase, in the presence of white Gaussian noise will be derived. The likelihood expressions for the cases where the phase and amplitude are unknown and also the pulse train cases easily follow from the simple case that will be presented. These various signal cases are extensively covered in Ref 22:Chapters 9,10, and 11.

To derive the likelihood ratio it is convenient to employ the sampling theorem waveform representation instead of the more general Karhunen-Loeve expansion (Ref 22:291). Given a low pass bandlimited $(-f_c, f_c)$ signal, $v(t)$, through application of the sampling theorem, sampling every $1/2f_c$ seconds, $v(t)$ can be completely specified by the samples using the expression

$$v(t) = \sum_{k=-\infty}^{\infty} v(k/2f_c) \text{sinc}[2\pi f_c (t - k/2f_c)] \quad (\text{II-82})$$

(Ref 22:53). From the sampling theorem it can be shown that

$$\int_0^T [v(t)]^2 dt = 1/2f_c \sum_{k=1}^{2f_c T} [v(k/2f_c)]^2 \quad (\text{II-83})$$

where T is the signal duration (Ref 22:56).

Assuming the signal is known and bandlimited, $(-f_c, f_c)$, with bandlimited noise, the detector processor input waveform, $v(t)$, is written in vector form as

$$\underline{v} = \underline{s} + \underline{n} \quad (\text{II-84})$$

where $v_k = v(k/2f_c)$, $s_k = s(k/2f_c)$, and $n_k = n(k/2f_c)$ for $k=1, 2, \dots, 2f_c T$. The conditional joint density function that describes the hypothesis H_1 (signal plus noise) is represented by

$$p(\underline{v}/H_1) = \frac{1}{(2\pi)^{N/2} (N f_c)} \exp[-1/2f_c N \sum_{k=1}^N (v_k - s_k)^2] \quad (\text{II-85})$$

where $N=2f_c T$ and the white noise PSD is $N/2$. Similarly the conditional joint density that describes the hypothesis H_0 (noise alone) is represented by

$$p(\underline{v}/H_0) = \frac{1}{(2\pi)^{N/2} (N f_c)} \exp[-1/2f_c N \sum_{k=1}^N (v_k)^2] \quad (\text{II-86})$$

From equation II-81 we see that the likelihood-ratio expression is

$$\begin{aligned}\Lambda(\underline{v}) &= \frac{p(\underline{v}/H_1)}{p(\underline{v}/H_0)} = \frac{\exp[-1/2f_{co} N \sum_{k=1}^N (v_k - s_k)^2]}{\exp[-1/2f_{co} N \sum_{k=1}^N (v_k)^2]} \\ &= \exp[-1/2f_{co} N (\sum_{k=1}^N (s_k)^2 - 2 \sum_{k=1}^N v_k s_k)] \quad (\text{II-87})\end{aligned}$$

Using equation II-83, equation II-87 may be rewritten as

$$\Lambda(\underline{v}) = \exp[-1/N \int_0^T s^2(t) dt + 2/N \int_0^T v(t)s(t) dt] \geq K \quad (\text{II-88})$$

Taking the natural logarithm of equation II-88 will not alter the inequality of equation because the function $\ln x$ is a monotonically increasing function of x , thus equation II-88 is

$$2/N \int_0^T v(t)s(t) dt \underset{H_0}{\overset{H_1}{>}} K + E/N \quad (\text{II-89})$$

The test statistic, the cross correlation between $v(t)$ and $s(t)$, is realized via a matched filter as suggested in the last section. If the output of the matched filter exceeds the threshold $K + E/N$ then a target is detected and tagged for

further processing.

The detection process just developed was for the case of white Gaussian noise. If the noise is assumed to be nonwhite, e.g. clutter, the inverse probability concept can again be applied to form the structure of the optimal detection processor. The processor based upon the likelihood-ratio to effectively cancel clutter, is an example of nondoppler processing. In an attempt to limit the size of the study, nondoppler processing will not be examined, however a deployed system must use a combination of nondoppler and doppler processing to cancel clutter.

It must be remembered that the detection processor developed is applied to each range-doppler bin to determine a target's presence. As mentioned before the filters to perform all the processing are generally matched filters, matched to each test cell. Because of the large number of bins a convenient way of implementing the filters other than with lumped constants must be obtained. With the advance of microelectronics, special purpose digital computers are used to implement the filters to perform the time and/or frequency domain analysis. The next section examines digital domain signal representation and analysis.

Digital Signal Processing

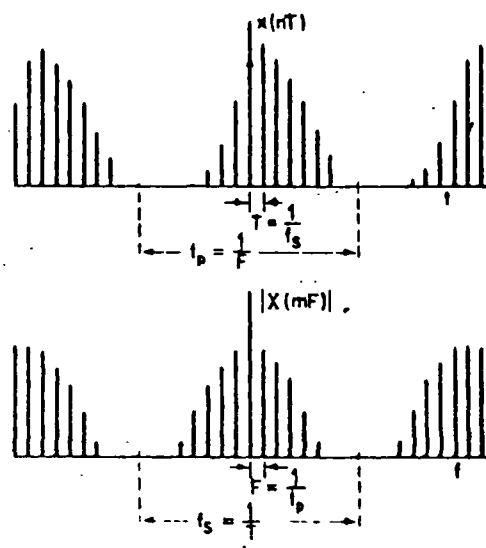
Following the pattern previously established when describing continuous signals and systems, this section first

covers the representation of digital signals and then describes digital signal analysis techniques. Because we are dealing with the radar problem, we assume that the digital signals and filters described, represent sampled versions of continuous analog signals and systems.

In the strict sense, a digital signal is a signal which has discrete values in time and in amplitude. However, in the ensuing discussion, digital signals will denote discrete time values of a continuous amplitude valued signal. Since amplitude quantization levels are the result of system choices, this limitation will not restrict the digital processing discussions. This limitation also eliminates the need for discussion of quantization noise, which can be found in Ref 29:Chapter 4 and Ref 43:Chapter 9.

A continuous analog signal is described digitally by applying the baseband sampling theorem. This theorem states that given a lowpass, bandlimited $(-f_c, f_c)$ signal $v(t)$, the signal can be uniquely characterized over all time by the samples of $v(t)$, if the samples are taken at intervals of $1/2f_c$ (Ref 22:53). The frequency $2f_c$, is the Nyquist frequency and sampling at less than the Nyquist rate results in aliasing. The sampling can be accomplished by 1) natural sampling : $v(nT) = v_a(t) * \text{sinc}[2\pi f_c t]$, 2) flat top sampling : $v(nT) = v_a(t) * \text{rect}[t/T]$, or 3) impulse sampling : $v(nT) = v_a(t) * \delta(t)$; where $v(nT)$ is the sampled version of the analog signal $v_a(t)$. There are N samples taken every T seconds. While the digital processing discussions will assume the

impulse sampling method, in practical situations natural or flat top sampling would be used. (Note: In the limit as $T \rightarrow 0$ both flat top and natural sampling reduce to impulse sampling.) Figure II-3 illustrates the impulse sampling of a periodic continuous signal and the corresponding frequency domain representation.



(Ref 59:243)

Fig. II-3 Impulse Sampling and its Fourier Transform

The relationship between the sampling period, T , and the sampling frequency, f_s ,

$$T = \frac{1}{f_s} \quad (\text{II-90})$$

and the relationship between the observation time, t_p , (generally t_p corresponds to the signal period for a periodic signal) and the frequency domain frequency interval, F ,

$$T = 1/F \quad (II-91)$$

both illustrated in Figure II-3, will be used when describing the discrete Fourier transform (DFT).

From Figure II-3 it is also seen that the sampled signal can be represented by

$$v(t) = \sum_{n=-\infty}^{\infty} v(nT) \delta(t - nT) \quad (II-92)$$

The Fourier transform of equation II-92 is

$$\begin{aligned} V(f) &= \sum_{n=-\infty}^{\infty} v(nT) \int \delta(t-nT) e^{-j2\pi ft} dt \\ &= \sum_{n=-\infty}^{\infty} v(nT) e^{-j2\pi fnT} \end{aligned} \quad (II-93)$$

Defining the complex variable $z = e^{j2\pi fT}$, the z-transform of the function $v(t)$ is defined as

$$V(z) = \sum_{n=-\infty}^{\infty} v(nT) z^{-n} \quad (II-94)$$

The z-transform is the frequency domain representation for discrete-time domain signals and systems, analogous to the Fourier transform for continuous time domain signals and systems. Difference equations, such as equation II-92, are changed into algebraic equations in the complex z domain through the use of the z-transform (Ref 28:511). The z-transform is defined for all real and complex functions for

which the series defined by equation II-94 converges, therefore the unique z-transform of a signal function, is obtained by applying equation II-94 and specifying the region of convergence. As with the Fourier transform, the z-transform has many useful properties that aid in analysis and design. (See Appendix C page C-7 for a list or Ref 29:Chapter 2 or Ref 43:Chapter 2.) Although the discussion thus far has dealt with digital representation of signals, the development also applies to systems.

The signals discussed in this section were assumed to be deterministic, however the theory also applies to random signals. As mentioned previously the statistical properties developed earlier for continuous signals applies equally well to discrete time signals by changing the integrals to summations. Although the probability theory for discrete time signals does not need to be redeveloped, the effect of sampling a stochastic signal must be examined.

Given a WSS random signal, $n(t)$, with zero mean and autocorrelation $R_n(\tau)$, the statistics of the sampled version, $n(mT)$, need to be determined. Assuming independence from sample time interval to sampling interval, $E[n(mT)] = 0$. To compute the autocorrelation of the sampled process, we assume flat top sampling. The autocorrelation of the sampled $n(t)$ is

$$R_{n(mT)}(\tau) = E\left[\left[\frac{1}{T} \int_{iT}^{(i+1)T} n(t_1) dt_1\right] \left[\frac{1}{T} \int_{iT}^{(i+1)T} n(t_2) dt_2\right]\right]$$

$$= 1/T \int_{iT}^{(i+1)T} \int_{t_1}^{t_2} R(t_1, t_2) dt_1 dt_2 \quad (\text{II-95})$$

For the WSS process, equation II-95 can be converted from a double integral to a single integral, thus

$$\begin{aligned} R_{n(mT)}(\tau) &= 1/T \int_{iT}^{(i+1)T} R_n(\tau) d\tau \\ &= R_n(\tau) / T \end{aligned} \quad (\text{II-96})$$

In the limit, as $T \rightarrow 0$, we have impulse sampling and thus

$$R_{n(mT)}(\tau) = R_n(\tau) \quad (\text{II-97})$$

For impulse sampling, the statistics of the sampled signal are the same as the continuous signal.

The z-transform just developed was for infinite length sequences. For the case in which the sequence to be represented is of finite duration, the discrete Fourier transform (DFT) is used. The DFT is a sequence rather than a continuous function, and corresponds to samples, equally spaced in frequency, of the Fourier transform. The development and interpretation of the DFT representation of a finite duration sequence is based upon the relationship between the finite-length and periodic sequences (Ref 43:87).

The complex Fourier series representation of periodic

signal $x(t)$, is

$$x(t) = 1/t \sum_{p, n=-\infty}^{\infty} X(k) e^{j2\pi k t} \quad (\text{II-98})$$

where

$$X(k) = \int_{-t/2}^{t/2} x(t) e^{-j2\pi k t} dt \quad (\text{II-99})$$

and t is the observation period as defined in Figure II-3. If $x(t)$ is sampled every T seconds, such that the Nyquist criterion is satisfied, equation II-99 becomes

$$X(k) = \sum_{p, -N/2}^{N/2} x(nT) \exp[-j2\pi k n T / t] \quad (\text{II-100})$$

where N is the total number of points in the sequence equalling t/T . Substituting $1/N = T/t$ into equation II-99, and also noting that $X(k)$ and $x(n)$ are symmetric for positive and negative values of N , the DFT of $x(nT)$ is defined

$$\begin{aligned} X(k) &= \sum_{n=0}^{N-1} x(nT) e^{-j2\pi k n / N} \\ &= \sum_{n=0}^{N-1} x(nT) W^{kn} \end{aligned} \quad (\text{II-101})$$

where $W = e^{-j2\pi/N}$. The inverse DFT is thus

$$x(nT) = 1/N \sum_{k=0}^{N-1} X(k) W^{-kn} \quad (\text{II-102})$$

The variable k in equations II-101 and II-102 represents the digital frequency index. It is related to the analog frequency variable f , by

$$f = k / NT \quad (\text{II-103})$$

The periodic sequence $X(k)$ can be interpreted as samples, equally spaced in angle, on the unit circle of the z -transform, for one period of the periodic sequence $x(n)$. Thus the relationship between the z -transform and the DFT is

$$X(k) = X(z) \Big|_{z = \exp[j2\pi k/N] = W^{-k}} \quad (\text{II-104})$$

(Ref 43:89-90). Because the DFT is a modified z -transform, the DFT properties are essentially the same as those for the z -transform.

Because the radar signals and systems can be represented by finite sequences, the DFT finds extensive usage for radar signal design and analysis. Although these radar sequences are generally aperiodic, by zero padding the sequences can be made to appear (for computational purposes) periodic with very long periods.

Since the digital signals described represent continuous analog signals, it is quite natural that the digital analysis of these signals be based upon the correlation principles previously established for analog signals. The correlation principle is implemented by a digital filter. The digital filter, assumed to be linear, causal, and time invariant, is usually an approximation of a desired analog filter.

Digital filtering, like analog filtering, can be developed in either the time domain or frequency domain. In the discrete time domain, digital filtering is accomplished by direct convolution

$$\begin{aligned}
 y(nT) &= x(nT) * h(nT) \\
 &= \sum_{k=-\infty}^{\infty} x(kT) h(nT - kT) \\
 &= \sum_{k=-\infty}^{\infty} x(nT - kT) h(kT)
 \end{aligned}
 \tag{II-105}$$

In the frequency domain, filtering is accomplished either by linear recursive or nonrecursive equations or by FFT (fast Fourier transform) operations. Because recursive equations cannot be implemented via FFT operations and also due to the transient period needed for the recursive filter to stabilize, this class of filters will not be discussed for use in clutter cancellation schemes. This is not to say that recursive filters do not find use in radar processing, for recursive

filters digitally implement the common Butterworth, Chebyshev and elliptical analog filters, however they will not be used in this study.

Nonrecursive, or finite impulse response (FIR), filters are of the form

$$H(Z) = \sum_{n=0}^{N-1} h(nT) z^{-n} \quad (\text{II-106})$$

indicating that nonrecursive filters are formed using input sequence values. The convolution of a signal $x(t)$ and filter response $h(t)$ can be accomplished in the frequency domain by multiplication of the z -transform of the FIR filter described in equation II-106 with the signal z -transform. Thus

$$Y(Z) = X(Z) H(Z) \quad (\text{II-107})$$

If the signal and filter sequences are represented by DFT's, the convolution is also accomplished by multiplication of the two DFT's. Due to the periodic nature of the DFT calculation, if the sequences are aperiodic, the two sequences need to be zero padded so as to appear periodic as described before. Both sequences should be of period L , where L is the smallest power of two greater than $M + N$, with M and N being the number of discrete points of the two sequences (Ref 61:379).

The most straightforward approach to obtain a nonrecursive filter is to truncate an infinite duration

impulse response sequence. Given the desired filter response $H(j\omega)$ then

$$H(j\omega) = \sum_{n=-\infty}^{\infty} h(nT) e^{-j\omega nT} \quad (\text{II-108})$$

where

$$h(nT) = \frac{1}{2\pi} \int_{-\pi/t}^{\pi/t} H(j\omega) e^{j\omega nT} d\omega \quad (\text{II-109})$$

Using the inverse DFT, equation II-102, a zero-order approximation to $h(nT)$ is obtained

$$h(nT) = \frac{1}{2k} \sum_{k=-M}^M H(k) e^{j\pi k n / M} \quad -N \leq n \leq N \quad (\text{II-110})$$

where M is generally larger than N .

Truncation of the ideal impulse response causes the FIR filter to experience sidelobes. These filter sidelobes appear to a digital clutter canceler system as clutter, thus degrading performance. By tapering the truncation window, the filter sidelobes can be reduced from -21 db to -74 db depending on the tapering scheme (Ref 43:250). Table II-1 illustrates various common tapering methods and their associated characteristics.

Table II-1
Tapering Methods

Type	Lag window ($W(r)$)	Spectral window ($w(f)$)	Equivalent bandwidth (B_s)
Rectangular	$= 1$ for $ r < T_m$ $= 0$ for $ r > T_m$	$= 2T_m \left[\frac{\sin 2\pi f T_m}{2\pi f T_m} \right] = W_0$	0.5
Bartlett	$= 1 - \frac{ r }{T_m}$ for $ r < T_m$ $= 0$ for $ r > T_m$	$= T_m \left[\frac{\sin \pi f T_m}{\pi f T_m} \right]^2$	1.5
Parzen	$= 1 - 6 \left(\frac{ r }{T_m} \right)^3 + 6 \left(\frac{ r }{T_m} \right)^5$ for $ r < \frac{T_m}{2}$ $= 2 \left(1 - \frac{ r }{T_m} \right)^3$ for $\frac{T_m}{2} < r < T_m$ $= 0$ for $ r > T_m$	$= 0.75 T_m \left[\frac{\sin \pi f \frac{1}{2} T_m}{\pi f \frac{1}{2} T_m} \right]^4$	1.9
Hanning	$= 0.5 + 0.5 \cos \left(\frac{\pi r}{T_m} \right)$ for $ r < T_m$ $= 0$ for $ r > T_m$	$= 0.5 W_0(f)$ $+ 0.25 W_0 \left[f + \frac{1}{2T_m} \right] + 0.25 W_0 \left[f - \frac{1}{2T_m} \right]$	1.3
Hamming	$= 0.54 + 0.46 \cos \left(\frac{\pi r}{T_m} \right)$ for $ r < T_m$ $= 0$ for $ r > T_m$	$= 0.54 W_0(f)$ $+ 0.23 W_0 \left[f + \frac{1}{2T_m} \right] + 0.23 W_0 \left[f - \frac{1}{2T_m} \right]$	1.3
Blackman	$= 0.42 + 0.5 \cos \left(\frac{\pi r}{T_m} \right) + 0.08 \cos \left(\frac{2\pi r}{T_m} \right)$ for $ r < T_m$ $= 0$ for $ r > T_m$	$= 0.42 W_0(f) + 0.25 W_0 \left[f + \frac{1}{2T_m} \right]$ $+ 0.25 W_0 \left[f - \frac{1}{2T_m} \right] + 0.04 W_0 \left[f + \frac{1}{T_m} \right]$ $+ 0.04 W_0 \left[f - \frac{1}{T_m} \right]$	1.4

where: $T_m = h_m$ = total time lag for window, h = sampling interval, and m = number of samples in lag window.

The modified filter thus becomes

$$h_m(nT) = h(nT) w(nT) \quad 0 \leq n \leq N-1 \quad (\text{II-111})$$

At the beginning of the digital filtering section it was stated that nonrecursive filters can be implemented via a FFT operation. The fast Fourier transform is simply a method, or algorithm, used to efficiently compute the discrete Fourier

transform (DFT) of a discrete time series of data samples (Ref 17:313). Equation II-110 illustrates the fact that nonrecursive filters can be implemented using the DFT of the desired frequency response, thus the nonrecursive filter can indeed be implemented via a FFT.

The unique feature of FFT algorithms is that they eliminate the redundancy in DFT calculations by reducing the DFT to shorter and smaller DFT sequences. Because of the binary operations of computers, FFT algorithms are most efficient if N is a power of two. Reduction in calculations are achieved by decimating the DFT in either time or frequency. The elegance of the DFT reduction techniques and the variety of methods available to accomplish the FFT calculations can be found in Ref 15, Ref 29 Chapter 6 and Ref 43 Chapter 6. Equations II-112 and II-113 summarize the FFT calculations after the DFT has been time and frequency decimated. Given the sequence $f(nT)$, the time decimation FFT is

$$F(k) = \sum_{n=0}^{N-1} g(nT)(W)^{2nk} + W^k \sum_{n=0}^{N-1} h(nT)(W)^{2nk} \quad (\text{II-112})$$

where $g(nT) = f(2nT)$ and $h(nT) = f((2n+1)T)$. The frequency decimation FFT of sequence $f(nT)$ is

$$F(2k) = \sum_{n=0}^{N/2-1} [g(nT) + h(nT)](W)^{2nk} \quad (\text{II-113})$$

$$F(2k+1) = \sum_{n=0}^{N/2-1} [[g(nT) - h(nT)]W^n](W)^{2nk}$$

By repeated application of the FFT algorithms described by equations II-112 and II-113, the filtering operations discussed for continuous signals can be accomplished. The convolution between a signal and a filter can be performed by fast Fourier transforming both the signal and filter, multiplying the two FFT's and then inverse Fourier transforming the result. The inverse FFT is accomplished by appropriate modification of the arguments of either II-112 or II-113. The FFT operation thus provides a means of accomplishing the signal analysis techniques described for continuous radar signals.

Ambiguity Function Development

Although the detectability of a target in the presence of interference, whether noise or clutter, is dependent on the signal strength, the ambiguity removal and resolution accuracy between multiple targets is a function of signal parameters, most notably the waveform duration and bandwidth. A high clutter environment, such as the one present in the spaceborne problem, can be thought of as a collection of multiple point scatterers. The detection of a target in the presence of clutter is thus heavily influenced by waveform selection. Because the reflections of point targets vary in range and doppler from the target, a response is induced in the matched filter radar receiver, matched to a specific delay and doppler, that is no longer the autocorrelation function of

the transmitted signal. The response of secondary targets, clutter, at a slightly different range and velocity may appear at the matched filter output when the desired target response is at its peak. As a result of signal overlap, due to multiple targets, a special set of mathematical functions called time-frequency autocorrelation functions, or ambiguity functions evolved (Ref 41:283). The ambiguity function describes the matched filter response to a complex signal envelope as a function of radar target radial velocity and range. This function is determined solely on the transmitted waveform and receiver filter characteristics (Ref 57:3-10). It provides an indication of the ability of a waveform-filter combination to resolve multiple radar reflectors at arbitrarily different range and velocities. The name "ambiguity function" is somewhat misleading in that the function describes more than just waveform ambiguities. Woodward used the word to show that the total volume under this function is a constant, equal to $(2E)^2$, independent of the shape of the waveform (Ref 56:42).

To obtain the time-frequency autocorrelation function, first the range ambiguity function and delay resolution constant will be determined, then the doppler ambiguity function and velocity resolution constant will be determined, and finally the combined range and velocity ambiguity function will be developed.

Using the complex signal notation developed earlier, the time domain transmitted function is

$$s(t) = \text{Re} [u(t) \exp[j2\pi f_o t]] = \text{Re} [s_a(t)] \quad (\text{II-114})$$

Given two stationary point targets which differ only in range, the received signal from target one is $s_a(t - t_o)$ and from target two $s_a(t - t_o - \tau)$ where t_o is the round trip delay time from target one and τ is the difference in time delay from target one and two. To resolve the range difference, or τ , we integrate the square of the difference between the two signals over all time

$$e^2 = \int |s_a(t) - s_a(t - \tau)|^2 dt \quad (\text{II-115})$$

Since we are only interested in the time difference we set $t_o = 0$ with no loss in generality. Expanding e^2 we obtain

$$\begin{aligned} e^2 = & \int |s_a(t)|^2 dt + \int |s_a(t - \tau)|^2 dt \\ & - \int s_a(t) s_a^*(t - \tau) dt - \int s_a^*(t) s_a(t - \tau) dt \end{aligned} \quad (\text{II-116})$$

Because of the periodicity of $s_a(t)$ we observe that

$$\int |s_a(t)|^2 dt = \int |s_a(t - \tau)|^2 dt = \int |u(t)|^2 dt \quad (\text{II-117})$$

Multiplying $s_a(t) s_a^*(t - \tau)$ and $s_a^*(t) s_a(t - \tau)$ out and summing the products we obtain

$$\begin{aligned}
& s_a(t) s_a^*(t-\tau) + s_a^*(t) s_a(t-\tau) = \\
& 2 \operatorname{Re} [s_a(t) s_a^*(t-\tau)] \quad (\text{II-118})
\end{aligned}$$

Combining equation II-117 and II-118 into equation II-116 we get

$$\begin{aligned}
e^2 &= 2 \int |u(t)|^2 dt - \\
& 2 \operatorname{Re} [\exp[-j2\pi f_0 t] \int u(t) u^*(t-\tau) dt] \quad (\text{II-119})
\end{aligned}$$

The measure e^2 shows the separation between $s_a(t)$ and $s_a(t-\tau)$ therefore if $\tau \neq 0$, e^2 should be made as large as possible. The first term in equation II-119 is constant and equals $4E_s$. The second term fluctuates because $\exp[-j2\pi f_0 t]$, which implies a high degree of range ambiguity. To maximize e^2 the magnitude of the second term needs to be minimized. The magnitude of the second term is defined as the range ambiguity function

$$|c(\tau)| = \int u(t) u^*(t-\tau) dt \quad (\text{II-120})$$

We see that $|c(\tau)|$ is the envelope of the output of a filter matched to the signal $s(t)$. The matched filter output forms the crosscorrelation between the received signal corrupted by interference and a replica of the transmitted signal. The replica of the transmitted signal is built into the filter

through the frequency response of the filter (equation II-71). If the input signal is the same as that for which the filter was designed (the filters can be designed for specific time delays and doppler) the output is the autocorrelation function (Ref 47:XVII-5).

A delay constant, T_r , is defined as the total area under the curve $|c(\tau)|^2$ normalized to one at $\tau=0$. The constant is

$$\begin{aligned} T_r &= \int |c(\tau)|^2 d\tau / c^2(0) \\ &= \frac{\int |U(f)|^4 df}{\left| \int |U(f)|^2 df \right|^2} \end{aligned} \quad (\text{II-121})$$

where $U(f)$ is the Fourier transform of $u(t)$. The inverse of the delay constant is defined as the effective bandwidth.

$$B_e = \frac{\left| \int |U(f)|^2 df \right|^2}{\int |U(f)|^4 df} \quad (\text{II-122})$$

A range resolution constant is also defined as

$$\Delta R = cT_r / 2 \quad (\text{II-123})$$

Thus to improve range resolution (i.e. reduce ΔR) the effective bandwidth must be increased.

Similar to the development of the range ambiguity function, the mean square difference is used to measure the velocity difference between two targets. Working in the frequency domain

$$e_f^2 = 2 \int [|s_a(f)|^2 - s_a^*(f) s_a(f-f)] df \quad (\text{II-124})$$

Again to minimize e_f^2 the second term in equation II-124 must be minimized. The doppler ambiguity function is thus defined

$$k(f_d) = \int |u(t)|^2 \exp[j2\pi f_d t] dt \quad (\text{II-125})$$

with $f_d = 0$. The doppler resolution constant is thus

$$\begin{aligned} F_r &= \int |k(f_d)|^2 df_d / k^2(0) \\ &= \frac{\int |u(t)|^4 dt}{\left| \int |u(t)|^2 dt \right|^2} \end{aligned} \quad (\text{II-126})$$

with the effective time duration defined as $T_e = 1/F_r$. Thus two targets at the same range can be resolved in velocity if

$$2 \Delta v_r / v_r < F_r \quad (\text{II-127})$$

To obtain the combined range and velocity resolution

function the same transmitted waveform as in the two previous cases is used. We assume the form

$$s_a(t) = u(t) \exp[j2\pi f_o t] \quad (\text{II-128})$$

The time delayed and doppler shifted signal is

$$s_a(t-\tau) = u(t-\tau) \exp[j2\pi(f_o - f_d)(t-\tau)] \quad (\text{II-129})$$

Using the mean square difference as before

$$e^2 = \int |s_a(t) - s_a(t-\tau)|^2 dt \quad (\text{II-130})$$

Expansion of the integrand yields

$$e^2 = 2 \int |u(t)|^2 dt - 2 \operatorname{Re}[\exp[j2\pi(f_o - f_d)\tau] \int u(t)u^*(t-\tau) \exp[j2\pi f_d t] dt] \quad (\text{II-131})$$

The combined range and velocity ambiguity function is then

$$|X(\tau, f_d)| = \int u(t)u^*(t-\tau) \exp[j2\pi f_d t] dt \quad (\text{II-132})$$

Thus we see that the ambiguity function describes the complex signal envelope at the matched filter receiver output as a function of target range and radial velocity.

A combined resolution constant can be obtained as in the

doppler and range developments

$$K = \frac{\iint |X(\tau, f_d)|^2 d\tau df_d}{|X(0,0)|^2} \quad (\text{II-133})$$

Assuming $|X(0,0)|^2$ is normalized to one, the delay and doppler resolution constants can be written respectively as

$$T_r = 1/B_e = \int |X(\tau, 0)|^2 d\tau \quad (\text{II-134})$$

$$F_r = 1/T_e = \int |X(0, f_d)|^2 df_d \quad (\text{II-135})$$

The plot of the square magnitude of the ambiguity function is called the ambiguity diagram. This ambiguity surface, in the τ and f_d plane, is used as a design tool to indicate the resolution and ambiguity of a waveform-filter combination. Ideally the ambiguity diagram should consist of a single spike of infinitesimal thickness at the origin and zero everywhere else. The single peak eliminates ambiguities, and its infinitesimal thickness at the origin permits simultaneous determination of frequency and echo time delay with a high degree of accuracy. The narrow spike permits the resolution of any two targets no matter how close they are together. In reality the ideal ambiguity diagram does not exist and depending on the specific application a suboptimal waveform can be chosen. The width of the ambiguity diagram

central peak indicates the resolution ability of multiple targets in delay and doppler. The sidelobes, or secondary peaks provide an indication of the amount of self-induced clutter and thus the masking of targets by mutual interference (Ref 49:25). For a given waveform-filter pair, the clutter power out of the filter, designed for a specific delay and doppler, is

$$C = \iint p(\tau, f_d) |x(\tau, f_d)|^2 d\tau df_d \quad (\text{II-136})$$

where $p(\tau, f_d)$ is the distribution of clutter scattering points in delay and doppler. Equation II-136 illustrates the fact that the clutter distribution as well as the waveform influences the amount of clutter power return. Waveforms having $|x(\tau, f_d)|^2 \rightarrow 0$ in the τ, f_d region where clutter exists, can be designed to reduce the amount of induced clutter. Ambiguity functions used in various applications are listed in Ref 57:3-15 - 3-30.

Having gained an understanding of how to represent and analyze signals in both time and frequency domain, and also having gained insight into methods of implementing the signal analysis techniques, clutter and clutter cancellation techniques can now easily be developed and described.

III Clutter Models and Cancellation Techniques

Introduction

The fundamental problem of radar design is the extraction of target range and velocity information from the return radar signal that is corrupted by clutter and noise energy. Target information is contained in the radar echo signal's amplitude, frequency and phase. To extract the target information buried in the echo signal the signal must be processed, which is essentially accomplished via comparison techniques, i.e. comparing the echo signal with the transmitted signal and/or comparing the echo signals with other echo signals which are varied in time or space. Depending on the type of information desired (mere indication of a target's presence, target range, relative elevation or azimuth angles, target velocity or target's physical characteristics) the echo signal is processed differently.

Effective extraction of range and velocity information from the echo signal is accomplished by first cancelling clutter. To effectively develop clutter cancellation techniques, it is necessary to first gain an understanding of the nature of clutter. Using the fundamentals that were established in Chapter II we will in this chapter first describe clutter, then briefly explain a typical MTI radar, and conclude with a description of various clutter cancellation techniques available to be employed on spaceborne radar systems.

Elements of Clutter

Radar clutter is the unwanted return or group of returns of reflected radar energy which results from distributed scattering elements such as buildings, chaff, birds, insects, precipitation, land and/or sea. The distributed scattering centers produce individual re-radiated electrical fields which are of vector-phasor nature having amplitude A_i and phase ϕ_i . The individual vectors (having both horizontal and vertical polarization) of all the illuminated scatterers may be summed to produce the unwanted electrical clutter field that is received by the radar. There are several models which attempt to explain the scattering of the transmitted electromagnetic waves produced by non-uniform surfaces, (Refs 19, 33, 35-37, 40, 55, 68) however they are not sufficiently well developed to be associated with every type of terrain of interest (Refs 19:9, 57:25-4). Attempts have also been made to characterize terrains probabalistically and then determine the return echo field. These models have met with some success (Ref 36:124, 57:25-4). While the exact interaction of the electromagnetic wave with various terrains is not known, experimental results show that ground, sea and weather clutter are dependent on: 1) radar parameters such as wavelength, power, polarization, pulse width, antenna scan rate, frequency agility, and resolution cell; 2) geometry parameters such as grazing angle, direction of illumination and range; 3) environmental conditions such as wind velocity, moisture content and season of the year and; 4) type of clutter, described by surface rough-

ness, number and orientation of scatterers in resolution cell, roughness of surface depth, surface conductivity and permittivity (Refs 47:XV-9, 55:63, 57:25-4). The fundamental relationship between all of the above listed parameters and the clutter returns are graphed in Skolnik's Radar Handbook (Ref 56) and Long's book Radar Reflectivity of Land and Sea (Ref 35). Since there are a large number of parameters which affect clutter returns, and the interactive mechanisms between the transmitted radar signal and the scatterers has not been firmly established, some manageable way of describing clutter must be obtained.

The clutter signal is of the form

$$c(t) = \sum_{i=1}^N A(t) s(t-\tau) e^{j\phi(t)} \quad (\text{III-1})$$

where $A(t)$ is the amplitude, τ is the time delay, $\phi(t)$ is the phase and N is the number of scattering centers. While these quantities may at times be considered deterministic, they are generally described as random variables. Clutter can therefore, under some conditions, be thought of as quasirandom noise. Experimental data, however, indicates that fluctuations in clutter returns, due to environmental or geometrical conditions, cause clutter to be more frequently considered as a nonstationary process. Clutter returns exhibit time dependence within resolution cells and spatial dependence from resolution cell to resolution cell (Ref 47:XV-8). Thus clutter can be described by not only average returns, but also by

statistical descriptions of temporal and spatial variations.

For a given set of radar, geometry and environmental conditions, clutter is usually described by any one or all three of the following methods: 1) an average radar cross section per unit area, 2) an amplitude probability distribution and 3) a power spectral density.

Since clutter comes from extended areas containing many scattering elements, clutter can be described statistically in terms of the average radar backscatter cross section per unit area, denoted σ^0 , or clutter reflectivity factor. Clutter reflectivity is a measure of the reflective ability of an area of the earth. Theoretically, clutter reflectivity is given by

$$\sigma^0 = \lim_{R \rightarrow \infty} \frac{1}{A_c} \left[\frac{1}{4\pi R^2} \frac{E_r^2}{E_i^2} \right] \quad (\text{III-2})$$

where E_r and E_i are the reflected and incident field strength respectively and A_c is the area illuminated by the radar beam. (Appendix B derives the area calculations.) Because of the spacial and temporal variations of the reflecting earth, the backscatter coefficient is generally calculated experimentally by applying the radar equation and solving for σ^0 given the observed power returns. The clutter reflectivity is then calculated by solving equation (III-3)

$$\sigma_c^0 = \sigma^0 (A_c) \quad (\text{III-3})$$

The clutter reflectivity factor is used in signal to clutter

calculations similar to those done in noise calculations. The signal to clutter ratio is

$$S/C = \sigma_t' / \sigma_c^0 A \quad (\text{III-4})$$

In many cases the clutter power is far greater than the signal power (i.e. when average backscatter reflectivity is large or the area of illumination is large) thus masking the presence of targets. Clutter cancellation techniques discussed later will show how the target signal can be extracted from the clutter when the S/C ratio is less than one.

Amplitude probability distributions are used to describe clutter so as to be able to predict the false alarm probabilities due to clutter (Ref 47:XV-11). Knowledge of the amplitude statistics is important in designing constant false alarm receivers, CFAR. Because the backscatter from clutter shows both temporal and spatial variation, a time varying probability distribution or random process is really needed to describe the clutter return statistics. The probability models which have found widest use in predicting clutter fluctuation statistics assure stationarity and independence of scatterers within a resolution cell (Ref 47:XV-11).

The simplest probability model is the Rayleigh or Gaussian model, which assumes a uniform spatial distribution of independent scatterers with equal amplitude and relatively uniform phase distribution from $0-2\pi$ (Ref 47:XV-14). The Gaussian envelope clutter model is used for land clutter with

vegetation that consists of non-dominant tree trunks or for sea clutter when large individual waves are not numerous at grazing angles greater than five degrees and pulse widths greater than .5 microseconds (Ref 52:38). The predetection clutter process in terms of its voltage envelope $v(t)$ and phase $\theta(t)$ is

$$c_G(t) = v(t) \cos[w_c t - \theta(t)]. \quad (\text{III-5})$$

Expanding the cosine term, $c(t)$ can be represented by its quadrature components as

$$c_G(t) = x(t) \cos[w_c t] - y(t) \sin[w_c t] \quad (\text{III-6})$$

where $x(t)$ and $y(t)$ are zero mean, identical distributed low pass, independent normal processes with variance σ^2 and w_c is the carrier frequency. The voltage envelope of $c(t)$ is

$$v(t) = \sqrt{x^2(t) + y^2(t)} \quad (\text{III-7})$$

and the phase of $c(t)$ is

$$\theta(t) = \tan^{-1} [y(t)/x(t)]. \quad (\text{III-8})$$

The joint probability density function of $x(t)$ and $y(t)$ is

$$q(x,y) = q(x)q(y) = (1/2\pi\sigma^2) \exp[-(x^2 + y^2)/2\sigma^2]. \quad (\text{III-9})$$

To find the density in terms of $v(t)$ and $\theta(t)$ we need to make a coordinate transformation and express the joint probability density function of $x(t)$ and $y(t)$ in the v, θ coordinate system. The joint density function, $q(x,y)$ is thus

$$q(x,y)dxdy = q(v \cos\theta, v \sin\theta) vdv d\theta \quad (\text{III-10})$$

since the element of the area $dxdy$ in the x,y plane corresponds to the element of area $vdv d\theta$. We state that

$$q(x,y)dxdy = p(v,\theta)dv d\theta \quad (\text{III-11})$$

and then see that

$$p(v,\theta)dv d\theta = q(v \cos\theta, v \sin\theta)vdv d\theta. \quad (\text{III-12})$$

Making the appropriate substitutions into equation (III-8) we obtain

$$p(v,\theta) = (v/2\pi\sigma^2) \exp[-(v^2 \cos^2 \theta + v^2 \sin^2 \theta)/2\sigma^2] \quad (\text{III-13})$$

$$\begin{aligned} p(v,\theta) &= (v/2\pi\sigma^2) \exp[-v^2/2\sigma^2] & v \geq 0 \\ &= 0 & v < 0. \end{aligned}$$

Equation III-13 implies that θ is uniformly distributed and

that the marginal density function of the phase is

$$p(\theta) = 1 / 2\pi \quad 0 \leq \theta \leq 2\pi \quad (\text{III-14})$$

The marginal density for the envelope, $v(t)$, can thus be found by integrating over $p(v, \theta)$ with respect to θ . Therefore we have

$$p(v) = \int_0^{2\pi} (v/2\pi\sigma_v^2) \exp[-v^2/2\sigma_v^2] d\theta \quad (\text{III-15})$$

$$\begin{aligned} p(v) &= (v / \sigma_v^2) \exp[-v^2/2\sigma_v^2] & v \geq 0 \\ &= 0 & v < 0 \end{aligned} \quad (\text{III-16})$$

which is a Rayleigh probability density function that is independent of time due to stationarity and is only a function of clutter power, $P_c = 2\sigma_v^2$ (Ref 52:38). P_c is the mean square value of the envelope.

The power spectral density for the Gaussian model is thus

$$S_G(f) = (P_c / \sqrt{2\pi}\sigma_f^2) \exp[-f^2/2\sigma_f^2] \quad (\text{III-17})$$

where P_c is the clutter power. The term σ_f^2 is the standard deviation of the spectrum and is related to the RMS velocity clutter spread σ_v by $\sigma_f^2 = 2\sigma_v^2 / \lambda$.

When the clutter process $c(t)$ is sampled by a pulsed radar, the probability density of the sample is given by the

multidimensional Gaussian distribution

$$p(x_1 \dots x_n) = [(2\pi)^n |M|]^{-.5} \exp[-.5 x^T M^{-1} x] \quad (\text{III-18})$$

where T is the transpose of the vector x and the covariance matrix is

$$M_x = \sigma_x^2 \begin{vmatrix} 1 & p_{12} & p_{13} & \dots & p_{1n} \\ p_{21} & 1 & & & p_{2n} \\ & & 1 & & \\ & & & \ddots & \\ p_{n1} & & & & 1 \end{vmatrix} \quad (\text{III-19})$$

and $p_{ij} = \exp[-(i-j) \frac{2\pi f}{T}]$. For analytical purposes the clutter process is assumed to be a Gaussian Markov process.

The Rician model is similar to the Gaussian model except that a predominant steady scatterer (S) is added to the distributed clutter. The random clutter process is given by

$$C_R(t) = (S - x(t)) \cos(w_c t) - y(t) \sin(w_c t) \quad (\text{III-20})$$

with voltage amplitude probability density function

$$p(v) = (1 + m^2) / \tilde{P} \exp[-m^2] \exp[(-v^2 / \tilde{P})(1 + m^2)]$$

$$I_0(2m\sqrt{(1 + m^2) v / P}) \quad (\text{III-21})$$

where m^2 is the ratio of the steady (S^2) to distributed (P^2) power and total power $\tilde{P} = S^2 + P^2$ (Ref 52:41). The power spectral density is

$$S_R(f) = m^2 P^2 S(f) + P^2 \exp\left[(-f/2\sigma_f^2)/\sqrt{2\pi}\sigma_f^2\right] \quad (\text{III-22})$$

The log-normal model has been used to model clutter obtained from high resolution (pulse width less than .5 microseconds) sea data, where the sea is observed at grazing angles less than five degrees. The log-normal model has also been fitted to ground clutter data observed at low grazing angles (Ref 52:42). The log-normal random clutter process is

$$c_{LN}(t) = v(t) \cos(\omega_c t + \theta) \quad (\text{III-23})$$

where $v(t)$ is the voltage envelope as in equation III-6 and θ is a uniformly distributed random phase variable. If the quadrature components are zero mean, uncorrelated and have identically band limited spectral densities, then $c_{LN}(t)$ is wide sense stationary and the voltage amplitude probability distribution is given by

$$p(v) = 1/(\sqrt{2\pi}\sigma_v v) \exp\left[(\ln v/v_m)^2 / 2\sigma_v^2\right] \quad (\text{III-24})$$

where $v \geq 0$, σ_v is the standard deviation of the normal distribution, and v_m is the median value of the distribution

(Ref 52:45). The log-normal model characterizes well the clutter from specular reflection associated with wave crests and from large directive scatterers that, depending on viewing aspect, produce bright ridges and shadowing (Ref 52:42). In the presence of sea clutter, the Gaussian pfd tends to underestimate the range of voltage amplitudes of the real clutter while the log-normal pdf tends to overestimate the range of values (Ref 56:479).

The Weibull clutter model has properties that lie between the Gaussian and log-normal clutter models. This model has the potential to represent real clutter over a wide range of conditions (Ref 52:48). It is used to model both land, sea, and atmospheric clutter. The Weibull clutter model voltage amplitude out of a clutter envelope detector is

$$p(v) = \ln 2 \left(\frac{v}{v_m} \right)^{\alpha - 1} \exp[-\ln 2 \left(\frac{v}{v_m} \right)] \quad (\text{III-25})$$

where α is a parameter that relates to the skewness of the distribution and v_m is the median value of the distribution (Ref 56:480).

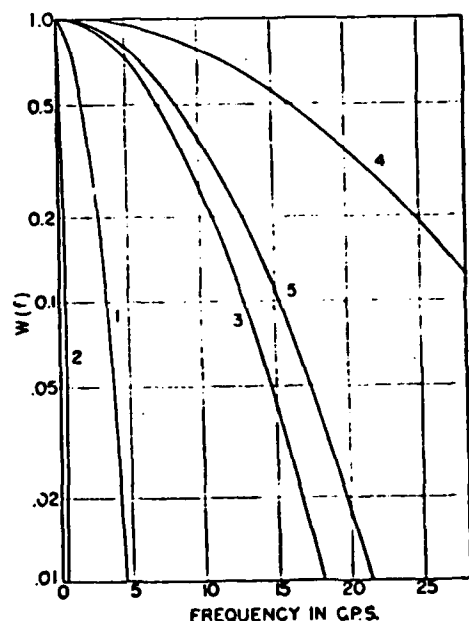
Several other distributions have been applied to empirical clutter data. These include the chi-square distribution, the K-distributions and the IIT model (complex overland airborne radar derived model). These models have not, however, had widespread use.

The power spectral density which describes clutter returns is probably the most useful for analyzing clutter

cancellation techniques. The most widely used discription of the clutter spectrum is that proposed by Barlow. Barlow, analyzing experimental data made from ground targets, sea echoes, and rain clouds, proposed a Gaussian model for the frequency distribution of clutter (Ref 5:351). The power spectrum from fixed targets is thus approximated by

$$W(f) = W_o \exp[-a(f/f_t)^2] \quad (III-26)$$

where W_o is the mean value of the power density, f_t is the radar transmitting frequency and "a" depends on the nature of clutter and weather conditions. Values of "a" range from 3.9×10^{19} for sparsely wooded hills on a calm day to 2.8×10^{15} for rain clouds (Ref 47:XV-25). Figure III-1 show the frequency spectra of various types of clutter.



Curve	Target	a
1	Heavily wooded hills, 20 mph wind blowing	2.3×10^{17}
2	Sparsely wooded hills, calm day	3.9×10^{19}
3	Sea echo, windy day	1.41×10^{16}
4	Rain clouds	2.8×10^{15}
5	Window "jamming"	1.0×10^{16}

(Ref 5:351)

Fig. III-1 Frequency spectra of various types of fixed targets

Equation III-26 can be written into the more familiar Gaussian form

$$W(f) = W_o \exp[-f^2 / 2\sigma_c^2] \quad (\text{III-27})$$

where $a = f^2 / 2\sigma_c^2$ and σ_c is the standard deviation of the clutter spectrum.

While the frequency spectrum for clutter is modeled as Gaussian, it is in actuality a filtered version of the transmitted signal spectrum envelope. The return radar signal resulting from clutter can be thought of as

$$C(f) = |H(f)|^2 S(f) \quad (\text{III-28})$$

where $C(f)$ is the clutter power spectrum, $S(f)$ is the signal power spectrum and $H(f)$ is the transfer function that describes the clutter response. Due to the effects of antenna tapering, smearing by the convolution of the IF spectrum with itself (Ref 11:484), system instabilities, movement by the radar and the random nature of the clutter, the fine grain structure of the transmitted signal spectrum is generally lost and the clutter power spectrum can be approximated by the Gaussian function as proposed by Barlow.

The spectrum of the clutter return results from the convolution of the Gaussian spectrum with the transmitted frequency and all harmonics. An example of a CW radar spectrum is shown in Figure III-2a while the spectrum of a

pulse doppler radar is shown in Figure III-2b.

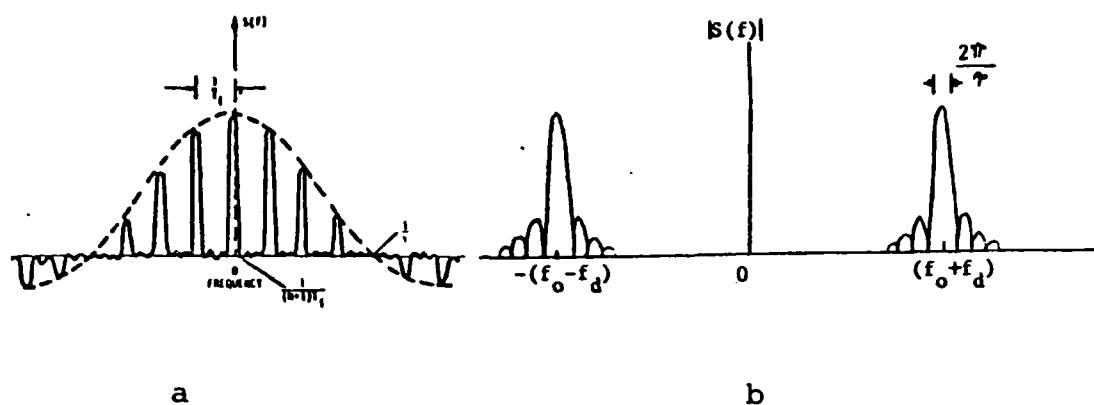


Fig. III-2 Clutter Spectrum

Figure III-2b illustrates why it is important for a doppler radar to use a high pulse repitition frequency so as to prevent aliasing between the harmonics, thereby eliminating velocity ambiguities.

The clutter spectrum shown in Figures III-2a,2b is spread primarily due to four effects: 1) antenna scanning modulation; 2) radar platform motion; 3) transmitter frequency and 4) internal clutter motion.

A scanning antenna induces a modulation that is characterized by a long pulse. Given a Gaussian antenna pattern, the contribution to clutter spread due to antenna scanning is

$$\sigma_s = \alpha / (\sqrt{2\pi}\theta_B) \text{ Hz} \quad (\text{III-29})$$

where α is the scan rate, and θ_B is the two way beamwidth (Refs 11:479, 24:133).

The platform motion has two effects on the clutter spectrum. First there is a translation of center frequencies due to the doppler shift induced by the platform. This doppler shift is

$$f_d = 2 (v_p / \lambda) \cos \phi \cos \theta \quad (\text{III-30})$$

where θ is the azimuth angle between the platform velocity and the direction of the radar beam and ϕ is the depression angle to clutter patch (Ref 53:210). Besides the shifting in the center frequency of the clutter, the spectrum is widened due to a relative rotation induced by the moving observer with respect to a fixed point. The platform motion contribution to clutter spread is

$$\sigma_p' = (.6/D) v_p \cos \phi \sin \theta \text{ Hz} \quad (\text{III-31})$$

where v_p is the radar velocity, the angles are defined as above and D is the diameter of the antenna (Ref 53:212).

The transmitter frequency instabilities cause a spreading of the clutter spectrum because of the decorrelation from pulse to pulse. The contribution to clutter spreading due to transmitter frequency instability is

$$\sigma_f' = (.42 / B) f'(t) \text{ Hz} \quad (\text{III-32})$$

where B is the transmitter pulse bandwidth and $f'(t)$ is the transmitter drift rate (Ref 53:216).

HD-A138 467

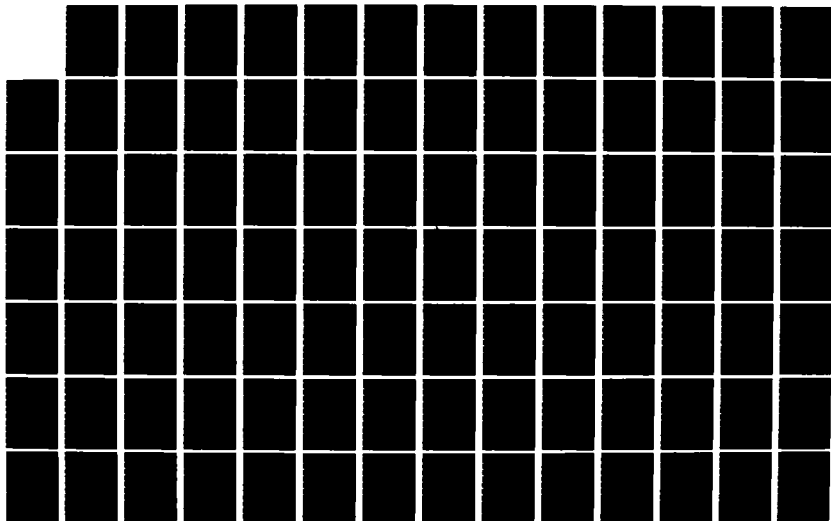
CLUTTER CANCELLATION TECHNIQUES FOR USE IN A
SPACE-BASED RADAR SYSTEM(U) AIR FORCE INST OF TECH
WRIGHT-PATTERSON AFB OH SCHOOL OF ENGINEERING
J DEVENUTO DEC 83 AFIT/GE/EE/83D-18

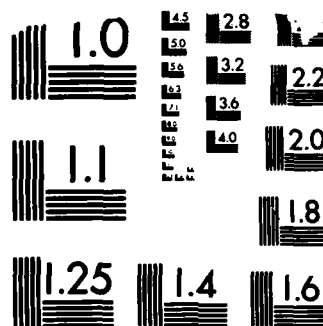
2/3

UNCLASSIFIED

F/G 77/9

NL





The scatterers often move relative to one another because of wind, thus causing a spread in the clutter spectrum. The standard deviation of the internal motion is

$$\sigma_v = 2 V_{\text{RMS}} / \lambda \text{ Hz} \quad (\text{III-33})$$

Typical values of σ_v are shown in Table III-1.

TABLE III-1
Characteristics of Clutter Spectra

Source of clutter	Wind speed (knots)	Ratio 2 m	Barlow's a	σ_c (cm/sec)	σ_v (ft/sec)
Sparse woods	calm		¹⁹ 3.9x10	3.5	0.057
Rocky terrain	10	30	¹⁸ 7.2x10	8	0.13
Wooded hills	10	5.2	¹⁷ 2.3x10	45	0.78
" "	20		¹⁷ 9x10	23	0.38
" "	25	0.8	¹⁷ 1.1x10	65	1.06
" "	40	0	¹⁶ 2.4x10	140	2.3
Sea echo			¹⁶ 0 (1-2)x10	165-205	2.5-3.3
" "	8-20		¹⁶ (0.6-2.6)x10	100-220	1.5-3.5
" "	(windy)		¹⁶ 1.4x10	183	3.0
Chaff	0-10	0	¹⁶ (1.4-8)x10	75-180	1.2-3.0
"	25	0	¹⁵ 7x10	250	4.1
Rain clouds		0	¹⁵ (0.7-3)x10	370-800	6-13
" "			¹⁵ 2.8x10	410	6.7

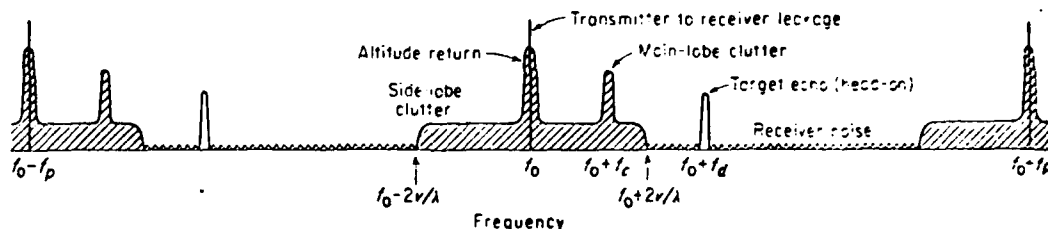
(Ref 6:100)

The four standard deviations combine together to give an overall clutter spread of

$$\sigma_c^2 = \sigma_s^2 + \sigma_p^2 + \sigma_v^2 + \sigma_f^2 \quad (\text{III-34})$$

$$\sigma_c^2 = \left(\alpha / (\sqrt{2} \pi \theta_B) \right)^2 + \left((.6v/D) \cos \phi \sin \theta \right)^2 + \left((.42/B) f'(t) \right)^2 + \left(2 v_{\text{RMS}} / \lambda \right)^2. \quad (\text{III-35})$$

For a spaceborne radar system the effects of the sidelobes must be added to the spreading of the clutter spectrum since the sidelobes can illuminate a large clutter area. The sidelobes in a spaceborne radar system will produce clutter returns which extend from $2v/\lambda$ on either side of the transmitter frequency (f) because the sidelobes extend in different directions around the main beam. The clutter returns resulting from sidelobes that point directly below the spacecraft will produce a strong return at f because the radial velocity at that point is zero. A typical clutter spectrum of a spaceborne radar system is shown in Figure III-3.



(Ref 56:146)

Fig. III-3 Spaceborne Radar Clutter Spectrum

Two other spectral models have found use to describe clutter returns in certain situations. These models are the Markoffian model and the cubic model. The Markoffian model describes the frequency spectrum of clutter that is bandlimited white noise like. The model is

$$W(f) = W_o \frac{f_c^2}{[f_c^2 + (f - f_c)^2]} \quad f > 0 \quad (\text{III-36})$$

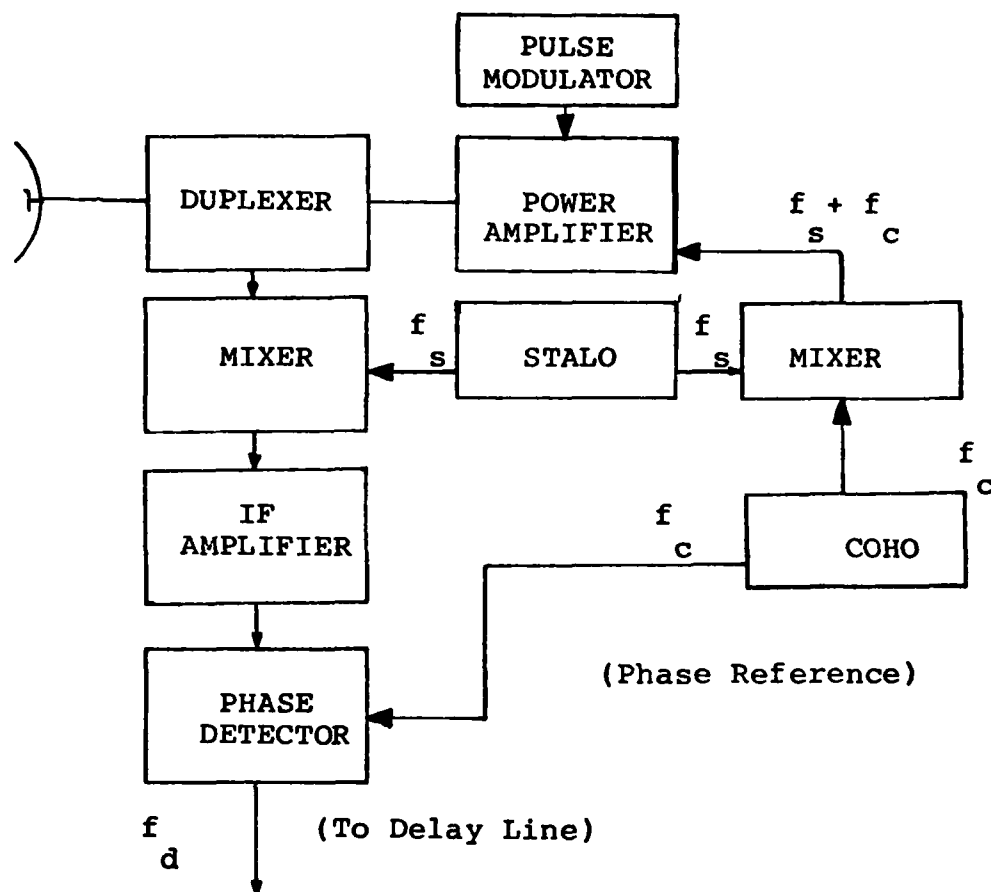
where W_o is the mean value of the power density and f_c is the half power frequency (Ref 47:XV-26). The cubic model has been proposed by Fishbein for clutter returns at X-band. The model is

$$W(f) = 1 / [1 + (f/f_c)^3] \quad (\text{III-37})$$

where $f_c = k e^{\beta v}$, with $k = 1.334$, $\beta = .356$ (knots)⁻¹ and v is the windspeed (knots) (Ref 47:XV-27).

Typical Radar Receiver

The clutter cancellation techniques analyzed in the next section assume a pulsed doppler radar system. Shown in Figure III-4 is a generalized block diagram of a coherent pulsed amplifier.



(Ref 56:105)

Fig. III-4 Block Diagram of a MTI Radar Receiver

Either a pulsed oscillator system or a pulse amplifier system can be used in a pulse doppler radar. Since the operation of the pulsed amplifier is very similar to that of the pulsed oscillator and for a spacecraft application a pulsed amplifier system would be used, only the pulsed amplifier operation will be described. An analysis of the pulsed oscillator operation can be found in Ref 6:192-195.

The system shown in Figure III-4 is one form of a co-

herent MTI radar, in which the phase reference is maintained in the radar itself (Ref 6:192). Coherent reference is maintained by a stable oscillator called the COHO, or coherent oscillator, operating at IF. Besides providing a reference signal from pulse to pulse, the output of the COHO, f_c , is mixed with the stable local oscillator, STALO, at frequency, f_l . The function of the STALO is to provide the necessary frequency translation from the IF to transmitted RF frequency. The transmitted signal is thus a combination of the COHO and STALO frequencies.

The RF echo signal is heterodyned with the STALO signal to produce the IF signal. The reference signal from the COHO is then mixed and low pass filtered with the IF echo signal in the phase detector. The phase detector output is proportional to any phase difference between the COHO and IF echo signal (Ref 56:105). The zero frequency output of the phase detector, sometimes called the video, is then processed to remove clutter.

Cancellation Techniques

Clutter masses can be considered as stationary targets, thus, relative to the radar antenna, targets and clutter masses exhibit different relative speeds. The differences of target and clutter velocities, conveyed by doppler shifts in the transmitted signal, are used to separate moving targets from undesired clutter. A radar that uses the doppler frequency shifts as a way of distinguishing moving targets

from clutter is called a MTI¹ (moving target indication) system (Ref 56:101). A MTI system essentially employs filtering networks (or their equivalent) which null the returns from fixed targets, which have no doppler shift, while passing the frequency shifted echoes of moving targets. Clutter cancellation by this means is limited by the extent that the energy spectrum from the clutter mass is distinguishable from that of the target (Ref 24:82). As illustrated in the previous section, the clutter power spectrum of a spaceborne radar occupies a range of frequencies, which at times is in the vicinity of components of the target radial velocity. This makes it difficult to distinguish between clutter and target energy. The ability of the MTI system to reject clutter and detect low velocity targets is in part based upon the clutter cancellation scheme employed.

A MTI radar system allows for operation in a high clutter environment with the minimum amount of dwell time for a given probability of detection. This is a necessary feature for a spaceborne surveillance and tracking system. A pulse doppler radar is a type of MTI system that uses a high pulse repetition frequency to allow unambiguous doppler measurements while also making it possible to make range measurements. Figure III-5 illustrates an example of a pulse doppler radar MTI

1The term MTI can either connote any radar system which uses velocity as a method of discriminating between targets and clutter or can connote a clutter cancellation scheme which uses delay line cancelers. While most clutter cancellation techniques employ some form of a delay line canceler, a distinction in the type of cancellation arrangement will be made and the first MTI definition will be used.

system. This general pulse doppler MTI system will be used in the description for this study. The MTI system basically solves the binary decision problem of whether a target is present or not. Given that a target is present, the system then provides an estimate, or mark, of target velocity and range. Depending on the task of the processor, cost and complexity desired and method of processing, certain element blocks may be added, eliminated, or just rearranged.

The receiver block, discussed in the previous section, performs the front end processing on the signal by converting the RF signal to either an IF or video signal. A possible modification to the receiver diagram shown in Figure III-4 is to add an adaptive velocity compensation mechanism which compensates for the platform motion. The compensation is accomplished by adjusting the frequency of the COHO as a function of the platform doppler frequency and sighting vector.

If a modulated waveform is transmitted, a pulse compression filter, in the form of a filter matched to the transmitted signal, is used to compress the receiver output signal. In delay line canceler systems, pulse compression is usually done after clutter processing. Following pulse compression, the signal is range gated to eliminate excess receiver noise and permit target range measurement (Ref 56:19-13). The number of range gates depends on the number of range bins, M , where $M = 2R / cT$ with R being the slant range, c being the speed of light and T being the compressed pulse

width. If pulse compression is accomplished digitally then the A/D conversion occurs before the pulse compression, otherwise the signal from each range gate is A/D converted.

The range gated signal is divided into quadrature and in-phase channels to eliminate the effects of blind phases. Blind phases occur when pulse sampling appears at the same point in the doppler cycle at each sampling instant (Ref 56:120). The quadrature channel is especially utilized when delay line cancelers are used as a clutter canceler. The digital signal in the I and Q channels are then digitally filtered to suppress clutter energy and enhance the target energy. Various clutter cancellation and filtering techniques will be discussed later. The filtered I and Q channels are then combined to produce a signal with no loss (Ref 56:121).

Following the combination of the I and Q channels, the signal from each filter is integrated, either coherently or incoherently, and then compared in the CFAR with an established threshold level to determine the presence or absence of a target. The CFAR circuitry, designed using the principles described in the Detection Processor Development section in Chapter II, maintains a constant, satisfactory number of false alarms for the radar system. The threshold value is generally calculated by applying the Neyman-Pearson criterion using either fixed or real time clutter and noise statistics. If real time (updated clutter and noise) statistics are used in modifying the threshold value, then the CFAR system is considered adaptive. Signals which exceed the

threshold value are then passed on to the data processor where target velocity and range estimation is made, and monopulse calculations, ambiguity removal and track initiation are all accomplished. The difference, Δ , and auxiliary, AUX, radar channels shown in Figure III-5 may or may not be employed. When employed they are used for monopulse calculations, jammer suppression and the adaptive loop calculations such as the one for the filters or the CFAR circuits. These channels contain block elements whose functions are similar to those just described for the sum, Σ , channel.

In designing the clutter cancellation techniques care must be taken to maintain perspective on the relationship of the variety of methods and techniques used for suppressing clutter. Doppler clutter cancellation is basically accomplished by spectrally analyzing each range gated signal. It can be seen that filter design and arrangement become the heart of any cancellation scheme. There are two problem areas in designing the filters. The first is designing the optimal filter so as to maximize the signal to interference (clutter + noise) ratio as discussed in References 21, 51, 58, 62. The second problem is to approximate the optimal filter as close as possible digitally so as to minimize filter sidelobes which introduce ambiguous interference. This second problem, discussed extensively in Reference 29, 43, and 60, essentially deals with choosing the proper windowing of the signal, proper weighting to implement the filter, whether to implement the filter with a finite

impulse response (FIR) circuit or an infinite impulse response (IIR) circuit or use a FFT software package. Windowing and weighting choices are influenced by the clutter spectrum which must be cancelled, while choice of implementation method is governed by system constraints.

The least complex and most widely used cancellation technique is the delay line canceler. Figure III-6 shows a single delay line.

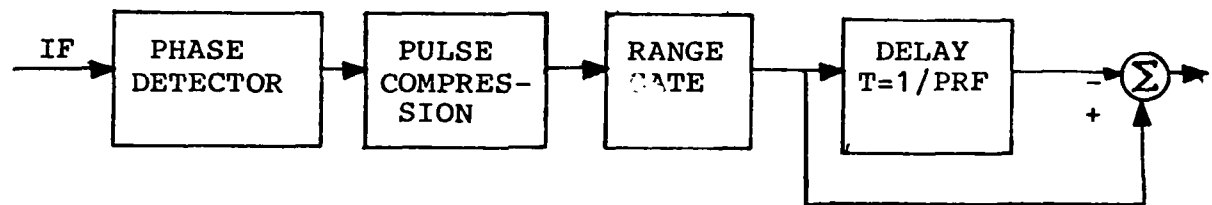


Fig. III-6 Single Delay line Canceler

While Figure III-6 shows the delay line canceler following pulse compression and range gating, the delay canceler may, and often does, follow the phase detector. The video output of the phase detector, for a specific range, for one complete interpulse period is fed into the delayed channel which has a delay time memory equal to the transmission interpulse period. During the next transmission period, the output of the phase detector is applied to the two channels of the canceler. At the summer junction the video output from the first interpulse period, which has been delayed, is subtracted from the most recent undelayed video signal. Theoretically, if there is no built-in system instability or radial motion caused by the

platform, the video output from fixed targets, clutter, will be unchanged between successive interpulse periods thus allowing for complete cancellation of the output of the summer. In contrast, moving targets detected during successive interpulse periods will have a finite phase difference causing a variance in signal level at the input of the subtracting unit thus producing a finite residue output. The signal present in the canceler due to a target return at time t is

$$E_1(t) = A \sin(2\pi f_d t + \theta + \phi) \quad (\text{III-38})$$

where θ is the initial phase and ϕ is the phase shift due to the target at range $4\pi R/\lambda$. The signal at an interpulse period later is

$$E_2(t) = A \sin[2\pi f_d (t + T) + \theta + \phi] \quad (\text{III-39})$$

Thus the output of the canceler is

$$E_0(t) = E_2(t) - E_1(t) = 2A \sin(\pi f_d T) \cos[2\pi f_d (t + .5T) + \theta + \phi] \quad (\text{III-40})$$

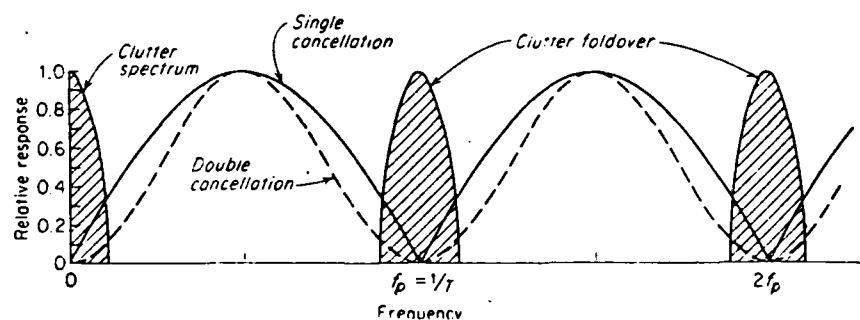
From equation III-40 we can see that the magnitude of the phase imbalance is thus proportional to the doppler frequency shift of the moving target. By envelope detecting and doppler filtering the signal described by equation III-40, the target doppler can be determined. From equation III-40 we can also

see that system instabilities such as pulse time jitter, pulse width jitter, pulse amplitude jitter, pulse distortion, and frequency modulation within the pulse all effect the cancellation ability of a delay line canceler.

The delay line canceler acts as a periodic filter notching out fixed clutter and signal energy around the dc and the PRF harmonic frequencies. The transfer function is

$$|H(f)| = 2 \sin (\pi f T) \quad (\text{III-41})$$

This filter, periodic in the frequency domain, is sometimes described as a "comb filter." Figure III-7 shows the response of a delay line canceler or comb filter.



(Ref 56:110)

Fig. III-7 Delay Line Frequency Response

The motion of the spaceborne radar platform induces a frequency translation of the clutter spectrum. To compensate for the doppler shift in clutter the frequency in the COHO can be modified to shift back the clutter spectrum. A phase

shift, inserted in one branch of the delay line canceler that shifts the null of the response to match the translated clutter spectrum, can also compensate for the translational effects of the platform motion. The appropriate phase shift is a function of the mainbeam sighting vector and platform velocity. The mean doppler shift due to platform motion can be removed by phase locking the receiver to the clutter as is done with time average clutter coherent airborne radar (TACCAR) (Ref 3:566). As in the airborne application, the clutter doppler shift for the space-based radar will be range dependent since the doppler frequency is a function of the sighting angle from the radar to the clutter cell. The average doppler frequency of the clutter, computed by averaging the clutter signal phase change from several range intervals, is used to cause the mean doppler frequency to coincide with the null of the delay line filter response over the rest of the range of observation (Ref 56:142). This system is an example of a clutter lock scheme. The clutter lock addition simply compensates for the doppler shift and then uses any conventional clutter canceler to remove the remaining clutter spectrum.

The clutter locking technique becomes ineffective when more than one type of clutter is present in the range of interest because of the wide disparity in the mean velocities. Furthermore, in the absense of clutter, the system compensates for only the target velocity, thus rejecting the target. Hence it is necessary to bypass the clutter locking circuits when

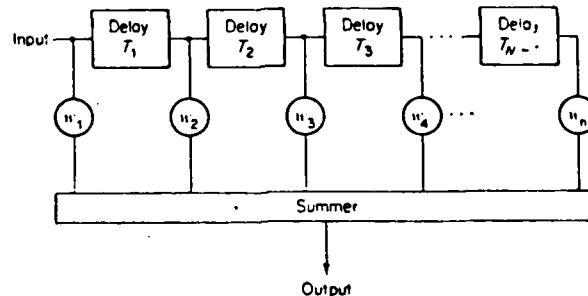
clutter power is small(Ref 40: 328).

The single canceler in many instances does not have a sufficiently broad enough null to reject the extended clutter spectrum which results from a moving platform. To reduce the clutter residue, the filter rejection notches can be widened by cascading several single cancelers. The filter transfer function for a cascaded delay line system is

$$|H(f)| = 2^n \sin^n(\pi f T) \quad (\text{III-42})$$

where n is the number of cascaded elements. Figure III-7 also shows the response of multiple cancelers. Care must be taken when widening the notch that target energy in the vicinity of the notch is not also rejected.

The multiple delay line pulse canceler is an example of a transversal or comb filter. The transversal filter finds much use in delay line cancelers because of its ease of digital implementation. Figure III-8 illustrates a nonrecursive or transversal filter.



(Ref 56:110)

Fig. III-8 Transversal Filter

The output of the filter can be written as

$$E_o(NT) = \sum_{k=1}^N w_k E_I(kT) \quad (\text{III-43})$$

where $E_o(NT)$ is the output of the filter and $E_I(kT)$ is the input to the filter. Since the filter response is controlled by adjusting the weights $w_1 \dots w_n$, much effort has been spent to optimally choose the weights and design methods to adaptively modify the weights as a function of the clutter return (Ref 2, 14, 24:91, 54). The transversal filter with alternating binomial weights

$$w_k = (-1)^{k-1} \binom{n}{k-1} \quad k = 1, 2, \dots, n+1 \quad (\text{III-44})$$

closely approximates the filter which maximizes the average improvement factor (Ref 56:111). By using alternate weighting schemes, i.e. Hanning, Butterworth, a different filter response results which maximizes performance criteria other than the improvement factor.

Since the transversal filter simply implements a cascaded delay line canceler network, as the number of delays increases, the notches at dc and all the PRF harmonics are widened and cancel an increasing amount of target energy. Ideally the filter response should have notches at dc and all PRF harmonics which match the clutter spectrum. The filter response can be shaped to approximately match the clutter by

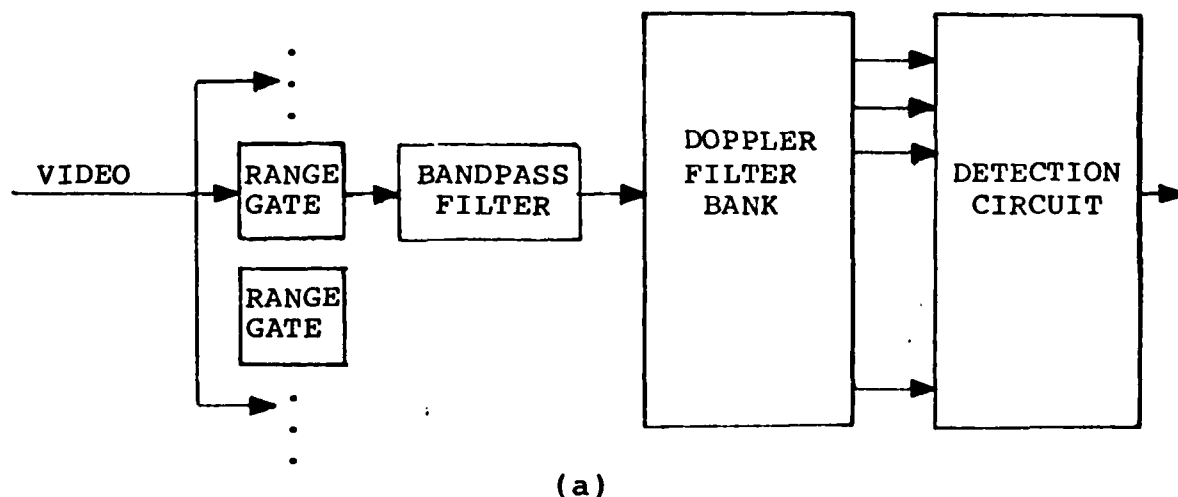
employing recursive, or feedback, filters. The z-plane frequency analysis techniques discussed in Chapter II are used to synthesize the desired frequency response. While recursive filters offer a better steady state response than nonrecursive filters, they exhibit severe ringing in the presence of large clutter (Ref 56:114) and require a number of pulses to be processed before the steady-state condition is met. For wide area surveillance application time is limited. Since the time required for the transient response of a recursive filter to die is large, recursive filters will not be considered for use in the delay line cancelers for this study.

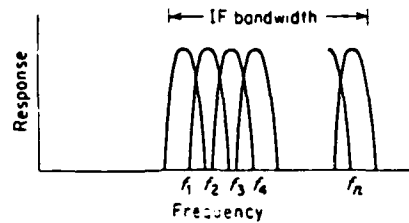
In a delay line canceler system, target doppler is obtained indirectly from the received signal. That is, the doppler information describing either a target or clutter is obtained from the comparison of several interpulse video signals. The relative change from one interpulse period to the next indicates the object's doppler. Low doppler objects are then eliminated through filtering. The next clutter cancellation technique obtains object doppler information directly by determining the frequency shift of the received signal from that of the transmitted signal frequency.

In this second cancellation scheme, fixed and moving targets are discriminated through the use of a single or a bank of contiguous doppler filters. In this scheme a typical clutter cancellation system would consist of a bandpass filter which passes the expected frequency response corresponding to targets and suppressing the response from fixed targets. A

bank of contiguous narrowband filters, which would extend over the expected target doppler frequencies, may follow the bandpass filter. The contiguous doppler filters are more complex than simple narrowband filters. These filters are designed to better match the characteristics of the clutter spectrum. The complex narrowband filters permit detection, measurement of target velocity, and resolution between targets having different velocities within the same beamwidth (Ref 32:16). Because the clutter spectrum is predominantly at low doppler frequencies, the low doppler filters of the contiguous bank of filters can be designed differently than the high doppler filters. The low doppler filters can be of the form suggested by Stutt and Spafford (Refs 58, 62) and Delong and Hofstetter (Ref 21), where the "mismatched" filters are a function of the clutter statistics. The major problem with these filters is their implementation, thus filters similar to those suggested by Urkowitz can be used (Ref 22:170).

Figure III-9 shows a system block diagram and a typical response for a doppler cancellation scheme.





(b)

Fig. III-9 (a) Block Diagram (b) Typical Response

The placement of the bandpass filter within the receiver is optional. The filter can be placed just beyond the maximum anticipated clutter spectrum with the knowledge that low radial velocity targets will be rejected. It is desirable when using a narrowband filtering scheme as just described to use a high PRF waveform to avoid doppler ambiguities.

The cancellation techniques discussed so far work well when there is a large differential between clutter and target doppler frequencies. A spaceborne radar system's ability to distinguish low velocity targets from clutter targets is however, severely impaired because the high platform velocity widely spreads the clutter. An additional compensation or cancellation technique is thus required to reduce the spread of clutter in a space-based radar if low velocity doppler targets are to be detected. A clutter spread compensation method, mostly employed on phased array radars, is the Displaced Phase Center Antenna (DPCA) MTI technique. The DPCA MTI technique attempts to remove the effects of platform motion, thereby improving the subclutter visibility of the low velocity targets. The elements which compose the DPCA MTI

system are shown in Figure III-10.

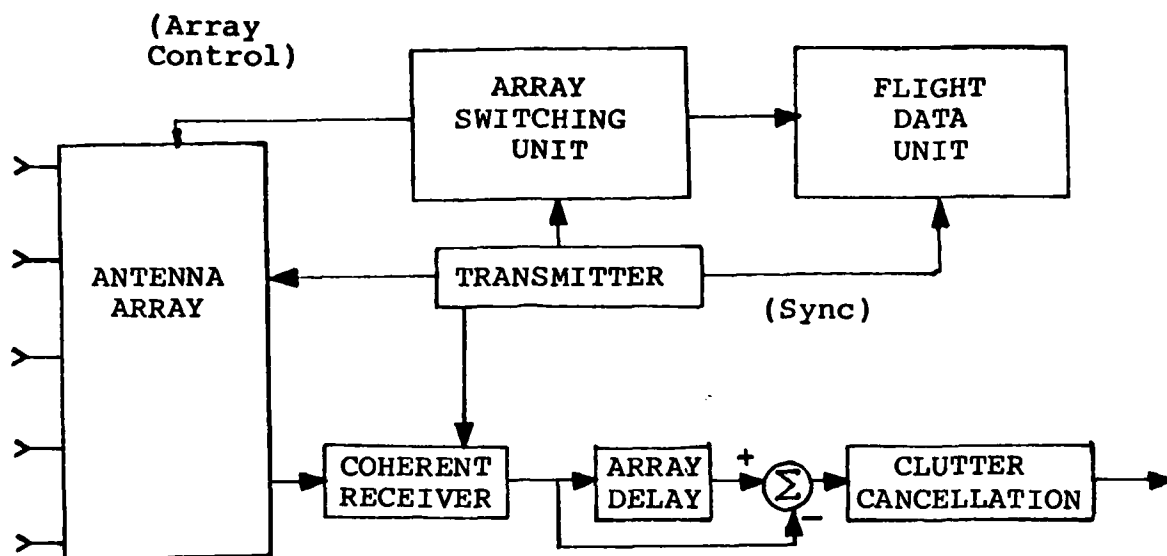


Fig. III-10 DPCA MTI Canceler

The linear array consists of two distinct sub-apertures or phase centers. In the DPCA MTI technique, energy from a single aperture is transmitted at a time t_1 . All the return energy is processed in the coherent receiver as in a conventional canceler. Returns from the initial interpulse period are stored in the array delay which is equal to the interpulse period. As the platform moves forward during Δt , where Δt corresponds to the interpulse period, the phase center of the array is shifted rearward and a second transmission is made from theoretically the same point in space. Fixed targets from the two successive transmissions will have identical phase and amplitudes thus being cancelled in the array delay processor. Moving targets would have changing

phase and amplitudes. The difference between the two periods will thus produce a residue voltage out of the processor that corresponds to their velocity. Theoretically, for perfectly matching aperture patterns, compatibility between switching time of the beam and the system PRF, and no vehicle motion effects, the DPCA system should provide high rejection of the mainbeam and sidelobe clutter, resulting in good subclutter visibility and detection of low velocity targets (Ref 36:27). Matching of system parameters and vehicle rotation have however limited the performance of the DPCA MTI technique. The output from the array cancelling is then further processed by one of the cancellation techniques previously discussed.

An improvement to the DPCA MTI concept is obtained by using a multiple phase center array combined with pulse compression and long integration time. This technique is employed on the Multiple Antenna Moving Target Surveillance Radar (MASR). The operation is identical to the DPCA MTI system except 1) a number of discrete phase centers from which beams are transmitted allow for multiple look integration 2) the output of the coherent receiver undergoes pulse compression before entering the MTI delay line canceler and 3) video integration is performed on the outputs of the canceler (Ref 32:33). The system limitations discussed with the DPCA MTI system are now compounded because of the multiple phase centers.

Both the DPCA and MASR compensation techniques need multiple "looks" to limit clutter spreading. Multiple looks

reduce the area search rate of the radar. Employing a technique similar to that used in monopulse tracking, clutter spreading can be compensated for without reducing the search rate. The monopulse anomolous nulling clutter compensation technique uses the normal sum pattern from the antenna and the difference pattern from the antenna to cancel the clutter in the mainbeam without canceling the target. A target in the mainbeam is near the peak of the sum pattern, thus having a large amplitude while having a low amplitude in the difference pattern. The clutter in the mainbeam is doppler spread by the platform motion as described before. The target doppler shift competes with the clutter doppler shift from a different angle within the mainbeam. Essentially the clutter is off the peak of the beam. The clutter on the other hand has a large gain in the difference pattern. Modifying the gain in the difference pattern to have the same amplitude as the sum pattern, the difference clutter pattern is subtracted from the sum clutter pattern, thus canceling out the clutter. Since the target amplitude in the difference pattern is nearly zero, while the target amplitude in the sum pattern is large, the resulting target amplitude is not sufficiently reduced when differencing occurs. Following the differencing, the signal is then processed further by one of the previously described cancellation techniques to eliminate the remaining clutter energy and provide for range and velocity measurements. While this method enhances the S/C ratio of the target in the mainbeam, sidelobe clutter is limited. This method, like the

DPCA and MASR techniques, is limited by the total system stability.

Various clutter cancellation techniques have been presented in this chapter which take advantage of the different spectral characteristics between targets and clutter. While this is not an exhaustive list of all the techniques available, the cancellation schemes presented are representative of the manner in which clutter for a spaceborne radar system would be cancelled. Essentially each of these techniques distinguish between targets and clutter doppler characteristics by using some form of a delay line canceler or a bank of contiguous doppler filters. To enhance the radar's ability to detect low doppler targets DPCA, MASR or monopulse anomalous nulling can be added to compensate for the clutter spreading due to the high platform velocity. Because the clutter spreading compensation techniques involve total radar system aspects, they will not be added in the modeling and analysis of the clutter cancellation techniques found in the next chapter.

IV Computer Models

Approach

The modeling of the clutter cancellation problem can be divided into three separate areas or subprograms. The calculation of the clutter power spectral density, for given radar parameters and given surveillance scenerio geometry is the first area. The routines used to calculate clutter PSD can be exercised to obtain insights and understanding into the magnitude and extent of the clutter PSD for various surveillance situations and clutter statistics. The second computer modeling area is the processing of the radar echo signal so as to cancel clutter and thus obtain target information. Since the analysis of Chapters II and III showed that the modeling of a clutter cancellation processor essentially becomes a matter of implementing a particular digital filtering scheme, the second subprogram simulates a digital filter. The final computer modeling area deals with the calculations to obtain the attenuation factor for the various clutter models - filtering scheme combinations. The output from this subprogram provides a quantitative measure of the clutter cancellation ability of various filtering schemes against different clutter backgrounds.

The computer simulation written for this study is structured such that variations in the clutter background, or cancellation scheme, can be easily implemented by simple substitutions of routines. The main program, CLUTCAN, calls

the subprograms that model each of the areas described above. These subprograms in turn call the subroutines that comprise each subprogram. The CLUTCAN program simulates the entire clutter cancellation problem, from the calculation of clutter PSD, the filtering schemes that cancel selected clutter spectral components, to the calculation of the attenuation factor of the cancellation scheme used. Figure IV-1, shown on the next page, shows the flowchart for the CLUTCAN program. Although the subprograms are exercised by the CLUTCAN program, they each can easily be used in separate programs to analyze specific problems. For example, the effects of various clutter statistics or variations in surveillance geometries on clutter PSD can be obtained by writing a separate program that only calls the clutter PSD calculation subprogram.

Since the main program, CLUTCAN, is only an initialization and calling program, and will not be discussed in detail. The CLUTCAN program listing can be found in Appendix D. The next three sections will discuss the three subprograms called by CLUTCAN. The subprograms' flowcharts and program listings can also be found in Appendix D.

Clutter PSD Calculations

The subprogram CLUT calculates the power spectral density that is received by a space-based doppler radar system given radar system parameters and the viewing geometry parameters for a specific surveillance scenerio. This subprogram computes the clutter PSD by one of two methods.

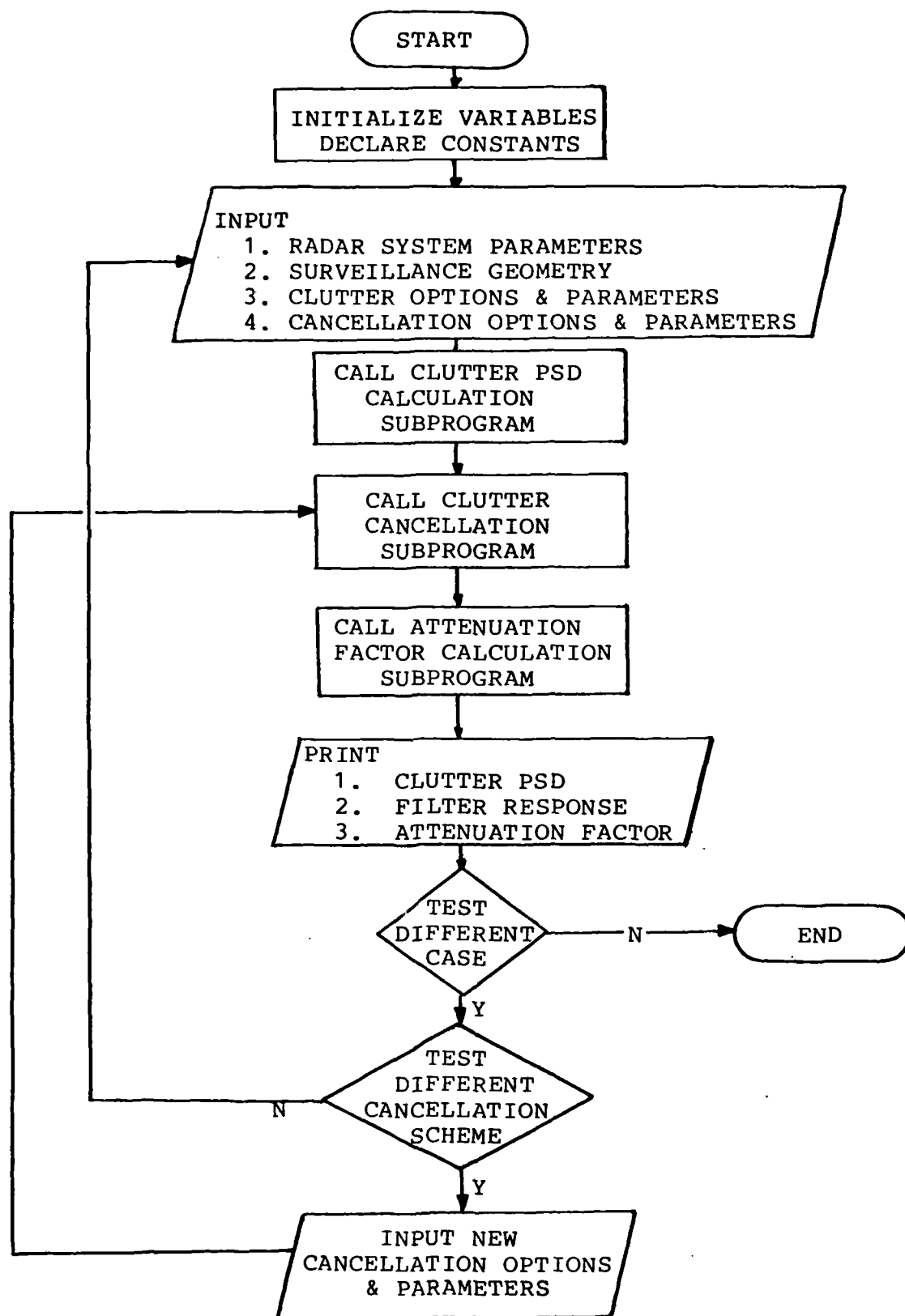


Fig. IV-1 Flowchart for CLUTCAN Program

The first method simply assumes a Gaussian power spectral distribution function, as described by equation III-27. The PSD mean power value is then computed by equation IV-1

$$W_o = \frac{P G^2 \lambda^2 \sigma_c}{(4\pi)^3 \frac{T}{L} \frac{R}{S}} \quad (IV-1)$$

where the spectrum variance, σ_c , is computed via equation III-35. The clutter spectrum is defined to be centered at zero frequency because it is assumed that platform induced frequency translation is compensated for by adjustments in the COHO.

The second clutter PSD calculation method is based upon the summation of power reflected from range and range rate distributed clutter. The region of distributed clutter that is of interest is defined by the area of the earth illuminated by the radar for a pair of depression and azimuth angles. These angles are measured relative to the velocity vector of the spaceborne platform as illustrated in Figure IV-2. The clutter level for an arbitrarily selected range-doppler cell within the illuminated area, where the clutter cell range width is defined by the range resolution constant, equation II-123, and the clutter cell doppler width is defined by the doppler resolution constant, equation II-126, is calculated by multiplying the average backscatter coefficient with the cell area.

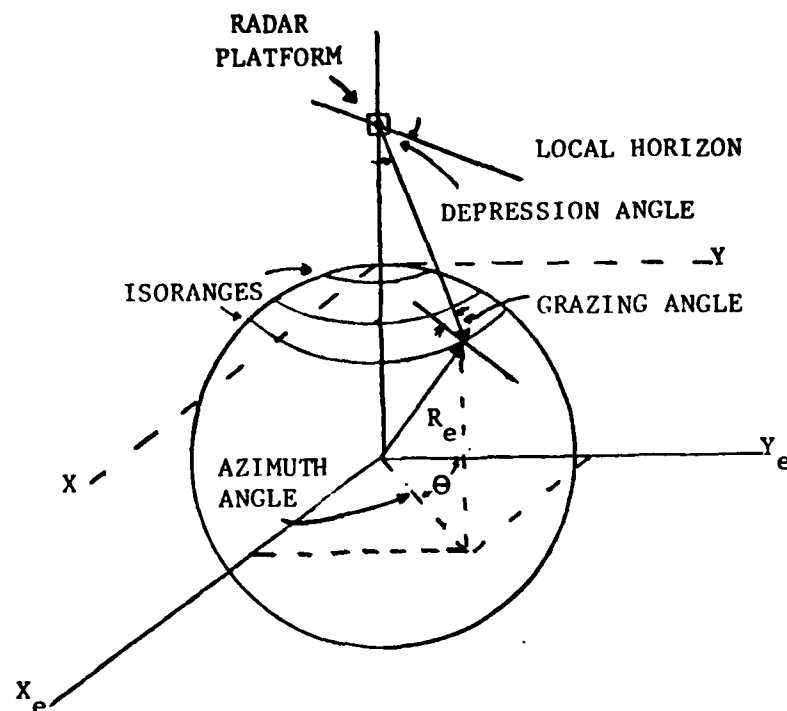


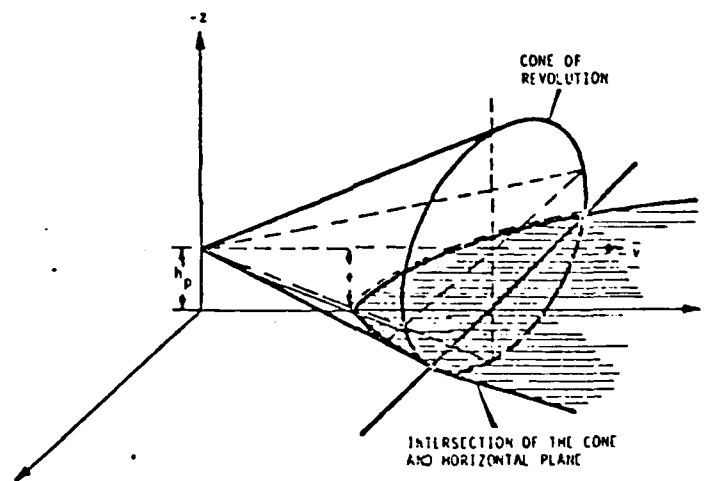
Fig IV-2 Situation Geometry

For the high PRF case, the clutter power from the ambiguous range cells are summed for an unambiguous doppler cell to obtain the clutter power for a specific doppler.

Projected beneath the radar is a locus of points which form a sphere centered at the radar nadir. This locus of points are instantaneously at a fixed range, R , from the radar. The intersection of the spheres with the earth forms a circle called an isorange, all points of which contribute to the range gate containing the range R . The earth isorange circles are also illustrated in Figure IV-2. A range gated return will contain clutter energy from the region between two isorange circles (Ref 50:375).

In the frequency domain, the locus of fixed points in

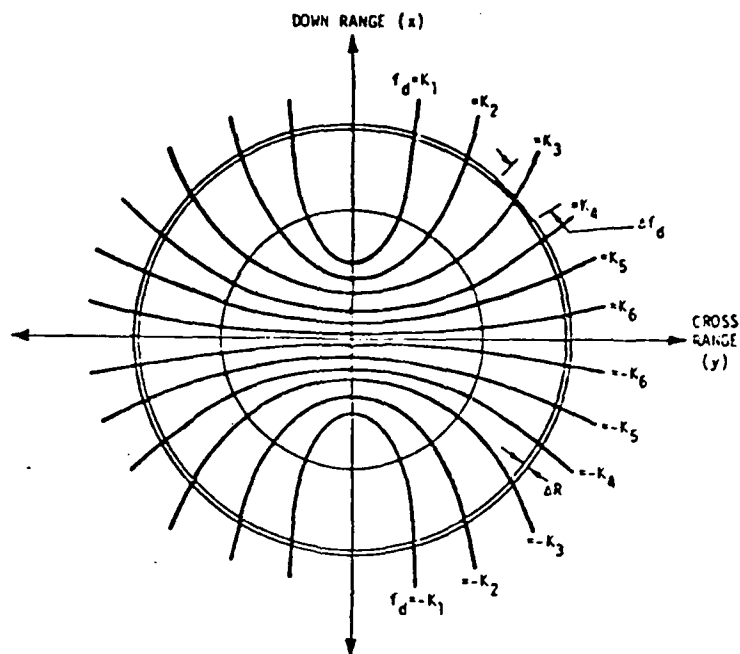
space, from which a return would have a given doppler shift, f_o , is a half cone whose vertex is at the radar and whose axis is the velocity vector of the radar. The half cone arises because the instantaneous relative speed between the radar and a fixed point, is the radar speed multiplied by the cosine of the angle formed by the velocity vector and the position vector of the point relative to the radar. The half cone formed by the set of points with fixed doppler is illustrated in Figure IV-3.



(Ref 47:XVI-7)

Fig. IV-3 Generation of Constant Doppler Contours

The intersection of the half cone with the earth forms a conic section called an isodop all points of which contribute to the doppler cell containing the doppler f_o . Figure IV-4 shows the projection of the isoranges and isodops on a flat surface.



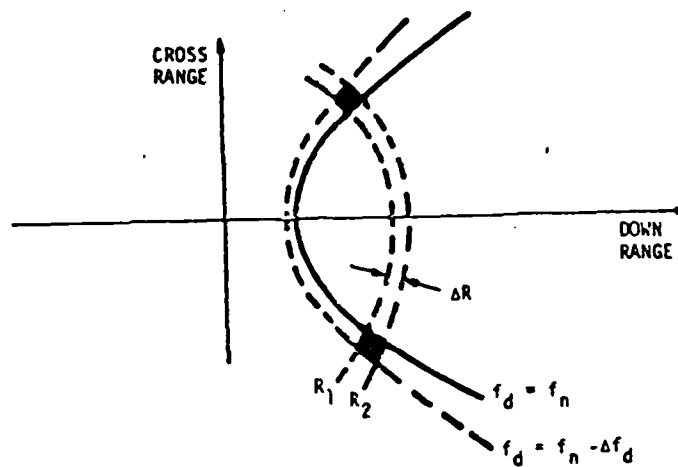
(Ref 47:XVI-8)

Fig. IV-4 Isodop and Isorange Points

The doppler cell thus contains the clutter returns from the region between two isodop conic sections (Ref 50:375).

To compute the PSD, the illuminated range cell region, shown in Figure IV-4 between the two isodops Δf_d a part, is first determined. This area is the clutter area for an arbitrarily selected range-doppler cell. This clutter area, multiplied by σ^1 is used in the radar range equation (along with the appropriate two way antenna gain defined along the observation line of sight) to calculate the region's contribution to the platform motion power spectrum. Figure IV-5 illustrates the region which generates the clutter for a range-doppler cell.

¹ Since σ^1 varies with problem geometry, the σ^1 value which corresponds to the problem grazing angle must be determined and used.



(Ref 47:XVI-9)

Fig. IV-5 Range-Doppler Clutter Cell

The complete power spectra can be computed by integrating over all isodop regions of interest. The high PRF used for a space-based radar causes ambiguities in range which necessitates integration over the entire ambiguous range region for each unambiguous doppler. The clutter PSD calculation for a doppler cell, f_o , is summarized by equation IV-2

$$C_{f_o, ik} (R_o, f_o) = \sum_k \frac{P \lambda^2}{(4\pi)^3 L} \int_{R_{ik} - R_o}^{R_{ik} + R_o} \frac{G^2(R, f_o)}{R^4} dR \quad (IV-2)$$

where R_o is the first unambiguous range between 0 and $c/2PRF$ on which the range gate is centered and R_{ik} forms the set of discrete ranges

$$R_{ik} = R_o + c/2PRF \quad (IV-3)$$

The range zone width, ΔR , is

$$\Delta R = c/2PRF \quad (IV-4)$$

The approach just described to calculate the clutter PSD is based upon the clutter modeling developed in Refs 4, 25-27, and 50. Chapter 2 of Ref 27 provides a complete mathematical description of this clutter PSD calculation method, therefore it will not be repeated in this text. The mathematical equations are, however, applied in the computer program.

Because of the iterations needed to calculate the clutter PSD and the ease with which variations in the problem can be accomplished, subroutines were used extensively in CLUT, especially in the second method of clutter computations. Method two of CLUT calls several geometry calculation routines to compute the angle and range relationships between the radar coordinate system and the coordinate system of the clutter scattering region. The subroutine SIGMA0 computes the mean backscatter coefficient for different grazing angles. The subroutine ANTG computes the antenna gain as seen by the doppler-range cell. A short description of each subroutine's usage is provided with the code listing found in Appendix D. The development of the equations used in the subroutines are straightforward geometric relationships, therefore will not be covered here. The calling sequence of these routines is shown in CLUT's flowchart, also found in Appendix D.

Clutter Canceler Simulator

The cancellation, or in some cases the reduction of clutter PSD, is accomplished by digital filtering the PSD calculated by subprogram CLUT. The subprogram CANCEL simulates the clutter cancellation via application of the digital filtering techniques discussed in the "Digital Signal Processing" section of Chapter II, primarily the application of equation II-51. Equation II-51 is

$$S_y(f) = |H(e^{j2\pi fT})|^2 S_c(f) \quad (\text{IV-5})$$

where $H(e^{j2\pi fT})$ is the transform of the filter $h(nT)$. The subroutine, FFT2C, from the Cyber IMSL library is used to compute the filter transform of the real valued sequence $h(nT)$. The subroutine requires as inputs the $h(nT)$ vector of sequence values and N , the number of data points to be transformed, where as mentioned before, N should be a power of two. The subroutine outputs the filter transform as a complex vector of length N . The magnitude of the components of $H(k)$, taken at each digital frequency, k , is obtained by taking the squared magnitude of the subroutine returned vector. The filtered clutter PSD is obtained by application of equation IV-5. The clutter power spectra, $S_c(f)$, is converted from the analog frequency axis, f , to the digital frequency axis, k , by $k=fNT$. The filtered clutter PSD, $S_y(k)$, is converted back to the analog frequency axis by equation II-103.

The subprogram CANCEL is designed such that either a nonrecursive filter with one of the following weighting schemes - binomial, Hanning, Hamming, Blackman, uniform, Butterworth or a filter impulse function, $h(t)$, is utilized to perform the filtering that accomplishes the clutter cancellation. The vector of filter sequence values is obtained by sampling either the weighting functions or $h(t)$ every T seconds such that N samples are taken with $n=0,1,2,\dots,N-1$.

The subprogram CANCEL returns to the main program, CLUTCAN, the filtered clutter PSD and the coefficients of the transformed filter. The flowchart and program listing for CANCEL can be found in Appendix D.

Attenuation Factor Calculation

The clutter attenuation factor, defined in Chapter I as

$$CA = \frac{C_{in}}{C_{out}} \quad (IV-6)$$

provides the quantitative measure for evaluating the merits of various cancellation schemes. The subprogram, CLTATT, computes the improvement factor by using the results of the subprograms CLUT and CANCEL.

The clutter power at the filter input is obtained by simply summing the clutter PSD values from the subprogram CLUT and likewise the clutter power at the output of the filter is obtained by summing the filtered clutter PSD values from subprogram CANCEL. The clutter attenuation factor is thus

determined by substitution of the clutter power, both at the input and output of the filter, into equation IV-7. The flowchart and program listing for CLTATT can also be found in Appendix D.

By utilizing the clutter cancellation problem simulator, CLUTCAN, the clutter rejection capability of various cancellation schemes against different clutter environments, different target parameters, and/or with different radar parameters can be tested. In the next chapter, various test cases and the associated clutter cancellation results will be presented and analyzed.

V Results and Analysis

Test Case

Using the computer simulation of the clutter cancellation problem outlined in the previous chapter, there are two areas in which analysis was performed. The first analysis area deals with the extent and magnitude of clutter PSD as seen by a space-based radar. Clutter PSD curves were generated for different depression/azimuth angle combinations using both clutter PSD calculation methods. Due to system constraints, (Ref 4:4-29) the grazing angle was limited between 2° and 70° , thereby limiting corresponding depression angles to between 35° and 75° . Since the calculation of clutter returns is symmetric in each of the four quadrants of the isodop-isorange plane (except for doppler sign changes) the azimuth angle is restricted between 0° and 90° . Clutter PSD calculations are computed with the depression angles having an initial value of 35° and incremented 10° and the azimuth angle having an initial value of 0° and incremented 30° with the exception of a data point taken at 45° . Thus, there are twenty-five depression angle/azimuth angle combinations used in calculating clutter PSD curves.

The clutter PSD curves generated assumed a land background. For comparison purposes, the clutter returns for sea and snow/ice were also generated. Since the backscatter coefficient, σ° , is not azimuth dependent, but rather depression angle dependent, an azimuth angle of 45° was used

with depression angles of 35° , 55° , and 75° . In all cases σ^2 was assumed constant.

The second area of analysis deals with the cancellation ability of the different filter systems. This study used a nonrecursive filter with a varying number of taps. Seven different weighting schemes were used: Bartlett, Hanning, Hamming, Blackman, Binomial, Uniform and Butterworth. Although these weighting schemes may not represent optimal weighting methods, they do illustrate the cancellation ability of easily generated weights. Through a subroutine change, more complicated, better "matched" filters, similar to those suggested by Delong and Hofstetter (Ref 21) and Spafford (Refs 58 and 62) could be implemented and tested. The cancellation ability of the seven filter schemes were tested against ground clutter, generated using the Gaussian function, with azimuth angle of 0° , 45° , and 90° and depression angles of 35° , 55° , and 75° .

Since this study was not intended to be a radar system design study, the radar parameters described in Appendix A were used for all test cases. A nonfluctuating target, with a 13 dbsm average RCS, at a range of 2350 kilometers was used for analysis. This range corresponds to a target at an altitude of 4.5 kilometers with a 45° depression angle relative to the radar system. The target was assumed to have a velocity of 617 m/s.

Clutter Comparisons

In this section the clutter spectrum, seen by a space based radar system is illustrated. Figures V-1 through V-5 show the clutter PSD for various depression angle/azimuth angle combinations generated using the Gaussian function approximation method. The various curves in each figure represent different azimuth boresight angles. The clutter returns from sea and snow/ice backgrounds are illustrated in Figures V-6 and V-7. The different curves in each figure represent different boresight depression angles. The sea and snow/ice clutter returns assumed a Gaussian function.

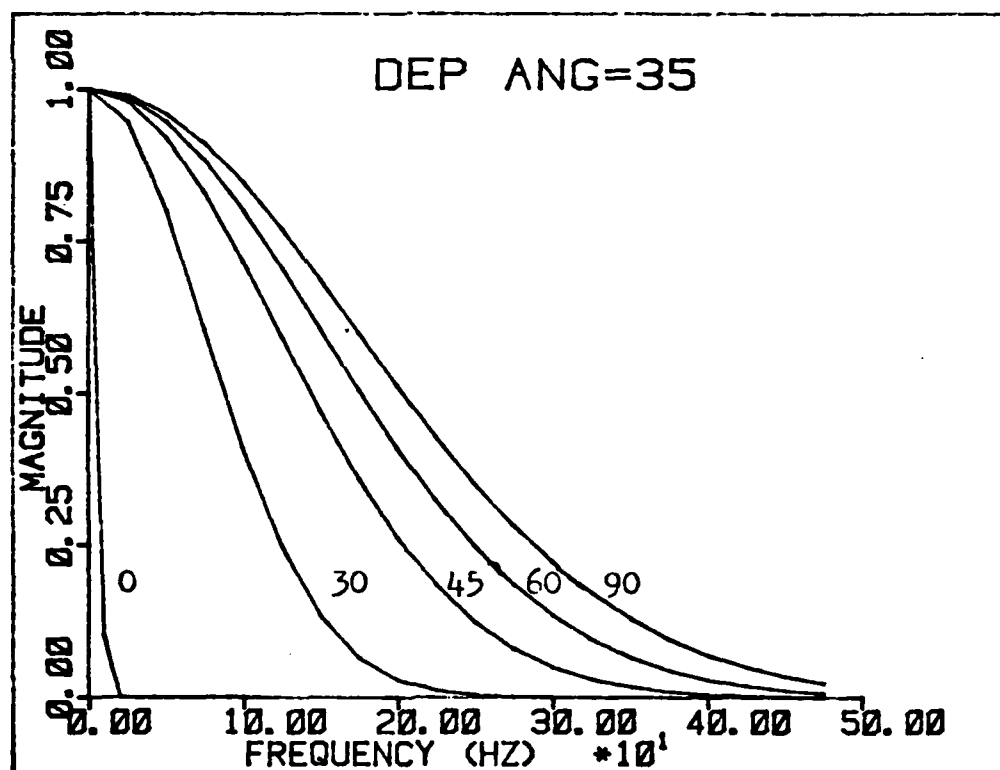


Fig. V-1 Ground Clutter PSD for 35° Boresight Depression Angle

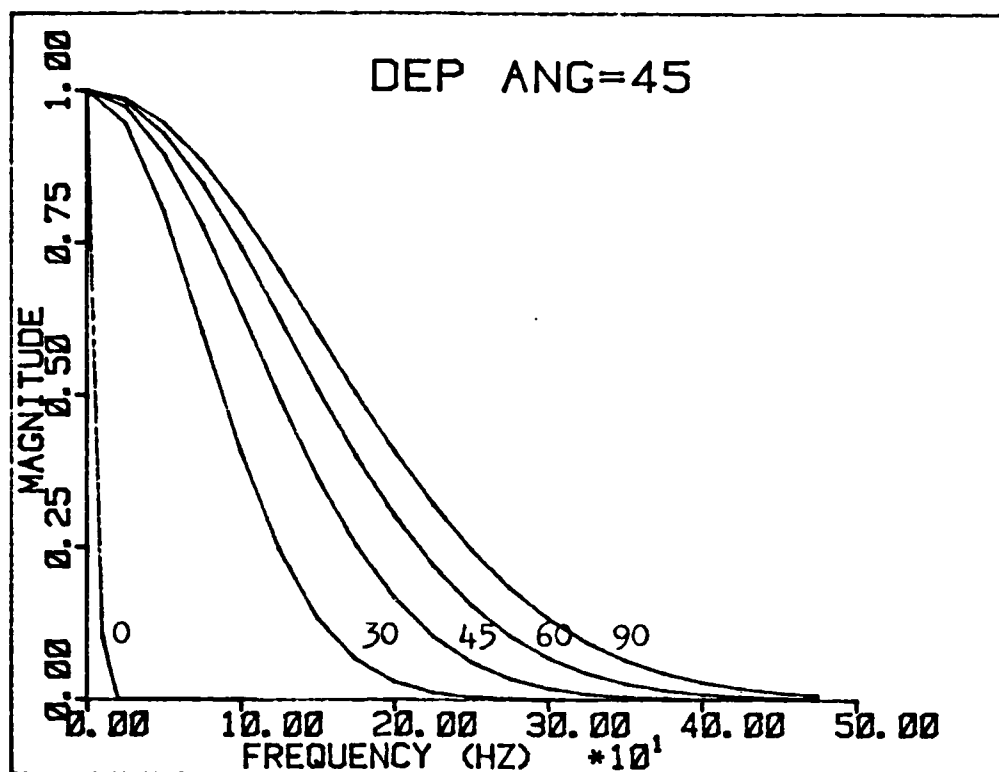


Fig. V-2 Ground Clutter PSD for 45° Boresight Depression angle

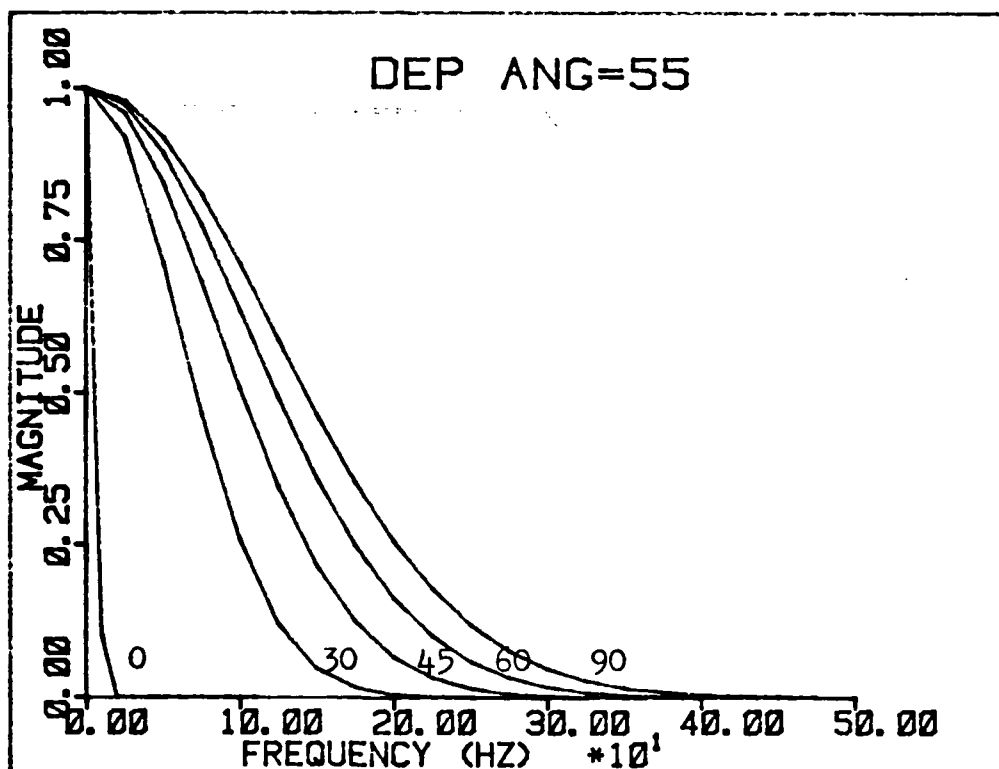


Fig. V-3 Ground Clutter PSD for 55° Boresight Depression Angle

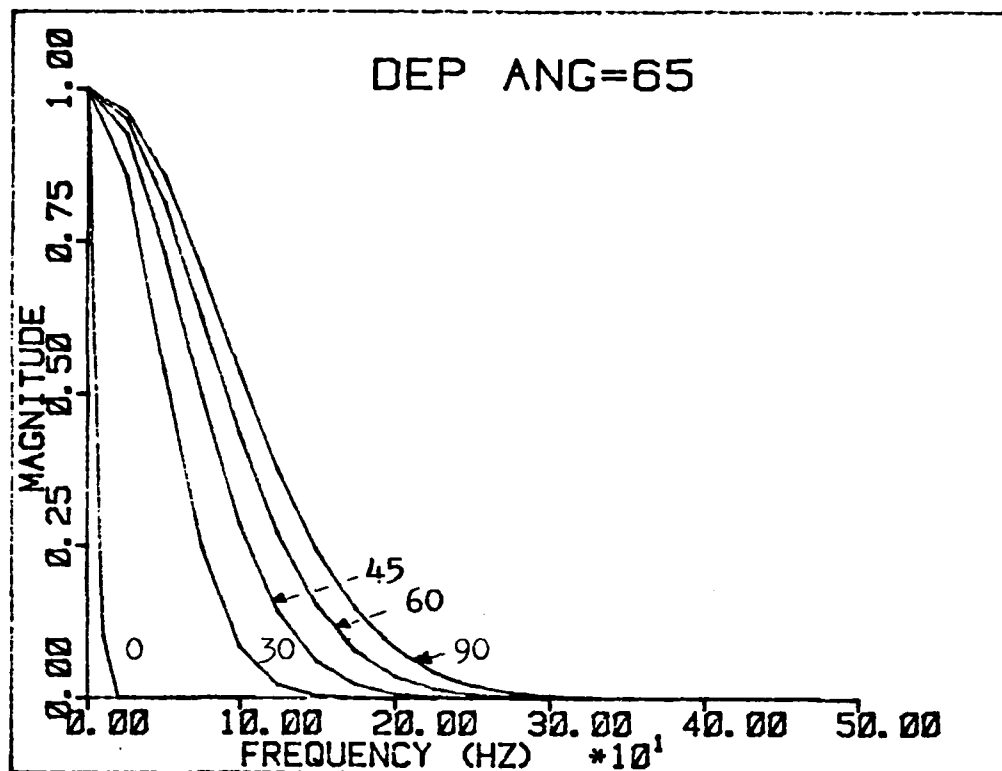


Fig. V-4 Ground Clutter PSD for 65° Boresight Depression Angle

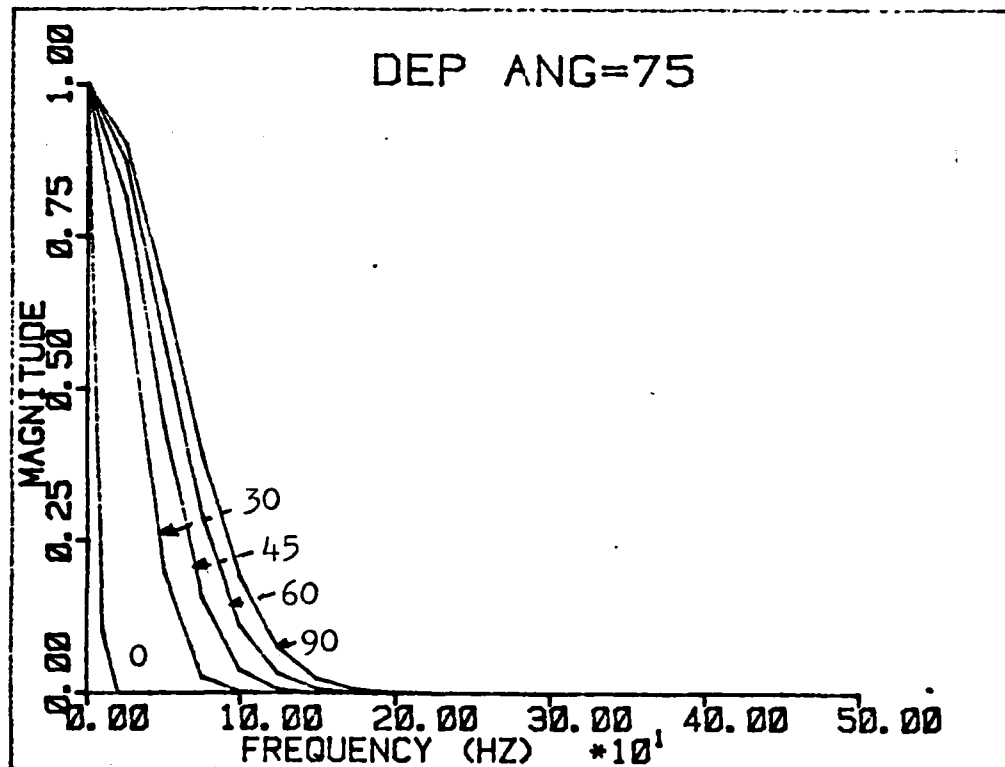


Fig. V-5 Ground Clutter PSD for 75° Boresight Depression Angle

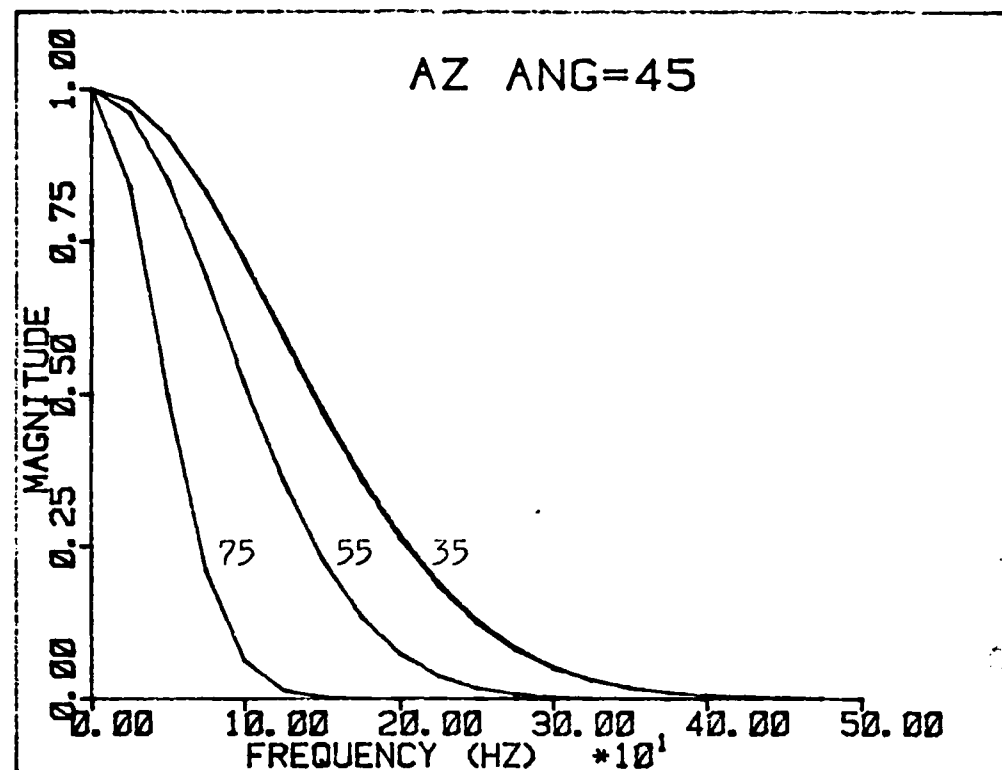


Fig. V-6 Sea Clutter PSD for 45° Boresight Azimuth Angle

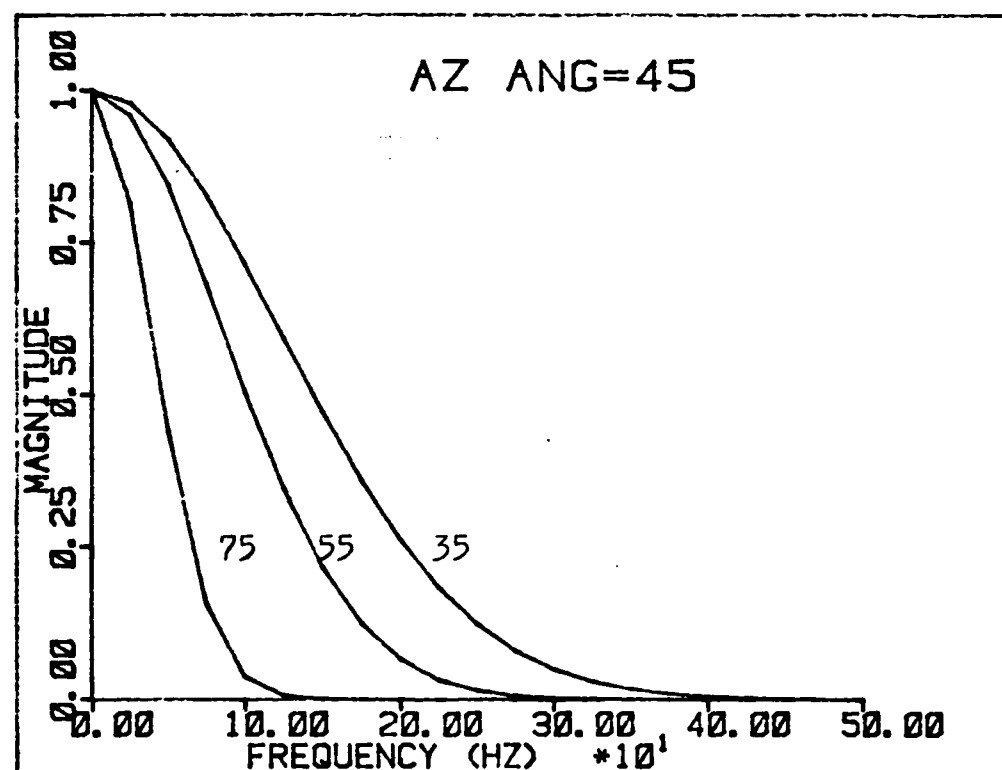


Fig. V-7 Snow/Ice Clutter PSD for 45° Boresight Azimuth Angle

From Figures V-1 through V-5, we observe that by increasing the antenna boresight azimuth angle the clutter spectrum spread increases. Using Figure V-3 for example, the 3db power point occurs at 6.25 Hz for 0° azimuth angle, at 73.75 Hz for 30° azimuth angle, at 100.98 Hz for 45° azimuth angle, at 124.96 Hz for 60° azimuth angle and at 142.5 Hz for 90° azimuth angle. This is as expected from equation III-35, which explained the causes of clutter spread.

Increasing the depression angle, which likewise increases the grazing angle, effects the clutter spectrum in two ways. First, the greater the depression angle the less the clutter spread, again per equation III-35. This is illustrated in Figures V-1 through V-5. Using the 45° azimuth angle as a comparison point, Table V-1 illustrates the decrease in frequency where the 3 db power point occurs for increasing depression angles.

Table V-1
Depression Angle Influence on Clutter Spread

Depression Angle	Frequency of 3 db Point
35°	148 Hz
45°	127.5 Hz
55°	105 Hz
65°	66.25 HZ
75°	47.50 Hz

From Table V-1 we see a 4.92 db reduction in frequency spread for a 75° depression angle relative to a 35° depression angle. Because MTI target detection is based upon doppler differential, it is important to understand the amount of clutter spread associated with different viewing geometries. Surveillance strategies should try to operate with look angles so as to minimize clutter spread.

The second effect depression angle has on clutter returns is an increase in clutter power with increasing depression angle. Table V-2 shows the increase in received clutter power for different depression angles over the clutter power received for a 35° depression angle.

Table V-2
Depression Angle Influence on Received Clutter Power

Depression Angle	Clutter Power Increase
45°	1.87 db
55°	4.61 db
65°	9.25 db
75°	15.76 db

The increase in power is because the range to the clutter patch is reduced with increasing depression angle.

Figure V-6 and V-7 show the clutter spectrum for sea and snow/ice backgrounds respectively. Comparing the curves of V-6 and V-7 with the 45° azimuth angle curves of Figures V-1

through V-5, we see very little change in clutter spread for different backgrounds. Although the clutter spread from sea and snow/ice backgrounds differs little from ground backgrounds, there is however, a reduction in amount of clutter power. Tables V-3 and V-4 indicate the reduction in clutter return from sea and snow/ice as compared to ground clutter returns.

Table V-3

Comparison of Ground / Sea Clutter Power

Depression Angle	Ground/Sea Power Ratio
35°	-23.26 db
55°	-12.83 db
75°	-7.64 db

Table V-4

Comparison of Ground / Snow-Ice Clutter Power

Depression Angle	Ground/Snow-Ice Power Ratio
35°	-8.5 db
55°	-3.86 db
75°	-4.0 db

The reduction in sea and snow/ice clutter power return is due

to the increase in diffuse reflection that occurs in sea and snow/ice backgrounds.

Due to a limitation in time, the second method for clutter PSD calculation was not executed and compared with the Gaussian clutter PSD calculation method. Had this second method been run, we would have seen a greater spread in clutter as compared to the first method and an increase in the amount of clutter. This is because the second method calculates the clutter contribution of all illuminated earth area and not just the area illuminated by the mainbeam.

Cancellation Scheme Comparison

The ability of a particular cancellation system to eliminate clutter is, as seen from the development in Chapter III, based upon the ability of a filter, or set of filters, to cancel the spectral components which correspond to clutter, while preserving target spectral energy. Regardless of whether the spectral information is obtained indirectly, as in a delay line canceler system, or directly, an indication of the cancellation ability of any doppler clutter cancellation method can be obtained by analyzing the filters.

Because the transversal filter can be used to implement a delay line canceler system or a filter bank system, it is used in this study as a basis for comparison of different clutter cancellation systems. That is, it is assumed that different configurations of the transversal filter represent

different cancellation systems. The filters analyzed are intended to represent front end filters, cancelling the clutter spectrum, while allowing for signal detection in separate filter circuitry. To maintain perspective as to where these filters fit into the radar signal processing chain, the transversal filters analyzed would be used at the doppler filter bank block in Figure III-5.

Before analyzing the clutter cancellation ability of a multitude of transversal filters against the various clutter spectrum described in Figures V-1 through V-5, a pragmatic approach to limit the number of filters studied was necessary. The ideal filter response for cancelling clutter, as described in Chapter III, was one that possessed a notch at dc and all PRF harmonics wide enough to cancel clutter yet not too wide so as to eliminate targets. There are three parameters in a transversal filter which can be varied to produce different spectral responses - 1) the weighting on each tap, 2) the time delay between taps, and 3) the number of taps. Figures V-8 through V-14 show the filter magnitude response due to Butterworth, Bartlett, Hanning, Hamming, Blackman, Binomial and uniform weighting schemes. Figures V-15 through V-18 show the filter response of a different delay time. Finally Figures V-19 through V-22 show the effect of varying the number of filter taps. The filters illustrated in all the figures, Figures V-8 through V-22 all have a periodic spectral response, with period $1/T$. T is the time delay between taps.

The number next to the curves in each figure indicates

the number of tap weights the filter has. The variable, N , indicates the number of points used to generate the filter curves.

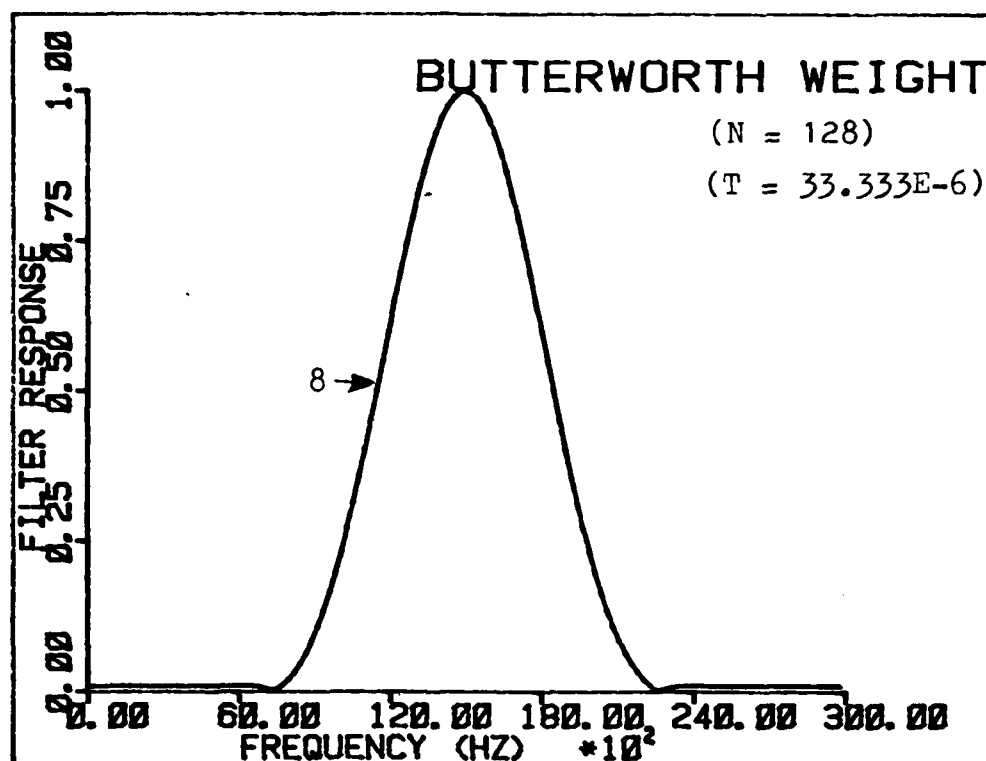


Fig. V-8 Transversal Filter with Butterworth Weights

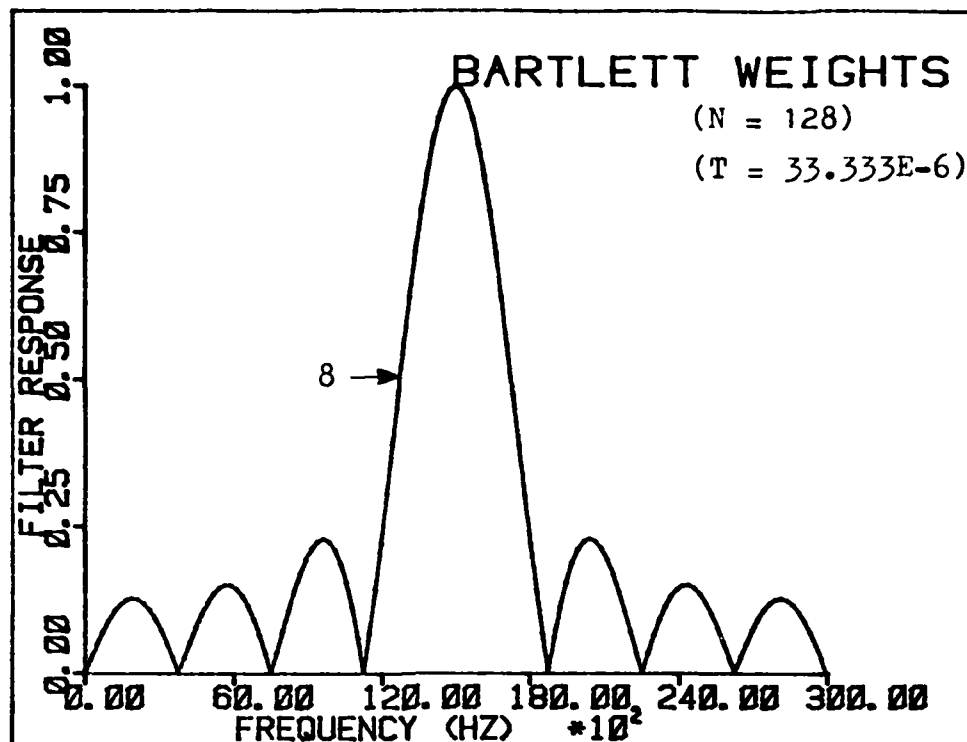


Fig. V-9 Transversal Filter with Hanning Weights

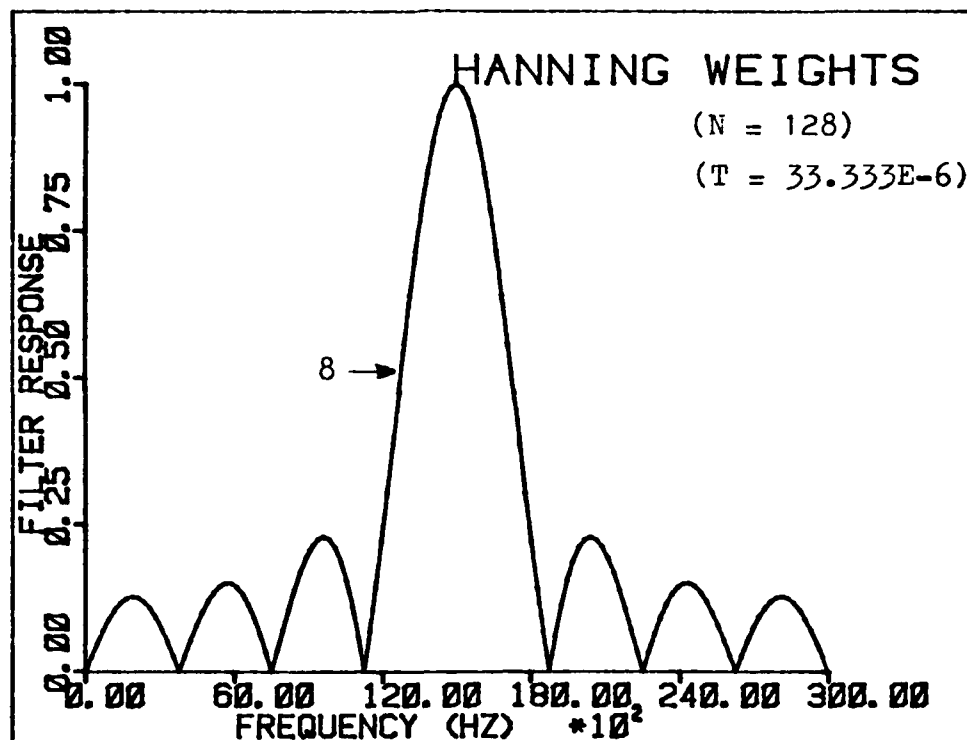


Fig. V-10 Transversal Filter with Hanning Weights

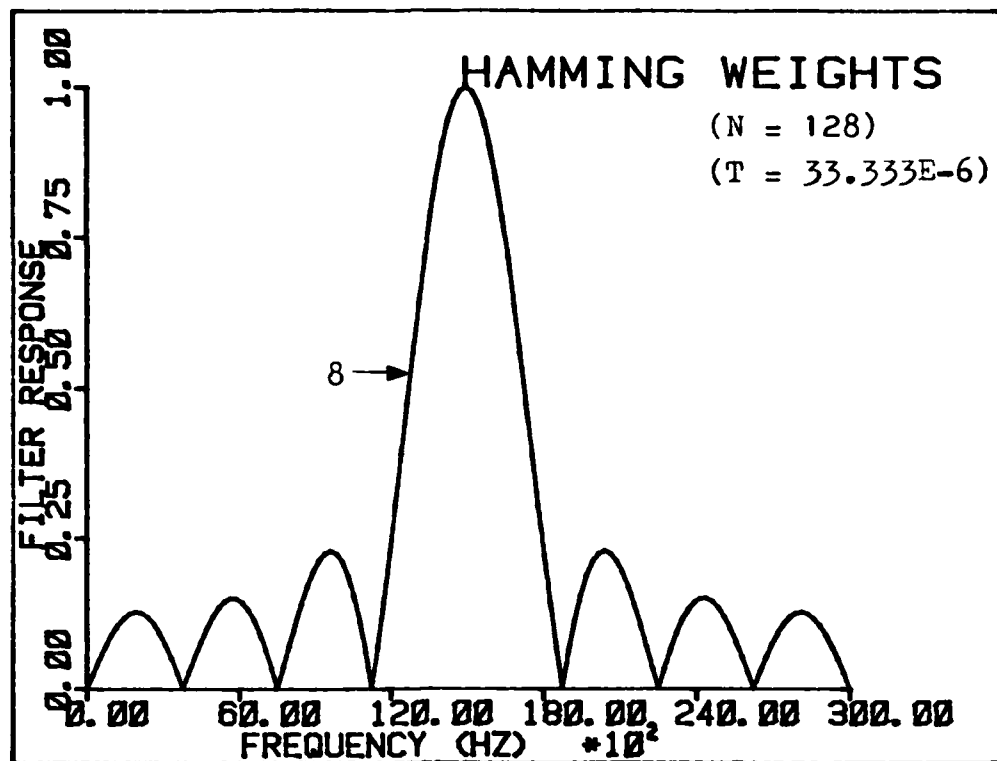


Fig. V-11 Transversal Filter with Hamming Weights

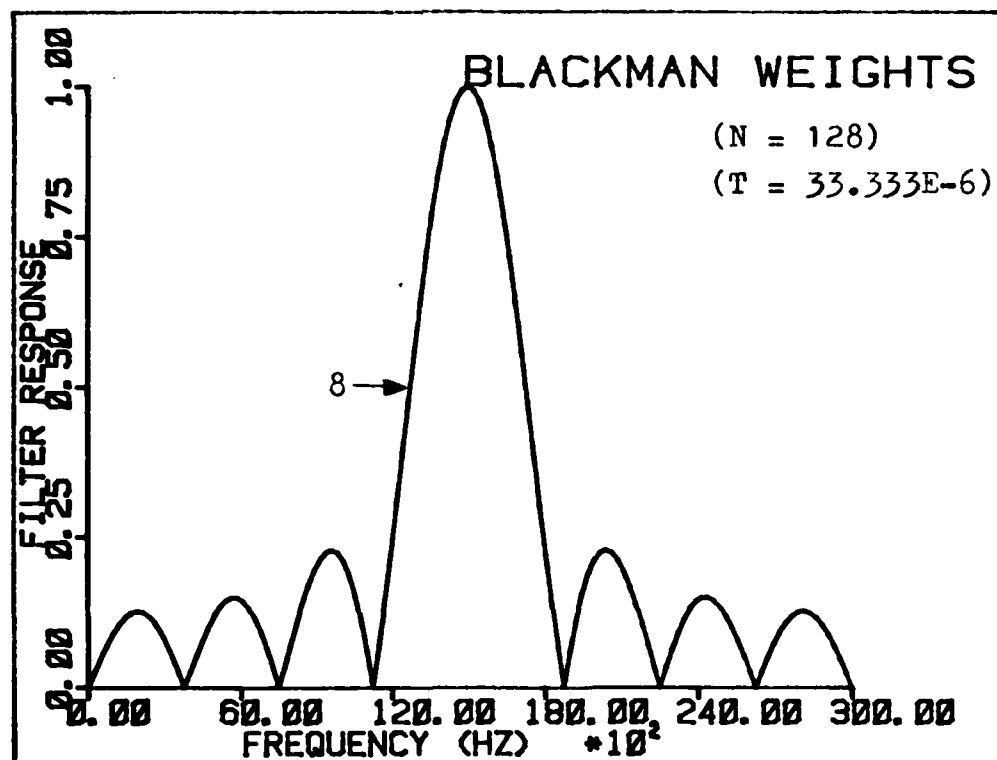


Fig. V-12 Transversal Filter with Blackman Weights

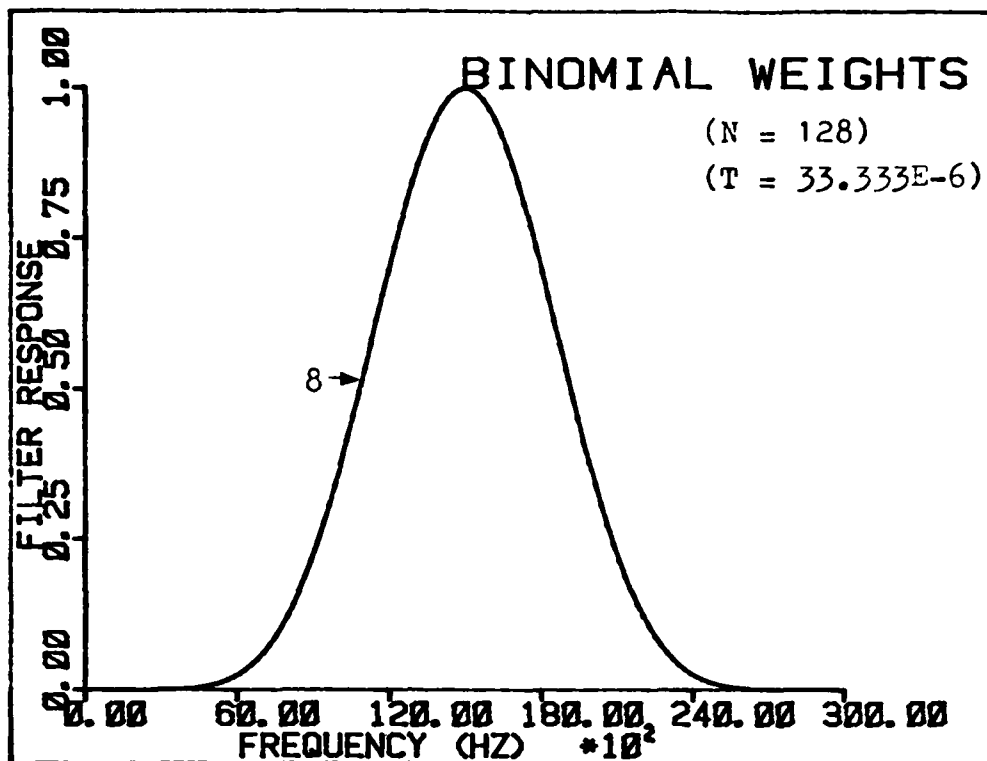


Fig. V-13 Transversal Filter with Binomial Weights

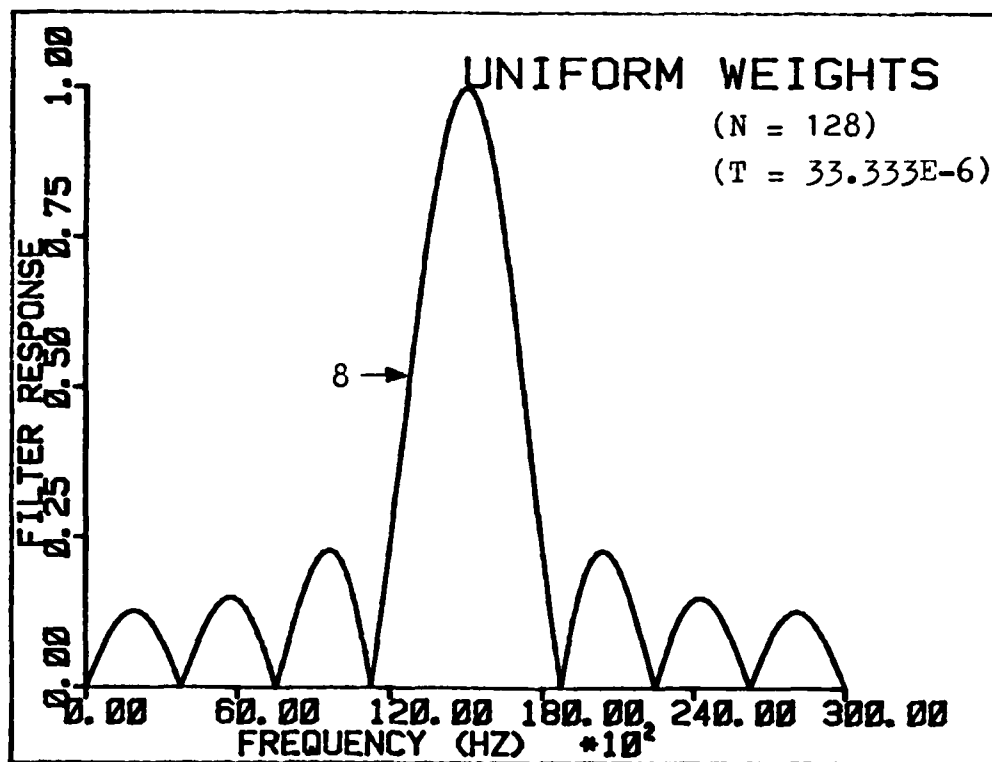


Fig. V-14 Transversal Filter with Uniform Weights

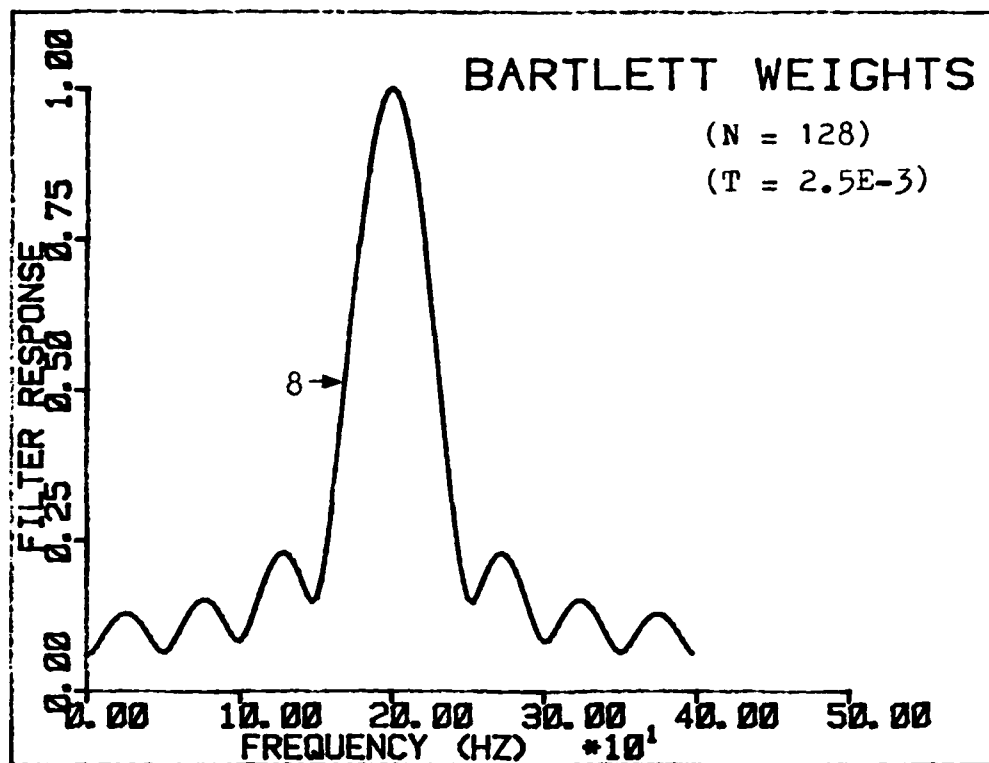


Fig. V-15 Transversal Filter with Bartlett Weights

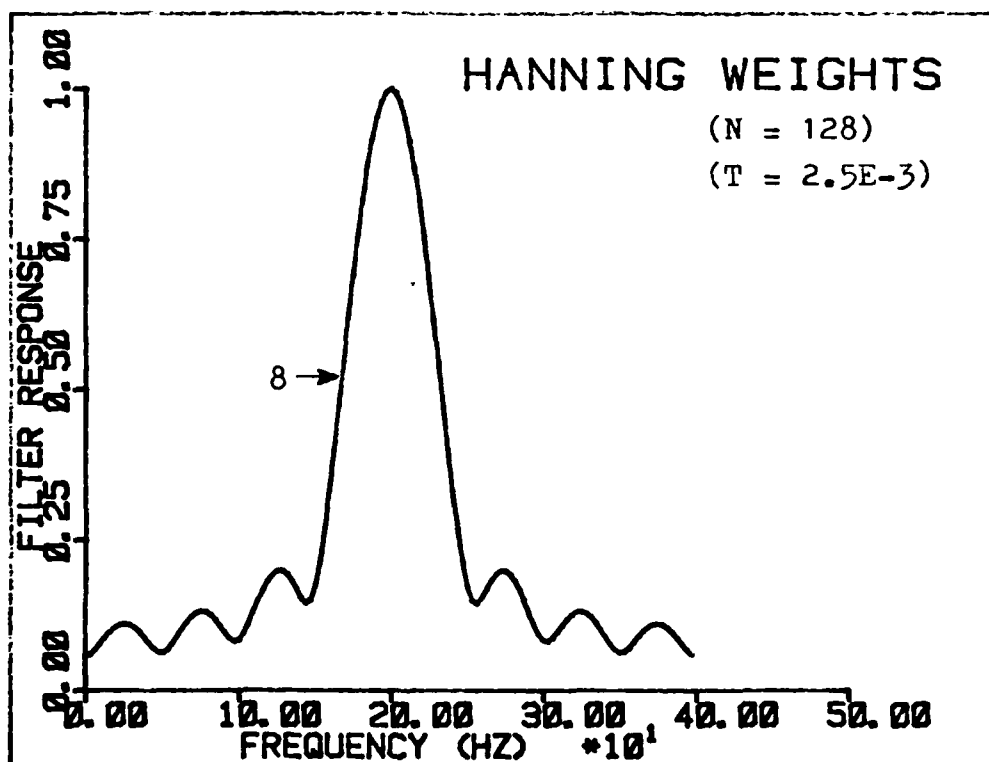


Fig. V-16 Transversal Filter with Hanning Weights

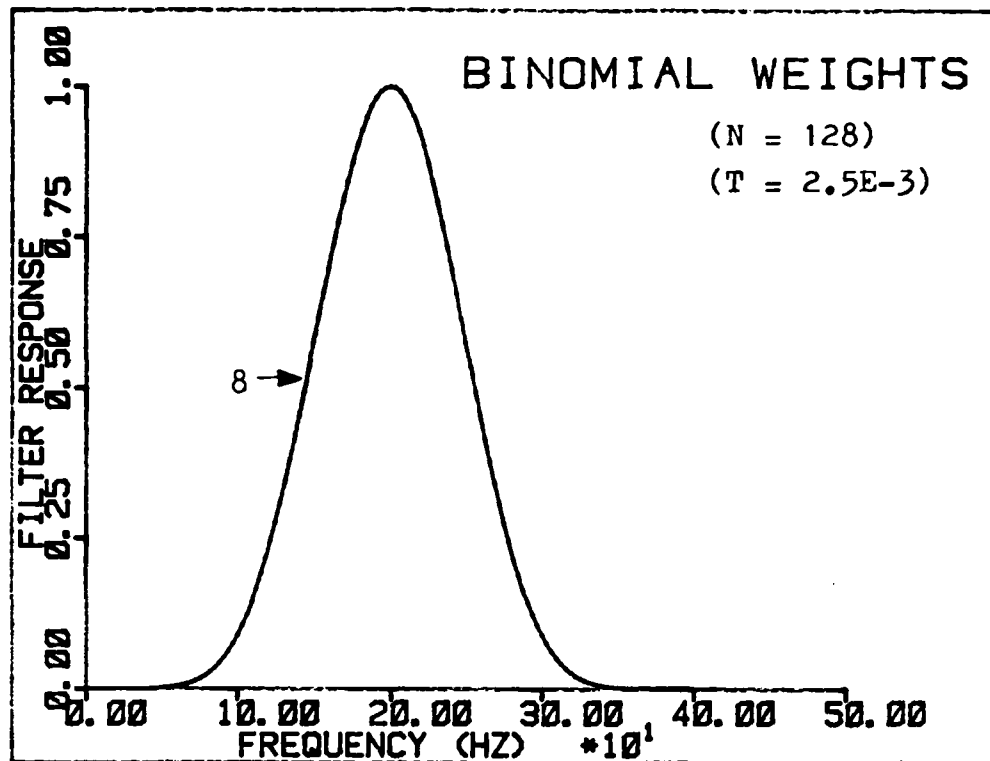


Fig. V-17 Transversal Filter with Binomial Weights

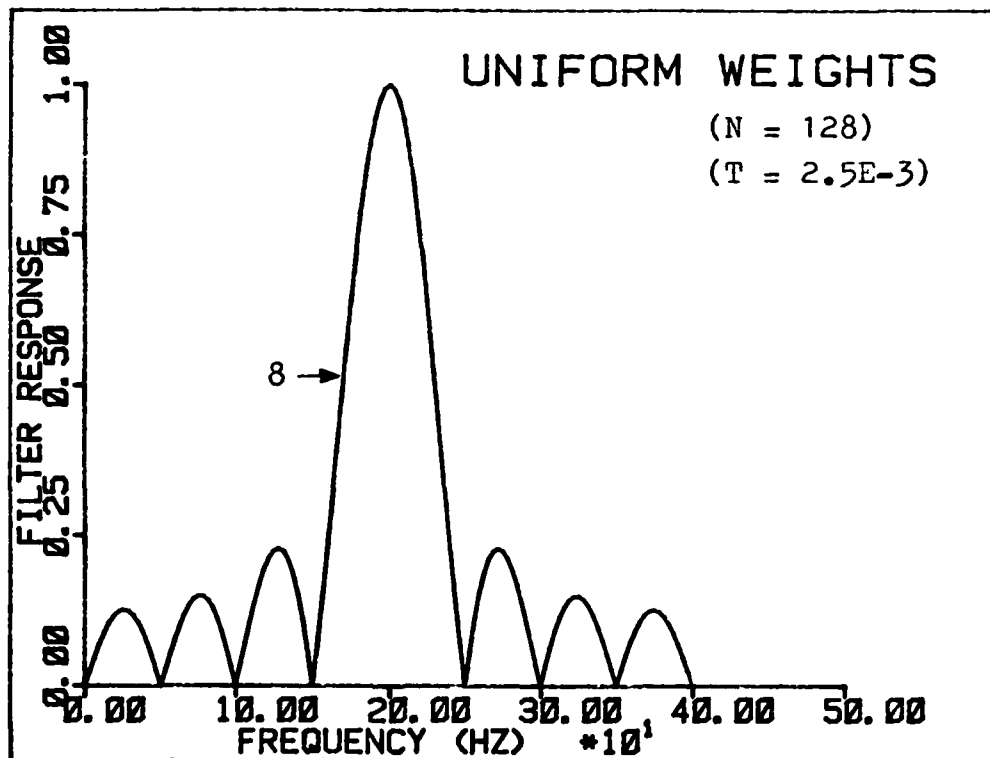


Fig. V-18 Transversal Filter with Uniform Weights

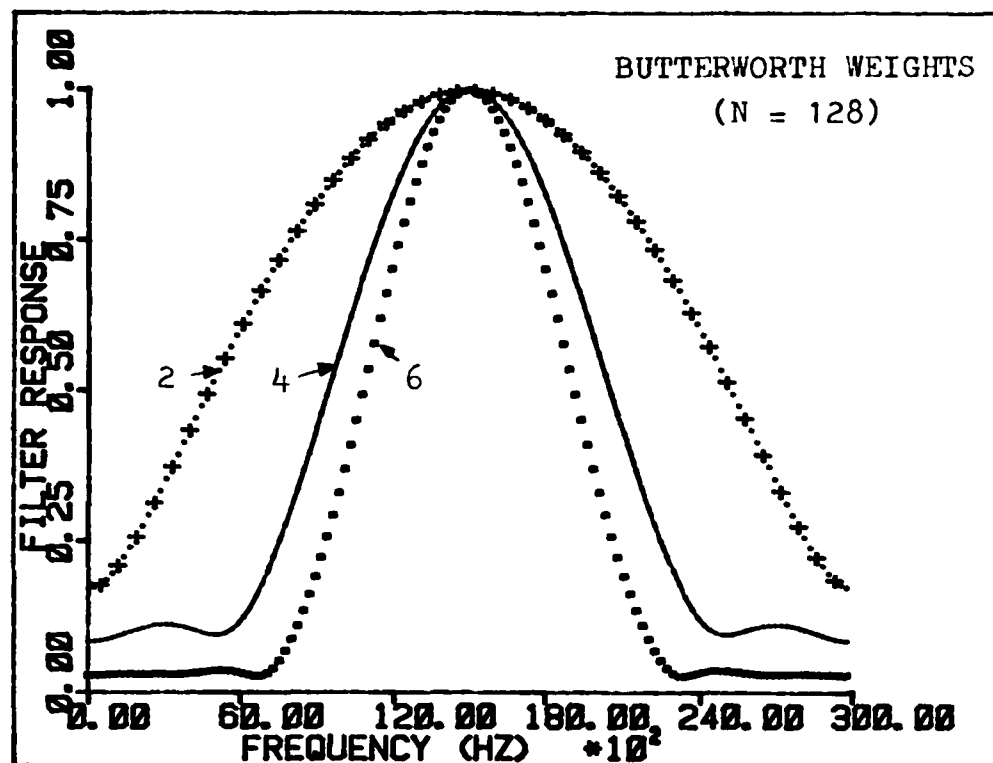


Fig. V-19 Butterworth Weighted Filter (Even number of Taps)

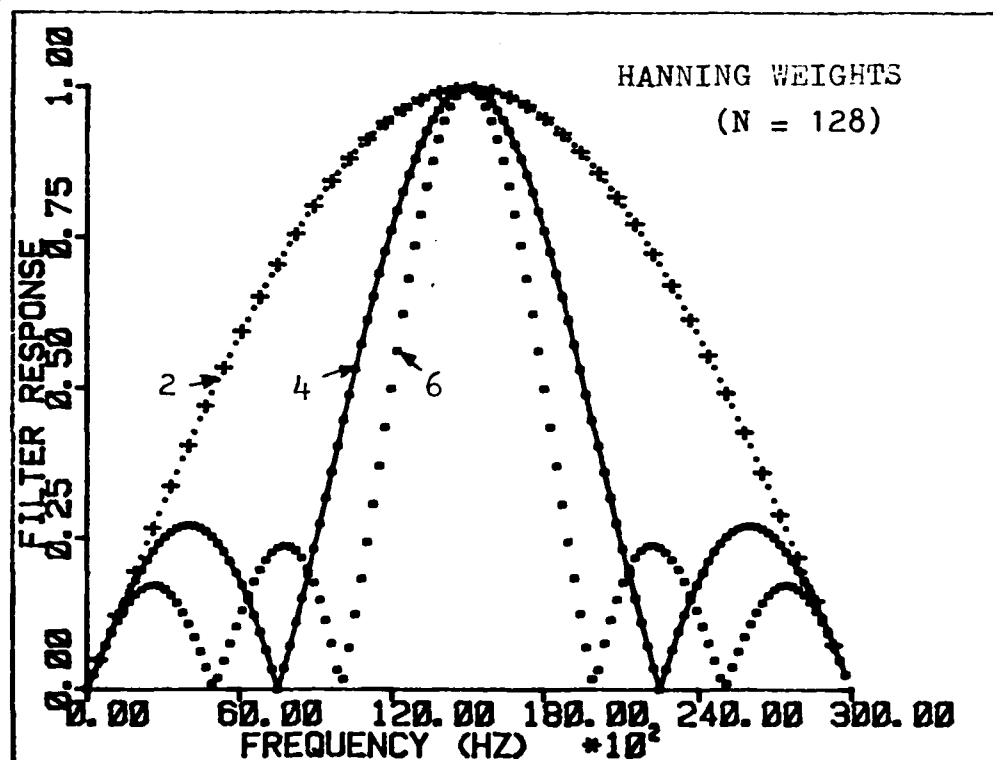


Fig. V-20 Hanning Weighted Filter (Even number of Taps)

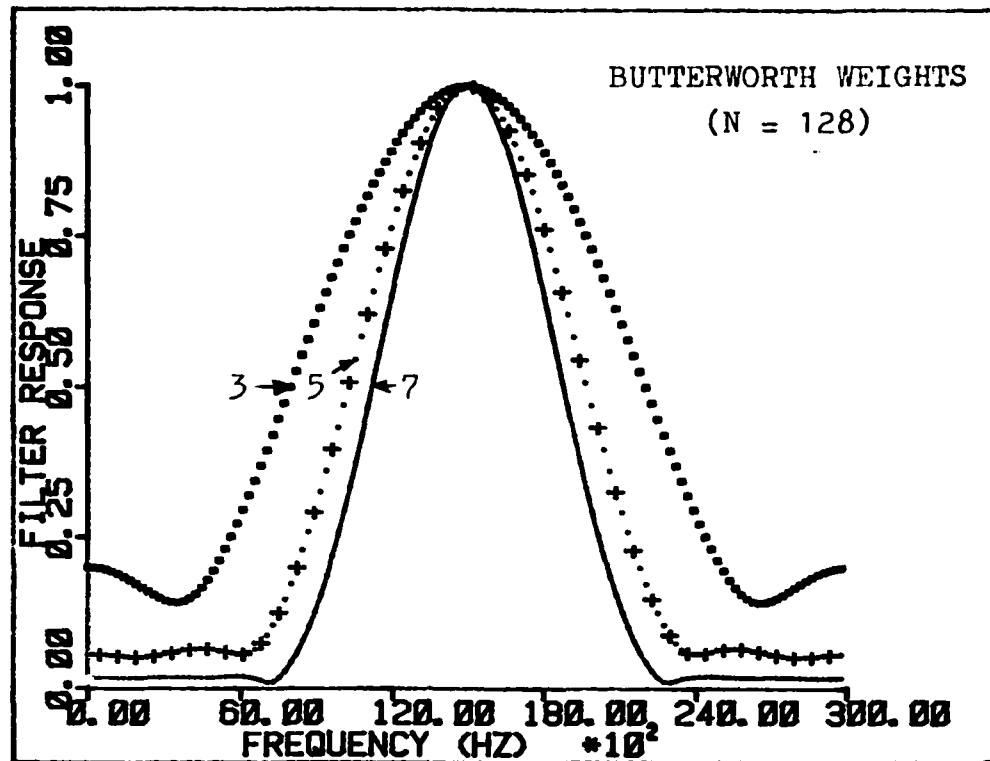


Fig. V-21 Butterworth Weighted Filter (Odd number of Taps)

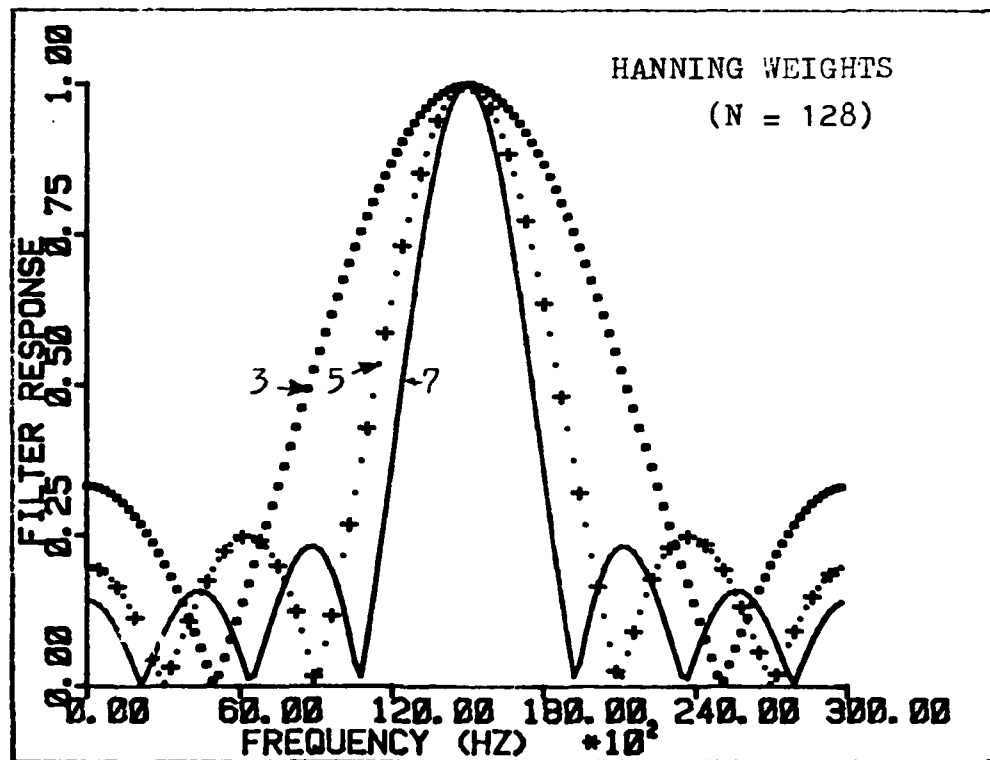


Fig. V-22 Hanning Weighted Filter (Odd number of Taps)

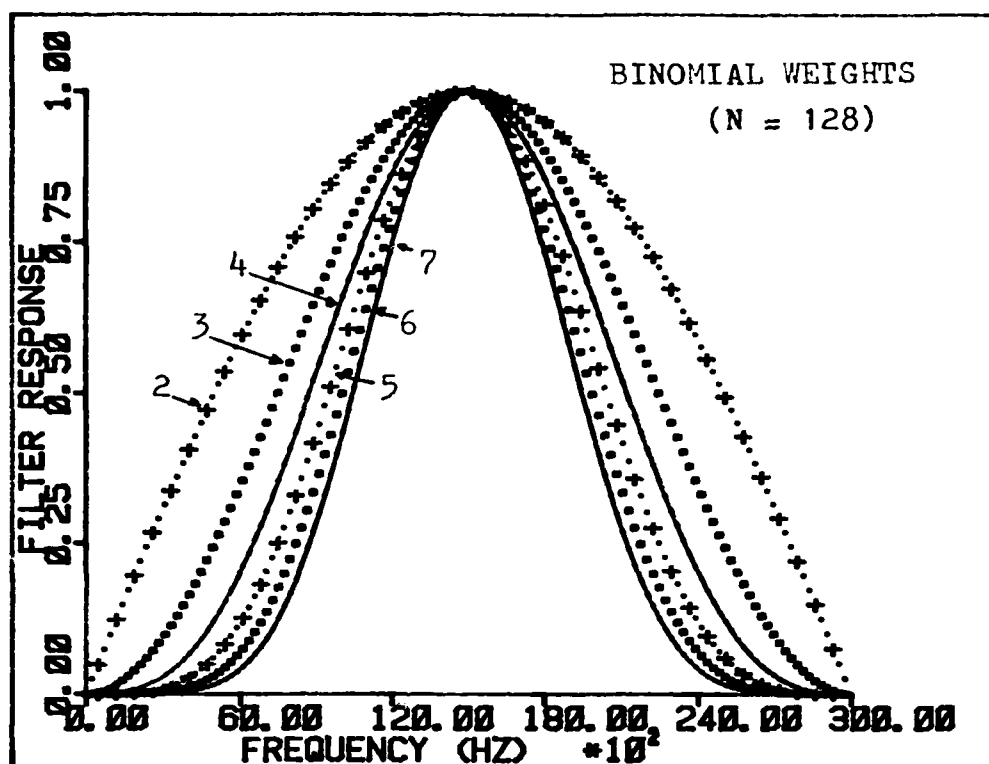


Fig. V-23 Binomial Weighted Filter with Different Number of Taps

Comparison of Figures V-8 through V-14 shows a great similarity between Bartlett, Hanning, Hamming, Blackman and uniform weighting schemes. This is to be expected since the weight values for these five schemes are similar, varying from between ± 1 . The Butterworth and Binomial responses are characterized by a broad mainlobe response, broader than the mainlobe response of the other five weighting schemes, and essentially nonexistent sidelobes. (The Butterworth filter has a 3 db bandwidth of 7125 Hz, the Binomial filter has a 3

db bandwidth of 8325 Hz and the Hanning filter has a 3 db bandwidth of only 4500 Hz.) The low sidelobes and broader mainlobes are due to the dynamic range of the Butterworth and Binomial weight values. The slight sidelobes which the Butterworth filter exhibits is due to the asymmetric nature of the Butterworth weights.

Figures V-15 through V-18 show the effect of changing the time delay between taps. Increasing the delay time has three effects on the filter response : 1) reduces the bandwidth of the filter, 2) reduces the depth of the sidelobe nulls, and 3) reduces the sidelobe levels. Because the filter response with delay times greater than $33.333\text{E-}6$ (reciprocal of the possible target doppler bandwidth) do not span the entire spectrum in which a target could be present, and delay times less than $33.333\text{E-}6$ span a spectral region greater than necessary, thereby increasing the amount of noise, only delay time equal to $33.333\text{E-}6$ seconds needs be used. If a bank of narrowband filters is to be implemented, then delay times greater than $33.333\text{E-}6$ would be necessary, with the delay dependent on the bandwidth of the filter desired. The trends that are seen with a filter having a delay time equal to $33.333\text{E-}6$ will, however, apply to a filter with different delay times.

Figures V-19 through V-22 illustrate Binomial, Butterworth and Hanning weighting schemes with different number of tap weights. The Bartlett, Hamming, Blackman, and uniform weighting schemes were eliminated because of the

similarity with the Hanning weighting scheme. The mainlobe of the filter response using either the Butterworth, Hanning, or Binomial weighting schemes, broadens as the number of taps is reduced. This is again due to the reduction in dynamic range of the weights. The Butterworth filter and the Hanning filter with an odd number of taps, both exhibit nonzero filter responses at frequencies less than 400 Hz where clutter is the greatest. This undesired high response worsens as the number of taps decreases. Because of the high filter response in the low doppler regions, the Butterworth filters and the Hanning filter with an odd number of taps, can be eliminated from further analysis.

After systematic analysis of various filters, only filters with Binomial weights and Hanning weights with an even number of taps, need to be analyzed for clutter cancellation ability. It is interesting to note that a Hanning filter with two taps has the same response as a Binomial with two taps, therefore the two tap Hanning filter can also be eliminated from further analysis. The curves in Figures V-1 through V-5 show that the most stressing clutter case is when the antenna boresight has a 35° depression angle and a 90° azimuth angle. Table V-5 illustrate the clutter attenuation factor of a transversal filter with Binomial weights with different number of taps and a filter with Hanning weights with four and six taps.

Table V-5

Clutter Attenuation Factor for Different Cancellation Schemes

Weighting Scheme	Number of Taps	Clutter Attenuation Factor
Binomial	2	30.697 db
Binomial	4	76.623 db
Binomial	5	96.904 db
Binomial	7	134.681 db
Binomial	8	152.363 db
Hanning	4	24.694 db
Hanning	6	21.201 db

From Table V-5 we see there is a 122 db improvement in clutter attenuation by using an eight tap Binomial filter instead of a two tap Binomial filter, however, this is at the expense of detecting targets. Comparing the Hanning and Binomial weighting schemes we observe a 32 db reduction in attenuation using a four tap Hanning filter instead of a four tap Binomial filter and a 94 db reduction in attenuation using a six tap Hanning instead of a six tap Binomial.

Table V-5 provides attenuation figures for only one particular viewing geometry. With different viewing geometries the clutter attenuation will vary because the clutter spread varies, thereby changing the ratio of the clutter into and out of the filter. Table V-6 shows the clutter attenuation factor for different viewing geometries using a four tap Binomial filter.

Table V-6

Clutter Attenuation Factor for Different Viewing Geometries

Azimuth Angle	Depression Angle	Clutter Attenuation Factor
45°	35°	86.144 db
90°	35°	76.623 db
45°	55°	94.857 db
90°	55°	86.374 db
45°	75°	157.264 db
90°	75°	118.190 db

The average clutter attenuation factor provides a better indication of the cancellation ability for a surveillance radar since the viewing geometries continually change. The mean clutter attenuation for a four tap Binomial transversal filter is 103.24 db.

From observation of Figures V-8 through V-22 and Table V-5, it is apparent that the Binomial weighted transversal filter provides the best cancellation ability of any of the filters tested. Variations on the Binomial weighting scheme were tested, but with no increase in attenuation factor.

Chapter VI Conclusions and Recommendations

Conclusions

To prudently handle the clutter cancellation problem a method of mathematically describing the target signal and clutter return was needed. It was found that the most efficient method for description was in the frequency domain, in terms of the power spectral density. In Chapter II it was proven that the power spectral density could be determined for a deterministic (i.e. target) and random (i.e. clutter) signal. Since both clutter and target returns were easier to describe in the frequency domain, signal analysis was also described in the frequency domain. It turned out that signal analysis essentially reduced to designing the matched filter which would accomplish the correlation principle, normally implemented via a convolution integral. The design and analysis of the matched filter were easier in the frequency domain because the transformation between the time and frequency domains, accomplished by the Fourier transformation, eliminates the need to perform convolution integral and instead performs simpler algebraic manipulations. If the clutter environment statistics are known, then with the aid of the ambiguity function an "optimal" waveform-filter pair could be defined.

The survey of doppler clutter cancellation methods showed that clutter cancellation is accomplished by distinguishing clutter returns from target returns by the

velocity differential between the two. This velocity differential manifests itself as power spectra located at different frequencies. The cancellation occurs by eliminating those spectral components which correspond to clutter. If the environment and the geometry of the particular surveillance situation are given, the PSD of the clutter can be predetermined, thus allowing for proper spectral nulling. This relatively straightforward approach to eliminating clutter is complicated when the target and clutter velocity differential is such that the target power spectral components overlap the spectral components of clutter. For a space-based radar system, the situation of a low velocity differential between clutter and target spectrum arises either because of the geometry of the particular surveillance situation and/or because of the radar system's platform motion. In the previous chapter we saw that the greatest clutter spread occurs at small depression angles and large azimuth angles. We also observed that clutter energy, after clutter locking compensation, is centered about zero Hz and spreads out to greater than 400 Hz. The cancellation of clutter in the low doppler (velocity) regions is the essence of the clutter cancellation problem.

If the system compensation methods are ignored, i.e. DPCA or monopulse anomalous nulling, the clutter cancellation problem reduces to a filter design problem. Because of the large area which the space-based radar must survey, there is a vast number of detection cells which must be analyzed. This

necessitates that the filters be implemented digitally. The choice must be made whether the filters should be implemented via recursive equation, thereby taking advantage of the vast experience in the design of analog filters or implementing the filters via nonrecursive equations, which can be computed using one of the various FFT algorithms. Because recursive equations cannot be implemented via FFT operations, and also because the transient period for stabilization tends to be longer for recursive filters, nonrecursive filters were utilized for various clutter cancellation schemes.

Since the transversal filter can be used to represent either a delay line canceler or a filter in a filter bank, analyzing the spectral nulling of different transient filters provides an indication of the clutter cancellation ability of different cancellation schemes. In Chapter V the spectral response of transversal filters with seven different weighting schemes, with different tap delay times, and with different numbers of taps were all examined to determine which transversal filter configuration provided sufficient clutter cancellation. It was shown that a transversal filter using the Binomial weighting scheme and a tap delay time equal to the reciprocal of the target doppler bandwidth provided the best clutter cancellation. Increasing the number of taps broadened the filter spectral null, thereby improving the clutter cancellation at the expense of eliminating more targets. A four tap Binomial weighted transversal filter provided 103.24 db of average clutter attenuation, a value

sufficiently adequate to cancel clutter and obtain target range and velocity information.

Recommendations

The primary objective of this study was to organize, define and develop the nature and description of the spaceborne radar clutter cancellation problem. Besides the development of the clutter problem, a secondary objective was to develop a computer tool that would 1) implement the equations and concepts which describe the clutter problem so a fuller understanding of the clutter problem could be gained and 2) provide a vehicle to test various clutter cancellation methods. This study concentrated on only doppler cancellation methods, which digitally filtered the radar echo signal by application of one of several FFT algorithms. Although this study has concisely tied together the clutter cancellation problem, there are still many areas which require further research.

In this study, the spectrum of the echo signal was canceled by a nonrecursive filter, implemented by FFT algorithms. There are several other methods of estimating the spectra based on modeling the clutter as a rational function and then determining the coefficients for the specific situation. The relative merits of these other spectral estimation techniques should be explored and compared in terms of the clutter attenuation factor and operational speed. Ref 34 provides an excellent reference to initiate the analysis.

The continuing change in the clutter statistics, especially due to the platform's motion results in filter mismatches. The use of an adaptive algorithm such as the one suggested by Applebaum, Ref 1, or Reed and Brennen, Refs 8 and 10 to modify the matched filters should be explored. This effort should compare the clutter attenuation factor of each of the algorithms with that of a fixed matched filter.

Several system platform motion compensation methods were discussed, but not analyzed. The effects of these methods on the total radar system and the gain in attenuation factor should be determined.

To limit the size of this study, nondoppler clutter cancellation techniques were not considered. The nondoppler cancellation techniques should be analyzed, and their clutter reduction ability quantitatively determined. Normally, the benefits of nondoppler techniques have been described in terms of probability of detection. A performance measure similar to the clutter attenuation factor should be developed and then the doppler and nondoppler cancellation techniques should be compared.

Finally, the simulation of the clutter cancellation problem was accomplished through the application of the radar range equation. This somewhat simplistic approach to the problem is based upon approximations to the power levels. A theoretically more accurate and thorough approach to the modeling of the clutter problem would be to perform a video signal simulation, simulating the interaction of the

transmitted video signal with the target and the clutter scatterers. Although a video simulation would be more complex and utilize more computer time, a finer sensitivity to the response of various filters could be obtained.

Bibliography

1. Applebaum, S.P. "Adaptive Arrays," IEEE Transactions on Antennas and Propagation. Vol. AP-24, No. 5: 585-597 (September 1976).
2. Andrews, G.H. Optimal Radar Doppler Processors. Washington, D.C.: Naval Research Laboratory, May 29, 1974. (AD920000).
3. -----, "Radar Antenna Pattern Design for Platform Motion Compensation," IEEE Transactions on Antennas and Propagation. Vol. AP-26. No. 4: 566-571 (July 1978).
- ✓ 4. Baily, J.C., Kluck, J.H., et al. Space Based Radar for Atmospheric Tactical Warning - Phase II (U). El Segundo, California: Aerospace Corporation, 25 January 1982. (TOR-0082(2411)-6) (Secret).
5. Barlow, E.J., "Doppler Radar," Proceedings of the IRE, Vol. 37, No. 4: 340-355 (April 1949).
6. Barton, D.K. Radar System Analysis. New Jersey: Prentice Hall, 1964.
7. Beauchamp, K.G. Signal Processing Using Analog and Digital Techniques. New York: John Wiley & Sons, 1973.
8. Brennan, L.E., Mallett, J.D., and Reed, I.S., "Adaptive Arrays in Airborne MTI Radar," IEEE Transactions on Antennas and Propagation, Vol. AP-24, No. 5: 607-615 (September 1976).
9. Brennan, L.E., and Reed, I.S., "Optimal Processing of Unequally Spaced Radar Pulse Trains for Clutter Rejection," in MTI Radar, Ed. by D.C. Schleder. Massachusetts: Artech House, Inc., 265-268 (1978).
10. -----, "Theory of Adaptive Radar," IEEE Transactions on Aerospace and Electronic Systems Vol. AES-9, No. 2: 237-251 (March 1973).
11. Berkowitz, R.S. Modern Radar Analysis, Evaluation, and System Design. New York: John Wiley and Sons, Inc., 1965.
12. Brookner, E. Radar Technology. Massachusetts: Artech House Inc., 1977.
13. Burdick, W.S. Radar Signal Analysis. New Jersey: Prentice Hall, Inc., 1968.
14. Capon, J., "Optimal Weighting Functions for the Detec-

- tion of Sample Signals in Noise," in MTI Radar, Ed. by D.C. Schleher. Massachusetts: Artech House, Inc., 255-262 (1978).
15. Cochran, W.T., et. al., "What is the Fast Fourier Transform?" in Digital Filters and the Fast Fourier Transform, Ed. by B. Liu. Pennsylvania: Dowden, Hutchinson & Row, Inc., 313-323 (1975).
 16. Cook, C.E. and Bernfeld M. Radar Signals An Introduction to Theory and Application. New York: Academic Press, 1967.
 17. Cooley, J.W., Lewis, P.A.W., Welch, P.D., "Application of the Fast Fourier Transform for Computation of Fourier Integrals, Fourier Series, and Convolution Integrals," in Digital Filters and the Fast Fourier Transform, Ed. by B. Liu. Pennsylvania: Dowden, Hutchinson & Row, Inc., 383-388 (1975).
 18. Cosgriff, R.L., Peake, W.H., and Taylor, R.C., "Terrain Scattering Properties for Sensor System Design (Terrain Handbook II)," in Radar Clutter, Volume 5, Ed. by D.K. Barton, Massachusetts: Artech House, Inc. 165-287 (1977).
 19. Dax, P.R., "Eliminating Clutter In Radar Systems," Microwaves: 34-43+ (April 1975).
 20. Deley, G.W., The Representation, Estimation and Design of Radar Signals. California: General Research Corporation, May 1967 (AD822609).
 21. Delong, D., F., Jr., and Hofstetter, E.M., "On the Design of Optimal Radar Waveforms for Clutter Rejection," IEEE Transaction on Information Theory Vol. IT-13, No. 3 454-463 (July 1967).
 22. DiFranco, J.V. and Rubin, W.L. Radar Detection. Massachusetts: Artech House Inc., 1980.
 23. DiNardo, U. and Nucci, G. "Synthesis Criteria of a Signal Processor for Pulse Doppler Radars," in CW and Doppler Radar, Volume 7, Ed. by D.K. Barton. Massachusetts: Artech House Inc., 247-260 (1978).
 24. Emerson, R.C., "Some Pulse Doppler MTI and AMTI Techniques," in MTI Radar, Ed. by D.C. Schleher, Massachusetts: Artech House, Inc., 77-142 (1978).
 25. Farrell, J.L., and Taylor, R.L., "Doppler Radar Clutter," in CW and Doppler Radar, Volume 7, Ed. by D.K. Barton. Massachusetts: Artech House Inc., 351-361 (1978).

26. Friedlander, A.L. and Greenstein, L.J., "A Generalized Clutter Computation Procedure for Airborne Pulse Doppler Radars," in CW and Doppler Radar, Volume 7, Ed. by D.K. Barton. Massachusetts: Artech House Inc., 364-373 (1978).
27. -----, A Program for Airborne Radar Clutter Analysis PARCA. Ohio: Aeronautical Systems Division, August 1979 (AD866369).
28. Glass, C.M. Linear Systems with Applications and Discrete Analysis. New York: West Publishing Co. 1976).
29. Gold B. and Rader, C.M. Digital Processing of Signals. New York: McGraw Hill, 1969.
30. Hansen, V.G. and Michelson, D., "A Comparison of the Performance Against Clutter of Optimum, Pulse Doppler & MTI Processors," in Record of IEEE 1980 International Radar Conference, New York: IEEE Aerospace & Electronic Systems Society, 1980.
31. Hansen, V.G., "Clutter Suppression in Search Radars," in CW and Doppler Radar, Volume 7, Ed. by D.K. Barton. Massachusetts: Artech House Inc., 397-404 (1978).
32. Johnson, P.E. MTI Investigation. Interoffice Correspondence, The Aerospace Corporation, February 1978. (78-5241.24-4).
33. Katzin, M., "On Mechanisms of Radar Sea Clutter," in Radar Clutter, Volume 5. Ed. by D.K. Barton. Massachusetts: Artech House Inc., 69-79 (1977).
34. Kay, S.M., and Marple, S.L., Jr., "Spectrum Analysis - A Modern Perspective," Proceedings of the IEEE, Vol. 69, No. 11: 1380-1419 (November 1981).
35. Long, M.W., "On Polarization and the Wavelength Dependence of Sea Echo," in Radar Clutter, Volume 5, Ed. by D. K. Batron. Massachusetts: Artech House Inc., 105-110 (1977).
36. -----, Radar Reflectivity of land & Sea. Massachusetts: D.C. Heath and Company, 1975.
37. Middleton, D., "Theory of Reveberation and Similar First Order Scattered Fields Part I: Waveforms and the General Process and Part II: Moments, Spectra, and Special Distributions," IEEE Transactions on Information Theory Vol. IT-13, No. 3, 372-414 (July 1967).
38. Mitchell, R.L. Radar Signal Simulation. Massachusetts:

Artech House Inc., 1976.

39. Mooney, D. and Ralston, G. "Performance of Clutter of Airborne Pulse MTI, CW Doppler, and Pulse Doppler Radar," in CW and Doppler Radar, Volume 7, Ed. by D.K. Barton. Massachusetts: Artech House Inc., 343-350 (1978).
40. Nathanson, P.E. and Reilly, J.P., "Clutter Statistics Which Affect Performance Analysis," in Radar Clutter, Volume 5, Ed. by D.K. Barton. Massachusetts: Artech House Inc., 29-35 (1977).
41. Nathanson, P.G. Radar Design Principles. New York: McGraw Hill, 1969.
42. Nussbaumer, H.J. Fast Fourier Transforms and Convolution Algorithms. Germany: Springer-Verlag Berlin Heidelberg, 1981.
43. Oppenheim, A.V. and Schafer, R.W. Digital Signal Processing. New Jersey: Prentice-Hall, Inc., 1975.
44. Papoulis, A. Probability, Random Variables, and Stochastic Processes. New York: McGraw Hill, 1965.
45. ----- Signal Analysis. New York: McGraw Hill, 1977.
46. Peebles, P.Z. Communication System Principles. Massachusetts: Addison-Wesley Publishing Company, 1976.
47. Principles of Modern Radar. Short Course Notes. Georgia: Georgia Institute of Technology, 1980.
48. Purdy, R.J., et al. Digital Signal Processing Designs for Radar Applications Vols I & II. Massachusetts: Lincoln Laboratory, 31 December 1974 (ADB001419 & ADB001420).
49. Reed, J. D., "Radar Waveform Selection Based on the Calculation and Application of Radar Ambiguity Functions," Thesis, Air Force Institute of Technology, June 1982.
50. Ringel, M.B., "An Advanced Computer Calculation for Ground Clutter in an Airborne Pulse Doppler Radar," in CW and Doppler Radar, Volume 7, Ed. by D.K. Barton, Massachusetts: Artech House, Inc., 375-382 (1978).
51. Rummler, W.D., "Complex Suppression by Complex Weighting of Coherent Pulse Trains," in Detection and Estimation Application to Radars, Ed. by S.S. Haykin, Pennsylvania: Dowden, Hutchinson & Ross, Inc., 318-328 (1976).

52. Schleder, D.C., "Clutter Models and Data," in MTI Radar, Ed. by D.C. Schleder, Massachusetts: Artech House, Inc., 37-61 (1978).@
53. -----, "MTI Performance Analysis," in MTI Radar, Ed. by D.C. Schleder, Massachusetts: Artech House, Inc., 181-251 (1978).
54. -----, and Schulkind, D., "Optimization of Nonrecursive MTI," in MTI Radar, Ed. by D.C. Schleder, Massachusetts: Artech House, Inc., 277-280 (1978).
55. Schooley, A.H., "Some Limiting Cases of Radar Sea Clutter Noise," in Radar Clutter, Volume 5, Ed. by D.K. Barton, Massachusetts: Artech House, Inc., 63-67 (1977).
56. Skolnik, M.L. Introduction to Radar Systems (Second Edition). New York: McGraw Hill, 1980.
57. -----, Radar Handbook. New York: McGraw Hill, 1970.
58. Spafford, L.J., "Optimal Radar Signal Processing in Clutter," in MTI Radar, Ed. by D.C. Schleder, Massachusetts: Artech House, Inc., 283-292 (1977).
59. Stanley, W.D. Digital Signal Processing. New Jersey: Prentice Hall, Inc. 1968.
60. Stearns, S.D. Digital Signal Analysis. New Jersey: Hayden Book Company, Inc., 1975.
61. Stockman, T.G., Jr., "High-Speed Convolution & Correlation," in Digital Filters and the Fast Fourier Transform, Ed. by B. Liu, Pennsylvania: Dowden, Hutchinson & Ross Inc., 378-382 (1975).
62. Stutt, C.A., and Spafford, L.J., "A 'Best' Mismatched Filter Response for Discrimination," in Detection and Estimation Application to Radars, Ed. by S.S. Haykin, Pennsylvania: Dowden, Hutchinson & Ross, Inc., 310-317 (1976).
63. Tomlinson, P.C. A Model for Space Radar Clutter. New York: Rome Air Development Center, June 1979 (AD-A072990).
64. Wardle, N.L., "Derivation of Equations Used in CR (Coherent Radar) and NCR (Noncoherent Radar) Program," Notes, 12 July 1980.
65. Westerfield, E.C., Prager, R.H. and Steward, J.L., "Processing Gains Against Reverberation (Clutter) Using

Matched Filters," in Detection and Estimation Applications to Radar, Ed. by S.S. Haykin, Pennsylvania: Dowden, Hutchinson & Ross, Inc., 309-309 (1976).

66. Whalen, A.D. Detection of Signals In Noise. New York: Academic Press, 1971.
67. Woodward. P.M. "Information Theory and the Design of Radar Receivers," in Detection and Estimation Application to Radars, Ed. by S.S. Haykin, Pennsylvania: Dowden, Hutchinson & Ross, Inc., 30-33 (1976).
68. Wright, J.W., "A New Model for Sea Clutter," in Radar Clutter, Volume 5, Ed. by D.K. Barton. Artech House Inc., 123-129 (1977).

APPENDIX A
PROBLEM PARAMETERS

Radar System

A S-Band, 20 meter diameter radar system was used for this study. Figure A-1 illustrates an example of an arbitrary space-based radar system.

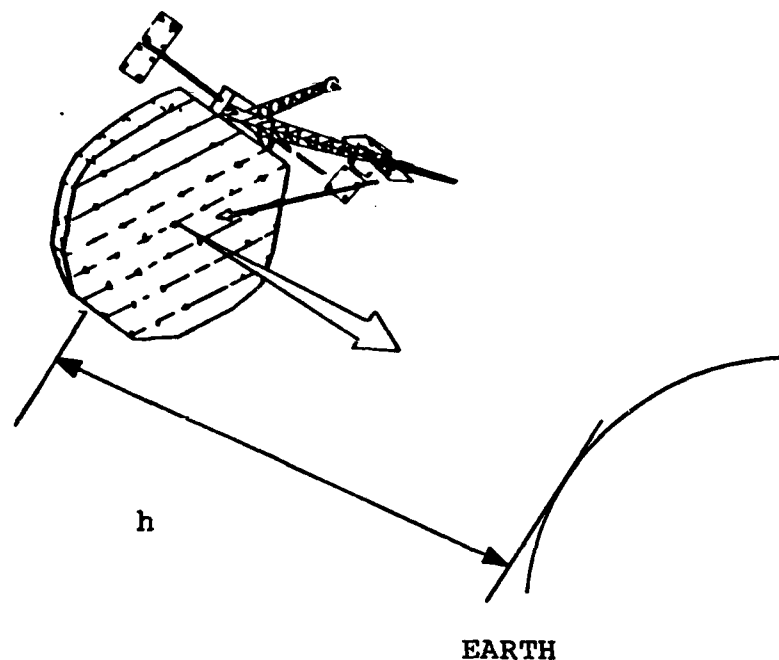


Fig. A-1 Radar System Configuration

The satellite, with the antenna's boresight pointed toward the horizon, is assumed at an altitude of 1667 kilometers.

Since this study is concerned with clutter cancelers, the radar system described is for the purpose of clutter analysis and should not be taken as a point design. The following radar parameters chosen for this study are, however, representative of a system that could be deployed to perform wide area surveillance.

1. Transmitted frequency - 3.0 GHz (S-Band)

2. Power / Burst	- 5.0 kW
3. Gain ($\alpha = .85$)	- 55 DB
4. System Noise Temperature	- 415 ^o Kelvin
5. System Losses	- 13 DB
6. Azimuth Beamwidth	- .5 ^o
7. Elevation Beamwidth	- .5 ^o
8. PRF	- 30 kHz
9. Scan Rate	- 5 ^o /sec

A simple rectangular pulse waveform, illustrated in Figure A-2, is used for the analysis.

DWELL REQUIRED FOR DETECTION

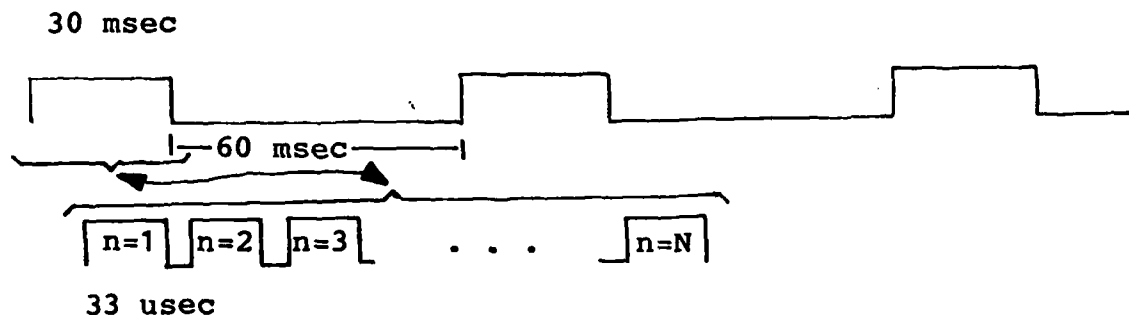
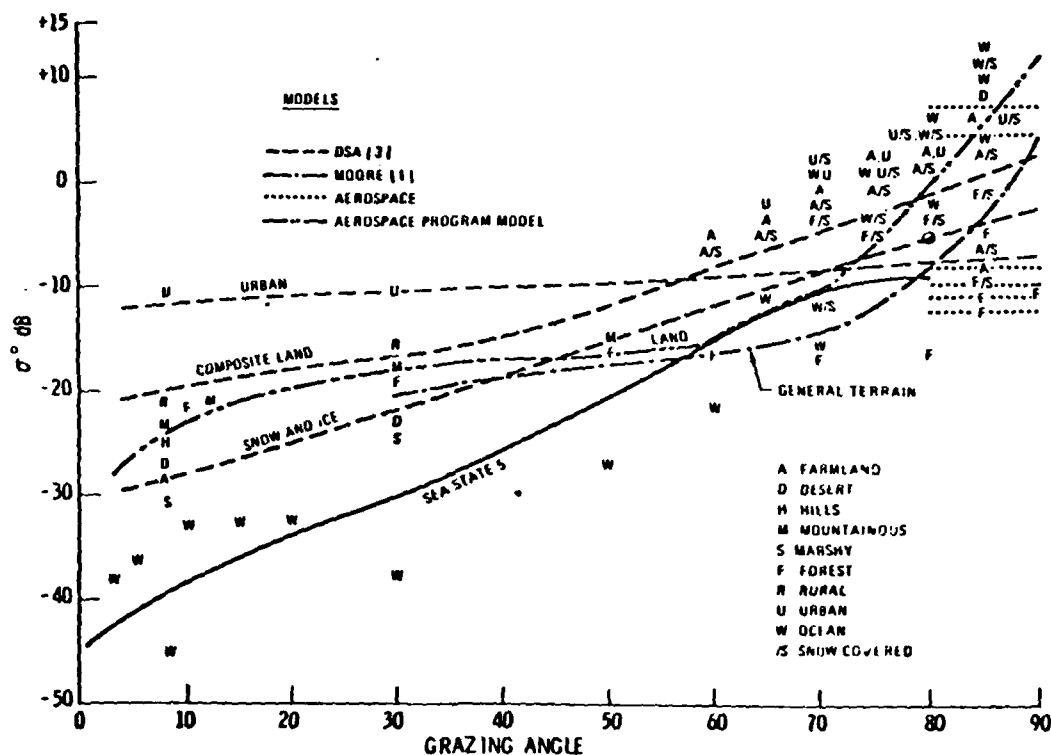


Fig. 2-A Pulse Doppler Waveform

Clutter Model

Due to the uncertain nature of the statistics of radar clutter as seen by a space-based radar system, the backscattering coefficient, σ^o , described in Ref 4:4-24, is used for this study. Figure A-3 illustrates the average

backscatter values for different terrains.



The values of σ° are for a S-Band radar.

The computer simulation of the clutter cancellation problem allows the user to choose either land, sea, or snow and ice terrain. Backscatter coefficient values, at every five degrees of grazing angle, are stored for the three types of terrain. The program stores the DSA backscatter model values for land and snow/ice. The sea σ° values are taken from the Sea State 5 curve for grazing angles less than 70 degrees. For grazing angles greater than 70 degrees the Aerospace Program Model is utilized. The change at 70 degrees is because the Aerospace Program Model better approximates the available data values.

APPENDIX B
CLUTTER AREA CALCULATIONS

For a pulse doppler radar, the amount of clutter surface area illuminated by the antenna mainbeam is dependent upon the platform's altitude above the earth's surface, the grazing angle and the mainbeam's azimuth and elevation beamwidths. Given a geometric description of the mainbeam with respect to the earth, the clutter surface area can be computed. Figure B-1 describes the angles used in describing the geometry between the radar and the surface area.

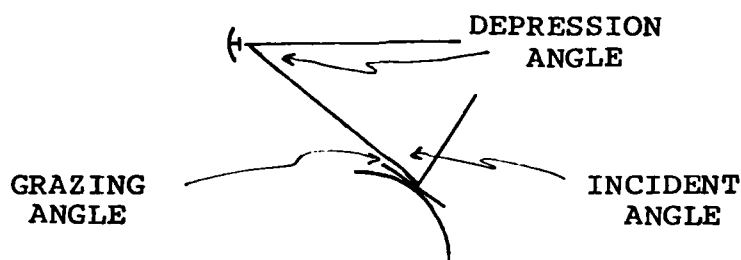
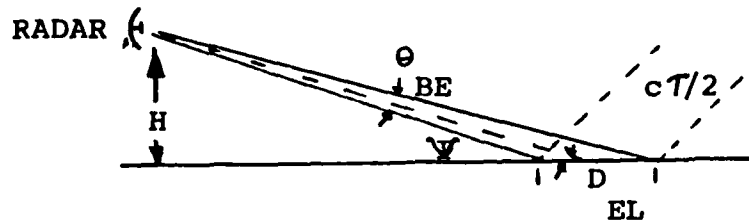


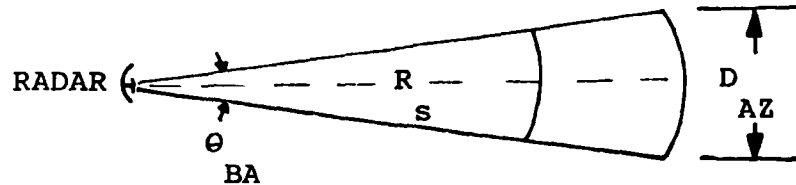
Fig. B-1 Radar Geometry Angles

Depending on the altitude of the radar platform certain assumptions can be made in computing the surface area. For an airborne or extremely low spaceborne platform, the radar is close enough to the ground such that the surface illuminated by the mainbeam is essentially flat. Depending on the situations, two different cases occur when computing the clutter area. The pulse limiting case occurs when the equivalent physical length of the pulse is less than the value of the elevation beamwidth dimension (dimension D_{EL} , Figure B-2). This case results when the relationship between the half power elevation beamwidth, the grazing angle γ , the range R , and the pulse width τ satisfy $\tan \gamma < \tan [2\theta_{BE} R / c\tau]$. Figure B-

2 illustrates the relationship between the various parameters.



a. Elevation view showing surface clutter.



b. Azimuth view showing surface clutter.

Fig. B-2 Illuminated Clutter Area for Pulse Limiting Case

Dimension D_{EL} can be calculated given the radar's grazing angle ψ , and the pulse width τ . The angle θ is defined as

$$\theta = 180 - (90 - \psi) - 90 = \psi \quad (B1)$$

Therefore D_{EL} is

$$\frac{c\tau/2}{D_{EL}} = \cos \psi \quad (B2)$$

or

$$D_{EL} = c\tau/2 \sec \psi \quad (B3)$$

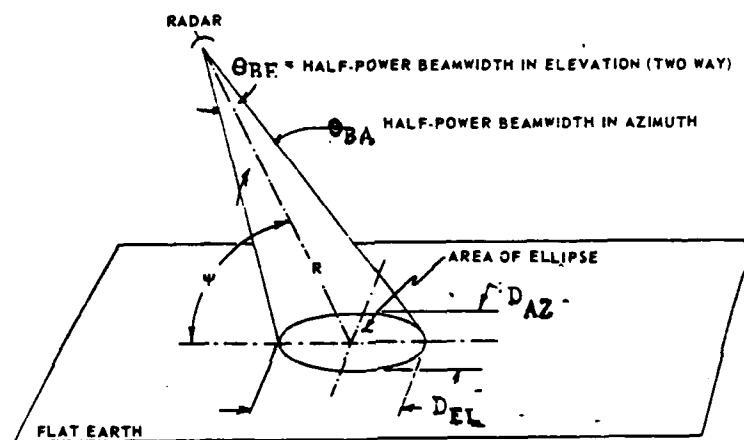
For a narrow azimuth beamwidth, the dimension D_{AZ} is

$$D_{AZ} = R \theta_{BA} \quad (B4)$$

and the illuminated area is approximated by multiplying the width dimension D_{AZ} , with the elevation length, D_{EL} .

$$A_c = (R \theta_{BA} c \tau) / 2 \sec \Psi \quad (B5)$$

The second case occurs when the illuminated area is limited by the beamwidth and not by the pulse length as shown in Figure B-3



(Ref 41:65)

Fig. B-3 Illuminated Clutter Area for Beamwidth Limiting Case

The beamwidth limiting case occurs when $\tan \Psi > \tan[2\theta_{BE}/c\tau]$. The mainbeam clutter is thus

$$A_c = .25 \pi R^2 \theta_{BA} \theta_{BE} \csc \Psi \quad (B6)$$

For equation B5 and B6 to apply, the beamwidths are assumed to be less than ten degrees.

For a high altitude radar system, the area illuminated is shown in Figure B-4 where h is the platform altitude, R_s is

the slant range to the toe of the footprint, the angles β_h , α_h , ϕ_h , and β_t , α_t , ϕ_t respectively correspond to the heel and toe of the footprint.

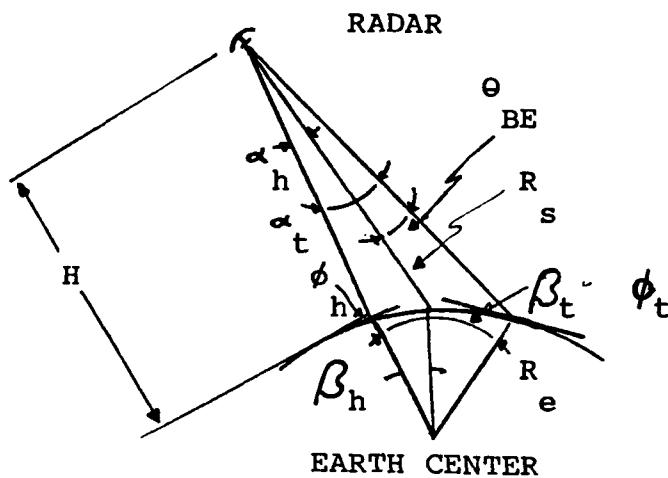


Fig. B-4 Radar - Earth Geometry

To calculate the area covered by the radiated energy the toe grazing angle must be calculated. From the law of sines

$$\frac{\sin(\phi_t + 90)}{H + R_e} = \frac{\sin \alpha_t}{R_e}$$

thus

$$\alpha_t = \sin^{-1} (R_e / (H + R_e) \cos \phi_t) \quad (B7)$$

Again using the law of sines, the heel grazing angle is computed

$$\frac{\sin(\phi_h + 90)}{H + R_e} = \frac{\sin \alpha_h}{R_e}$$

where $\alpha_h = \alpha_t - \theta_{BE}$. Thus

$$\phi_h = \cos^{-1}((H + R_e)/R_e \sin \alpha_h) \quad (B8)$$

The toe earth central angle β_t , is

$$\beta_t = 90 - \phi_t - \alpha_t \quad (B9)$$

and the heel earth central angle, β_h , is

$$\begin{aligned} \beta_h &= 90 - \phi_h - \alpha_h \\ &= 90 - \cos^{-1}((H + R_e)/R_e \sin \alpha_h) - \alpha_t + \theta_{BE} \end{aligned} \quad (B10)$$

Thus the length is

$$\begin{aligned} D_{EL} &= (\beta_t - \beta_h) R_e \\ &= [\cos^{-1}((H + R_e)/R_e \sin(\alpha_t - \theta_{BE})) - \phi_t - \theta_{BE}] R_e \end{aligned} \quad (B11)$$

To calculate the width of the footprint, D_{AZ} , the slant range must first be obtained. Again using the law of sines

$$\frac{R_s}{\sin \beta_t} = \frac{R_e}{\sin \beta_t}$$

thus

$$R_s = R_e \sin \beta_t / \sin \alpha_t \quad (B12)$$

The footprint width is

$$D_{AZ} = R_s \theta_{BA} \quad (B13)$$

The clutter surface area is then the length of the footprint times the width, or

$$A_c = [\cos^{-1} ((H + R_e) / R_e \sin(\alpha_t - \theta_{BE})) - \phi_t - \theta_{BE}] \theta_{BA} R_e \quad (B14)$$

(Note: The area calculated by equation B14 is slightly larger than the actual area covered by the mainbeam. This is because in calculating the width, the heel of the footprint was assumed to have the same width as the toe of the footprint.)

APPENDIX C
USEFUL FORMULAS

Trigonometric Identities

$$\sin(x \pm y) = \sin(x) \cos(y) \pm \cos(x) \sin(y)$$

$$\cos(x \pm y) = \cos(x) \cos(y) \mp \sin(x) \sin(y)$$

$$\sin(x) \pm \sin(y) = 2 \sin[(x \pm y)/2] \cos[(x \mp y)/2]$$

$$\cos(x) + \cos(y) = 2 \cos[(x + y)/2] \cos[(x - y)/2]$$

$$\cos(x) - \cos(y) = 2 \sin[(x + y)/2] \sin[(y - x)/2]$$

$$2 \cos(x) \cos(y) = [\cos(x + y) + \cos(x - y)]$$

$$2 \sin(x) \sin(y) = [\cos(x - y) - \cos(x + y)]$$

$$2 \sin(x) \cos(y) = [\sin(x + y) + \sin(x - y)]$$

$$\sin(2x) = 2 \sin(x) \cos(x)$$

$$\cos(2x) = \cos^2(x) - \sin^2(x)$$

$$\sin(x/2) = \pm \sqrt{[1 - \cos(x)]/2}$$

$$\cos(x/2) = \pm \sqrt{[1 + \cos(x)]/2}$$

Select sign for radical
consistent with left side.

$$2 \sin^2(x) = 1 - \cos(2x)$$

$$2 \cos^2(x) = 1 + \cos(2x)$$

$$4 \cos^3(x) = 3 \cos(x) + \cos(3x)$$

$$A \cos(x) - B \sin(x) = R \cos(x + \theta)$$

where

$$R = \sqrt{A^2 + B^2}$$

$$\theta = \tan^{-1} \left[\frac{B}{A} \right]$$

$$e^{\pm j\theta} = \cos \theta \pm j \sin \theta$$

$$\cos \theta = \frac{e^{j\theta} + e^{-j\theta}}{2}$$

$$\sin \theta = \frac{e^{j\theta} - e^{-j\theta}}{2j}$$

$$\tan \theta = \frac{j\theta - e^{-j\theta}}{e^{j\theta} - e^{-j\theta}} = \frac{2j\theta}{e^{2j\theta} - 1}$$

$$\frac{a}{\sin A} = \frac{b}{\sin B} = \frac{c}{\sin C}$$

$$a^2 = b^2 + c^2 - 2bc \cos A$$

Following

Reproduced from
best available copy.

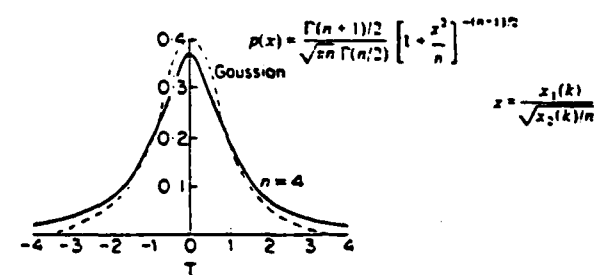
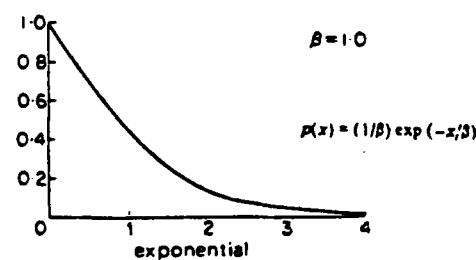
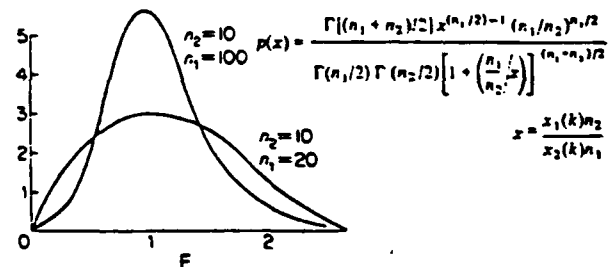
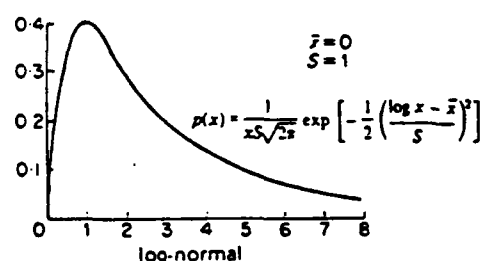
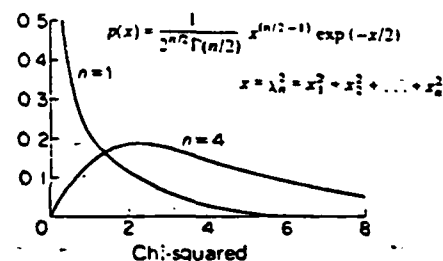
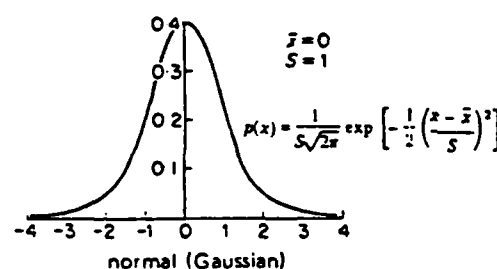
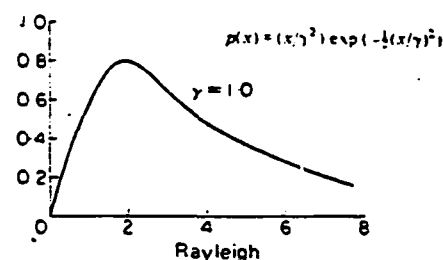
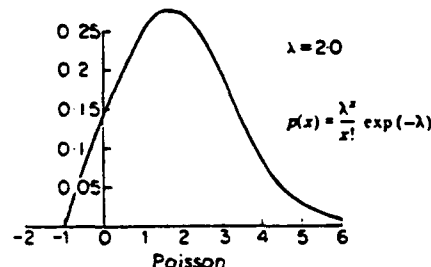
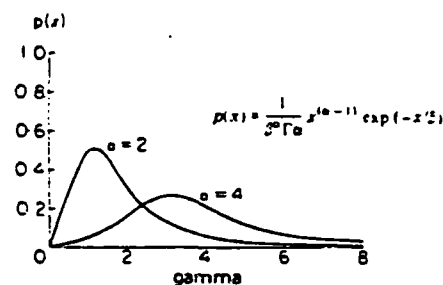
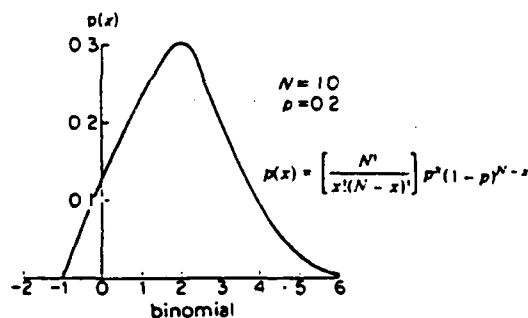
PAGE'S

Table of Elementary Fourier Transform Pairs

DESCRIPTION	TIME DOMAIN		FREQUENCY DOMAIN
Pulse	$A\rho\left(-\frac{\tau}{2}, \frac{\tau}{2}\right)$	\longleftrightarrow	$A\tau \operatorname{sinc}(\tau f)$
Delta	$A\delta(t)$	\longleftrightarrow	A
Constant	A	\longleftrightarrow	$A\delta(f)$
One-sided Exponential	$e^{-at}u(t)$	\longleftrightarrow	$\frac{1}{a + j2\pi f}$
Two-sided Exponential	$e^{-a t }$	\longleftrightarrow	$\frac{2a}{a^2 + (2\pi f)^2}$
Unit Step	$u(t) = \begin{cases} 1, & t > 0 \\ 0, & t < 0 \end{cases}$	\longleftrightarrow	$\frac{1}{2}\delta(f) + \frac{1}{j2\pi f}$
Signum	$\operatorname{sgn}(t) = \begin{cases} 1, & t > 0 \\ -1, & t < 0 \end{cases}$	\longleftrightarrow	$\frac{1}{j\pi f}$
Triangle	$\left[1 - \frac{ t }{\tau}\right]\rho(-\tau, \tau)$	\longleftrightarrow	$\tau \operatorname{sinc}^2(\tau f)$
Gaussian	$\frac{1}{\sqrt{2\pi}\sigma} \exp[-t^2/2\sigma^2]$	\longleftrightarrow	$\exp[-(2\pi\sigma f)^2/2]$
Cosine	$\cos(2\pi f_0 t)$	\longleftrightarrow	$\frac{1}{2}[\delta(f+f_0) + \delta(f-f_0)]$
Sine	$\sin(2\pi f_0 t)$	\longleftrightarrow	$j\frac{1}{2}[\delta(f+f_0) - \delta(f-f_0)]$
Periodic	$g_p(t) = g_p(t + nT_0)$	\longleftrightarrow	$\sum_n G(nf_0)\delta(f - nf_0)$
Sampling	$\sum_n \delta(t - nT_0)$	\longleftrightarrow	$\sum_n f_0 \delta(f - nf_0)$
Hilbert	$\hat{g}(t)$	\longleftrightarrow	$-jG(f) \operatorname{sgn}(f)$

Fourier Transform Theorems

A. Superposition	$\sum_{n=1}^N a_n g_n(t)$	\longleftrightarrow	$\sum_{n=1}^N a_n G_n(f)$
B. Symmetry	$G(t)$	\longleftrightarrow	$g(-f)$
C. Time Scaling	$g(at)$	\longleftrightarrow	$\frac{1}{ a } G(f/a)$
D. Time Shifting	$g(t - t_0)$	\longleftrightarrow	$G(f) \exp[-j2\pi f t_0]$
E. Frequency Shifting	$g(t) \exp[+j2\pi f_0 t]$	\longleftrightarrow	$G(f - f_0)$
F. Time Differentiation	$\frac{d^n}{dt^n}[g(t)]$	\longleftrightarrow	$(j2\pi f)^n G(f)$
G. Frequency Differentiation	$(-j2\pi t)^n g(t)$	\longleftrightarrow	$\frac{d^n}{df^n}[G(f)]$
H. Integration	$\int_{-\infty}^t g(x) dx$	\longleftrightarrow	$\frac{G(0)}{2}\delta(f) + \frac{1}{j2\pi f} G(f)$
I. Convolution	$g(t) * h(t)$	\longleftrightarrow	$G(f) H(f)$
J. Multiplication	$g(t)h(t)$	\longleftrightarrow	$G(f) \cdot H(f)$



Some probability density functions.

SUMMARY OF STATISTICAL AVERAGES*

NAME	DEFINITION	INDICATED OPERATION	
		Discrete case	Continuous case
Mean = m . Also called average, expectation, ensemble average	$E\{X\}$	$\sum_{i=1}^N x_i P(x_i)$	$\int_{-\infty}^{\infty} xp(x) dx$
Variance = σ^2 (standard deviation = σ)	$E\{(X - m_x)^2\}$	$\sum_{i=1}^N (x_i - m_x)^2 P(x_i)$	$\int_{-\infty}^{\infty} (x - m_x)^2 p(x) dx$
n th moment	$E\{X^n\}$	$\sum_{i=1}^N x_i^n P(x_i)$	$\int_{-\infty}^{\infty} x^n p(x) dx$
n th central moment or n th moment about the mean	$E\{(X - m_x)^n\}$ (= 0 for $n = 1$)	$\sum_{i=1}^N (x_i - m_x)^n P(x_i)$	$\int_{-\infty}^{\infty} (x - m_x)^n p(x) dx$
Mean of a function $g(x)$	$E\{g(X)\}$	$\sum_{i=1}^N g(x_i) P(x_i)$	$\int_{-\infty}^{\infty} g(x) p(x) dx$
$(n + k)$ th joint moment	$E\{X^n Y^k\}$	$\sum_{i=1}^N \sum_{j=1}^M x_i^n y_j^k P(x_i, y_j)$	$\int_{-\infty}^{\infty} \int_{-\infty}^{\infty} x^n y^k p(x, y) dx dy$
$(n + k)$ th joint central moment	$E\{(X - m_x)^n (Y - m_y)^k\}$	$\sum_{i=1}^N \sum_{j=1}^M (x_i - m_x)^n (y_j - m_y)^k P(x_i, y_j)$	$\int_{-\infty}^{\infty} \int_{-\infty}^{\infty} (x - m_x)^n (y - m_y)^k p(x, y) dx dy$
Covariance	$E\{(X - m_x)(Y - m_y)\}$	$\sum_{i=1}^N \sum_{j=1}^M (x_i - m_x)(y_j - m_y) P(x_i, y_j)$	$\int_{-\infty}^{\infty} \int_{-\infty}^{\infty} (x - m_x)(y - m_y) p(x, y) dx dy$
Mean of a function $g(x, y)$	$E\{g(X, Y)\}$	$\sum_{i=1}^N \sum_{j=1}^M g(x_i, y_j) P(x_i, y_j)$	$\int_{-\infty}^{\infty} \int_{-\infty}^{\infty} g(x, y) p(x, y) dx dy$

* For the discrete cases, outcomes are $x_i (i = 1, \dots, N)$ and $y_j (j = 1, \dots, M)$ with probability $P(x_i)$ and $P(y_j)$ respectively. For the continuous cases X and Y are defined over the interval $(-\infty < x, y < \infty)$ and have continuous density functions $p(x)$ and $p(y)$ respectively. The means are indicated by m_x and m_y .

TABLE 1. Values of the Standard Normal Distribution Function*

$$\Phi(z) = \int_{-\infty}^z \frac{1}{\sqrt{2\pi}} e^{-t^2/2} dt = P(Z \leq z)$$

z	0	1	2	3	4	5	6	7	8	9
-3.0	0.0013	0.0010	0.0007	0.0005	0.0003	0.0002	0.0002	0.0001	0.0001	0.0000
-2.9	0.0014	0.0011	0.0008	0.0006	0.0004	0.0003	0.0002	0.0001	0.0001	0.0000
-2.8	0.0016	0.0012	0.0009	0.0007	0.0005	0.0003	0.0002	0.0001	0.0001	0.0000
-2.7	0.0018	0.0014	0.0011	0.0008	0.0006	0.0004	0.0003	0.0002	0.0001	0.0000
-2.6	0.0020	0.0016	0.0012	0.0009	0.0007	0.0005	0.0003	0.0002	0.0001	0.0000
-2.5	0.0022	0.0018	0.0014	0.0011	0.0008	0.0006	0.0004	0.0003	0.0002	0.0001
-2.4	0.0024	0.0020	0.0016	0.0012	0.0009	0.0007	0.0005	0.0003	0.0002	0.0001
-2.3	0.0026	0.0022	0.0018	0.0014	0.0011	0.0008	0.0006	0.0004	0.0003	0.0002
-2.2	0.0028	0.0024	0.0020	0.0016	0.0012	0.0009	0.0007	0.0005	0.0003	0.0002
-2.1	0.0030	0.0026	0.0022	0.0018	0.0014	0.0011	0.0008	0.0006	0.0004	0.0003
-2.0	0.0032	0.0028	0.0024	0.0020	0.0016	0.0012	0.0009	0.0007	0.0005	0.0003
-1.9	0.0034	0.0030	0.0026	0.0022	0.0018	0.0014	0.0011	0.0008	0.0006	0.0004
-1.8	0.0036	0.0032	0.0028	0.0024	0.0020	0.0016	0.0012	0.0009	0.0007	0.0005
-1.7	0.0038	0.0034	0.0030	0.0026	0.0022	0.0018	0.0014	0.0011	0.0008	0.0006
-1.6	0.0040	0.0036	0.0032	0.0028	0.0024	0.0020	0.0016	0.0012	0.0009	0.0007
-1.5	0.0042	0.0038	0.0034	0.0030	0.0026	0.0022	0.0018	0.0014	0.0011	0.0008
-1.4	0.0044	0.0040	0.0036	0.0032	0.0028	0.0024	0.0020	0.0016	0.0012	0.0009
-1.3	0.0046	0.0042	0.0038	0.0034	0.0030	0.0026	0.0022	0.0018	0.0014	0.0011
-1.2	0.0048	0.0044	0.0040	0.0036	0.0032	0.0028	0.0024	0.0020	0.0016	0.0012
-1.1	0.0050	0.0046	0.0042	0.0038	0.0034	0.0030	0.0026	0.0022	0.0018	0.0014
-1.0	0.0052	0.0048	0.0044	0.0040	0.0036	0.0032	0.0028	0.0024	0.0020	0.0016
-0.9	0.0054	0.0050	0.0046	0.0042	0.0038	0.0034	0.0030	0.0026	0.0022	0.0018
-0.8	0.0056	0.0052	0.0048	0.0044	0.0040	0.0036	0.0032	0.0028	0.0024	0.0020
-0.7	0.0058	0.0054	0.0050	0.0046	0.0042	0.0038	0.0034	0.0030	0.0026	0.0022
-0.6	0.0060	0.0056	0.0052	0.0048	0.0044	0.0040	0.0036	0.0032	0.0028	0.0024
-0.5	0.0062	0.0058	0.0054	0.0050	0.0046	0.0042	0.0038	0.0034	0.0030	0.0026
-0.4	0.0064	0.0060	0.0056	0.0052	0.0048	0.0044	0.0040	0.0036	0.0032	0.0028
-0.3	0.0066	0.0062	0.0058	0.0054	0.0050	0.0046	0.0042	0.0038	0.0034	0.0030
-0.2	0.0068	0.0064	0.0060	0.0056	0.0052	0.0048	0.0044	0.0040	0.0036	0.0032
-0.1	0.0070	0.0066	0.0062	0.0058	0.0054	0.0050	0.0046	0.0042	0.0038	0.0034
-0.0	0.0072	0.0068	0.0064	0.0060	0.0056	0.0052	0.0048	0.0044	0.0040	0.0036

*B. W. Lindgren, *Statistical Theory*, The Macmillan Company, 1960.

TABLE 1 (Continued)

$$\Phi(z) = \int_{-\infty}^z \frac{1}{\sqrt{2\pi}} e^{-t^2/2} dt = P(Z \leq z)$$

z	0	1	2	3	4	5	6	7	8	9
0.0	0.5000	0.5040	0.5080	0.5120	0.5160	0.5199	0.5239	0.5279	0.5319	0.5359
0.1	0.5398	0.5438	0.5478	0.5517	0.5557	0.5596	0.5636	0.5675	0.5714	0.5753
0.2	0.5793	0.5832	0.5871	0.5910	0.5948	0.5987	0.6026	0.6064	0.6103	0.6141
0.3	0.6179	0.6217	0.6255	0.6293	0.6331	0.6368	0.6406	0.6443	0.6480	0.6517
0.4	0.6554	0.6591	0.6628	0.6664	0.6700	0.6736	0.6772	0.6808	0.6844	0.6879
0.5	0.6915	0.6950	0.6985	0.7019	0.7054	0.7088	0.7123	0.7157	0.7190	0.7224
0.6	0.7257	0.7291	0.7324	0.7357	0.7389	0.7422	0.7454	0.7486	0.7517	0.7549
0.7	0.7580	0.7611	0.7642	0.7673	0.7703	0.7734	0.7764	0.7794	0.7823	0.7852
0.8	0.7881	0.7910	0.7939	0.7967	0.7995	0.8023	0.8051	0.8078	0.8106	0.8133
0.9	0.8159	0.8186	0.8212	0.8238	0.8264	0.8289	0.8315	0.8340	0.8365	0.8389
1.0	0.8413	0.8438	0.8461	0.8485	0.8508	0.8531	0.8554	0.8577	0.8599	0.8621
1.1	0.8643	0.8665	0.8686	0.8708	0.8729	0.8749	0.8770	0.8790	0.8810	0.8830
1.2	0.8849	0.8869	0.8888	0.8907	0.8925	0.8944	0.8962	0.8980	0.8997	0.9015
1.3	0.9032	0.9049	0.9066	0.9082	0.9099	0.9115	0.9131	0.9147	0.9162	0.9177
1.4	0.9192	0.9207	0.9222	0.9236	0.9251	0.9265	0.9278	0.9292	0.9306	0.9319
1.5	0.9332	0.9345	0.9357	0.9370	0.9382	0.9394	0.9406	0.9418	0.9430	0.9441
1.6	0.9452	0.9463	0.9474	0.9484	0.9495	0.9505	0.9515	0.9525	0.9535	0.9545
1.7	0.9554	0.9564	0.9573	0.9582	0.9591	0.9599	0.9608	0.9616	0.9625	0.9633
1.8	0.9641	0.9648	0.9656	0.9664	0.9671	0.9678	0.9686	0.9693	0.9700	0.9706
1.9	0.9713	0.9719	0.9726	0.9732	0.9738	0.9744	0.9750	0.9756	0.9762	0.9767
2.0	0.9772	0.9778	0.9783	0.9788	0.9793	0.9798	0.9803	0.9808	0.9812	0.9817
2.1	0.9821	0.9826	0.9830	0.9834	0.9838	0.9842	0.9846	0.9850	0.9854	0.9857
2.2	0.9861	0.9864	0.9868	0.9871	0.9874	0.9878	0.9881	0.9884	0.9887	0.9890
2.3	0.9893	0.9896	0.9898	0.9901	0.9904	0.9906	0.9909	0.9911	0.9913	0.9916
2.4	0.9918	0.9920	0.9922	0.9925	0.9927	0.9929	0.9931	0.9932	0.9934	0.9936
2.5	0.9938	0.9940	0.9941	0.9943	0.9945	0.9946	0.9948	0.9949	0.9951	0.9952
2.6	0.9953	0.9955	0.9956	0.9957	0.9959	0.9960	0.9962	0.9963	0.9965	0.9966
2.7	0.9967	0.9968	0.9969	0.9970	0.9971	0.9972	0.9973	0.9974	0.9975	0.9976
2.8	0.9977	0.9978	0.9979	0.9980	0.9981	0.9982	0.9983	0.9984	0.9985	0.9986
2.9	0.9987	0.9988	0.9989	0.9990	0.9991	0.9992	0.9993	0.9994	0.9995	0.9996
3.0	0.9997	0.9998	0.9999	0.9999	0.9999	0.9999	0.9999	0.9999	0.9999	1.0000

Z - Transform Theorems

Sequence		z-Transform
1. $x(n)$	$X(z)$	$R_{s-} < z < R_{s+}$
2. $y(n)$	$Y(z)$	$R_{y-} < z < R_{y+}$
3. $ax(n) + by(n)$	$aX(z) + bY(z)$	$\max[R_{s-}, R_{y-}] < z < \min[R_{s+}, R_{y+}]$
4. $x(n + n_0)$	$z^{n_0}X(z)$	$R_{s-} < z < R_{s+}$
5. $a^n x(n)$	$X(a^{-1}z)$	$ a R_{s-} < z < a R_{s+}$
6. $nx(n)$	$-z \frac{dX(z)}{dz}$	$R_{s-} < z < R_{s+}$
7. $x^*(n)$	$X^*(z^*)$	$R_{s-} < z < R_{s+}$
8. $x(-n)$	$X(1/z)$	$1/R_{s+} < z < 1/R_{s-}$
9. $\text{Re } [x(n)]$	$\frac{1}{2}[X(z) + X^*(z^*)]$	$R_{s-} < z < R_{s+}$
10. $\text{Im } [x(n)]$	$\frac{1}{2j}[X(z) - X^*(z^*)]$	$R_{s-} < z < R_{s+}$
11. $x(n) * y(n)$	$X(z)Y(z)$	$\max[R_{s-}, R_{y-}] < z < \min[R_{s+}, R_{y+}]$
12. $x(n)y(n)$	$\frac{1}{2\pi j} \oint_C X(v)Y\left(\frac{z}{v}\right)v^{-1} dv$	$R_{s-}R_{y-} < z < R_{s+}R_{y+}$

DFT Transform Theorems

Finite-Length Sequence (length N)	DFT
1. $x(n)$	$X(k)$
2. $y(n)$	$Y(k)$
3. $ax(n) + by(n)$	$aX(k) + bY(k)$
4. $x((n+m))_N \mathcal{R}_N(n)$	$W_N^{km} X(k)$
5. $W_N^{ln} x(n)$	$X((k+l))_N \mathcal{R}_N(k)$
6. $\left[\sum_{m=0}^{N-1} x((m))_N y((n-m))_N \right] \mathcal{R}_N(n)$	$X(k)Y(k)$
7. $x(n)y(n)$	$\frac{1}{N} \left[\sum_{l=0}^{N-1} X((l))_N Y((k-l))_N \right] \mathcal{R}_N(k)$
8. $x^*(n)$	$X^*((-k))_N \mathcal{R}_N(k)$
9. $x^*((-n))_N \mathcal{R}_N(n)$	$X^*(k)$
10. $\text{Re } [x(n)]$	$X_{re}(k) = \frac{1}{2}[X((k))_N + X^*((-k))_N] \mathcal{R}_N(k)$
11. $j \text{Im } [x(n)]$	$X_{im}(k) = \frac{1}{2j}[X((k))_N - X^*((-k))_N] \mathcal{R}_N(k)$
12. $x_{re}(n)$	$\text{Re } [X(k)]$
13. $x_{im}(n)$	$j \text{Im } [X(k)]$

The following properties apply only when $x(n)$ is real:

14. Any real $x(n)$	$\begin{cases} X(k) = X^*((-k))_N \mathcal{R}_N(k) \\ \text{Re } [X(k)] = \text{Re } [X^*((-k))_N] \mathcal{R}_N(k) \\ \text{Im } [X(k)] = -\text{Im } [X^*((-k))_N] \mathcal{R}_N(k) \\ X(k) = X^*((-k))_N \mathcal{R}_N(k) \\ \arg [X(k)] = -\arg [X^*((-k))_N] \mathcal{R}_N(k) \end{cases}$
15. $x_{re}(n)$	$\text{Re } [X(k)]$
16. $x_{im}(n)$	$j \text{Im } [X(k)]$

Table of Elementary
Z - Transform Pairs

	$f(k)$	$F(z)$
1	$\delta(k)$	1
2	$\delta(k-i)$	z^{-i}
3	$u(k)$	$\frac{z}{z-1}$
4	$u(k-i)$	$z^{-i} \left\{ \frac{z}{z-1} \right\}$
5	$ku(k)$	$\frac{z}{(z-1)^2}$
6	$k^2 u(k)$	$\frac{z(z+1)}{(z-1)^3}$
7	e^{-akT}	$\frac{z}{z - \exp(-aT)}$
8	ke^{-akT}	$\frac{z \exp(-aT)}{\{z - \exp(-aT)\}^2}$
9	$1 - e^{-akT}$	$\frac{z\{1 - \exp(-aT)\}}{(z-1)\{z - \exp(-aT)\}}$
10	a^k	$\frac{z}{z-a}$
11	ka^k	$\frac{az}{(z-a)^2}$
12	$(k+1)a^k$	$\frac{z^2}{(z-a)^2}$
13	$(k+1)(k+2)a^{k/2}$	$\frac{z^3}{(z-a)^3}$
14	$\sin(\omega kT)$	$\frac{z \sin(\omega T)}{z^2 - 2z \cos(\omega T) + 1}$
15	$\cos(\omega kT)$	$\frac{z\{z - \cos(\omega T)\}}{z^2 - 2z \cos(\omega T) + 1}$
16	$e^{-akT} \sin(\omega kT)$	$\frac{z \exp(-aT) \sin(\omega T)}{z^2 - 2z \exp(-aT) \cos(\omega T) + \exp(-2aT)}$
17	$e^{-akT} \cos(\omega kT)$	$\frac{z^2 - z \exp(-aT) \cos(\omega T)}{z^2 - 2z \exp(-aT) \cos(\omega T) + \exp(-2aT)}$

Integral Relationships

$$\int \sin^2(ax) dx = \frac{x}{2} - \frac{\sin(2ax)}{4a}$$

$$\int x \sin(ax) dx = \frac{1}{a^2} [\sin(ax) - ax \cos(ax)]$$

$$\int \sin(ax) \sin(bx) dx = \frac{\sin[(a-b)x]}{2(a-b)} - \frac{\sin[(a+b)x]}{2(a+b)} \quad a^2 \neq b^2$$

$$\int \sin(ax) \cos(bx) dx = - \left[\frac{\cos[(a-b)x]}{2(a-b)} + \frac{\cos[(a+b)x]}{2(a+b)} \right] \quad a^2 \neq b^2$$

$$\int \sin(ax) \cos(ax) dx = \frac{\sin^2(ax)}{2a}$$

$$\int \cos^2(ax) dx = \frac{x}{2} + \frac{\sin(2ax)}{4a}$$

$$\int x \cos(ax) dx = \frac{1}{a^2} [\cos(ax) + ax \sin(ax)]$$

$$\int \cos(ax) \cos(bx) dx = \frac{\sin[(a-b)x]}{2(a-b)} + \frac{\sin[(a+b)x]}{2(a+b)} \quad a^2 \neq b^2$$

$$\int \exp[ax] \sin(bx) dx = \frac{\exp[ax]}{a^2 + b^2} [a \sin(bx) - b \cos(bx)]$$

$$\int \exp[ax] \cos(bx) dx = \frac{\exp[ax]}{a^2 + b^2} [a \cos(bx) + b \sin(bx)]$$

$$\int \frac{dx}{a^2 + x^2} = \frac{1}{a} \tan^{-1} \left[\frac{x}{a} \right]$$

$$\int x \exp[ax] dx = \frac{ax-1}{a^2} \exp[ax]$$

$$\int_0^{\infty} \exp[-(ax)^2] \cos(bx) dx = \frac{\sqrt{\pi}}{2a} \exp \left[- \left(\frac{b}{2a} \right)^2 \right] \quad a > 0$$

$$\int u^n du = \frac{u^{n+1}}{n+1} + C \quad (n \neq -1)$$

$$\int \frac{du}{u} = \log |u| + C$$

$$\int e^u du = e^u + C$$

$$\int \sin u du = -\cos u + C$$

$$\int \cos u du = \sin u + C$$

$$\int \tan u du = -\log |\cos u| + C$$

$$\int \cot u du = \log |\sin u| + C$$

$$\int \sec u du = \log |\sec u + \tan u| + C$$

$$\int \csc u du = \log |\csc u - \cot u| + C$$

$$\int \sec^2 u du = \tan u + C$$

$$\int \csc^2 u du = -\cot u + C$$

$$\int \sec u \tan u du = \sec u + C$$

$$\int \csc u \cot u du = -\csc u + C$$

$$\int \frac{du}{\sqrt{a^2 - u^2}} = \sin^{-1} \frac{u}{a} + C$$

$$\int \frac{du}{a^2 + u^2} = \frac{1}{a} \tan^{-1} \frac{u}{a} + C$$

Series Identities

$$\sum_{n=0}^{N-1} x^n = \frac{1-x^N}{1-x} ; \quad |x| < 1$$

$$\sum_{n=0}^{N-1} x^n = \frac{1-x^N}{1-x} ; \quad |x| < 1$$

$$\sum_{n=1}^{\infty} x^n = \frac{x}{1-x} ; \quad |x| < 1$$

$$\sum_{n=a}^{\infty} x^n = \frac{x^a}{1-x} ; \quad |x| < 1$$

$$\sum_{n=0}^{\infty} nx^n = \frac{x}{1-x^2} \frac{d}{dx} \sum_{n=0}^{\infty} x^n = \frac{x}{1-x^2} ; \quad |x| < 1$$

$$\sum_{n=-\infty}^{-1} x^{-n} = \sum_{n=1}^{\infty} x^n$$

APPENDIX D
PROGRAM LISTINGS

```

PROGRAM CLTCAN
*****
*   PROGRAM CLUTCAN   *
*   WRITTEN BY: JOE DEVENUTO   *
*   15 SEPTEMBER 1983   *
*****

    THE PROGRAM CLUTCAN IS AN INITIALIZATION AND
    CALLING PROGRAM THAT SIMULATES THE CLUTTER CAN-
    CELLATION PROBLEM. CLUTCAN CALLS THE SUBPROGRAM CLUT
    TO CALCULATE THE CLUTTER POWER SPECTRAL DENSITY AS SEEN BY
    A SPACEBASED DOPPLER RADAR SYSTEM. CLUTCAN THEN CALLS THE
    SUBPROGRAM CANCEL, A PROGRAM WHICH SIMULATES THE VARIOUS
    CANCELLATION SCHEMES, TO FILTER THE CLUTTER PSD THAT WAS
    CALCULATED BY CLUT. CLUTCAN THEN CALLS THE SUBPROGRAM CLTATT
    TO CALCULATE THE CLUTTER ATTENUATION FACTOR AS A RESULT OF
    THE CANCELLATION SCHEME SIMULATED BY CANCEL.

    CLUTCAN CALLS THE FOLLOWING SUBPROGRAMS
        CLUT
        CANCEL
        CLTATT

    THE FOLLOWING VARIABLES ARE USED IN "CLUTCAN"
        INPUT RADAR PARAMETERS
            FREQ-RADAR OPERATING FREQUENCY (HZ)
            PRF-PULSE REPETITION FREQUENCY (HZ)
            TAU-PULSE WIDTH (SEC)
            PT-PEAK POWER TRANSMITTED PER BURST (WATTS)
            BURST-BURST WIDTH (SEC)
            BURPRF-BURST PRF (HZ)
            LS-SYSTEM LOSSES
            NT-SYSTEM NOISE TEMPERATURE (DEGREES KELVIN)
            CANT-INPUT TO CONTROL ANTENNA FUNCTION
                1-COMPUTE ANTENNA GAIN
                2-FIXED ANTENNA GAIN
            GMAX-MAXIMUM 1-WAY GAIN OF ANTENNA MAINBEAM (DB)
            GMIN-MINIMUM 1-WAY GAIN OF ANTENNA SIDELOBES (DB)
            GCK1-CONSTANT TO COMPUTE 1-WAY ANTENNA GAIN BETWEEN
                ANGMB AND ANGSL
            GCK2-CONSTANT TO COMPUTE ANTENNA 1-WAY GAIN BETWEEN
                ANGMB AND ANGSL
            GCK3-ANGLE SCALE FACTOR TO COMPUTE 1-WAY ANT. GAIN
            CN-EXPONENT TO COMPUTE ANTENNA 1-WAY GAIN BETWEEN
                ANGMB AND ANGSL
            ANGSL-RADIAL ANGLE (DEG) BEYOND WHICH MIN SIDE-
                LOBE GAIN IS COMPUTED
            CMB-ANTENNA ANGLE SCALE FACTOR FOR COMPUTING MAIN
                BEAM GAIN
            BEL-ANTENNA ELEVATION BEAMWIDTH (DEG)
            BAZ-ANTENNA AZIMUTH BEAMWIDTH (DEG)
            D-ANTENNA DIAMETER (M)
            ALPHA-SCAN RATE (DEG/SEC)
        OUTPUT VARIABLES

```

```

C      KRAD-RADAR POWER CONSTANT GIVEN PT,PRF,BAZ,ALPHA (W)
C
C      INPUT GEOMETRY PARAMETERS
C      H-SATELLITE ALTITUDE (KM)
C      ANTAZ-AZIMUTH ANGLE OF ANT. MAINBEAM BORESIGHT (DEG)
C      DEPAZ-DEPRESSION ANGLE OF MAINBEAM BORESIGHT (DEG)
C
C      INPUT TARGET PARAMETERS
C      VT-TARGET VELOCITY (M/SEC)
C      RT-TARGET RANGE (KM)
C      RCS-TARGET RADAR CROSS SECTION (M*M)
C
C      CLUTTER PARAMETERS
C      INPUT VARIABLES
C      CCLUT-INPUT TO CONTROL CLUTTER OPTION
C      1-ASSUME GAUSSIAN CLUTTER SPECTRUM
C      2-COMPUTE CLUTTER SPECTRUM
C      CTER-INPUT TO CONTROL TERRAIN TYPE
C      1-LAND
C      2-SEA
C      3-SNOW AND ICE
C      CSGPDF-INPUT TO CONTROL PDF OF SIGMA-0
C      1-CONSTANT
C      2-GAUSSIAN
C      3-LOG-NORMAL
C      OUTPUT VARIABLES
C      CLTPSD(N)-ARRAY OF CLUTTER PSD VALUES
C      DELFQ-FREQUENCY INTERVAL BETWEEN FREQ SPECTRAL
C
C      CANCELLATION PARAMETERS
C      INPUT VARIABLES
C      CCNSCH-INPUT TO CONTROL CANCELLATION SCHEME
C      1-BARTLETT WEIGHTS
C      2-HANNING WEIGHTS
C      3-HAMMING WEIGHTS
C      4-BLACKMAN WEIGHTS
C      5-BINOMIAL WEIGHTS
C      6-IMPULSE RESPONSE
C      7-UNIFORM WEIGHTS
C      8-BUTTERWORTH WEIGHTS
C      N-NUMBER OF POINTS
C      T-SAMPLING INTERVAL
C      TAP-NUMBER OF FILTER TAPS
C      OUTPUT VARIABLES
C      FLCPSD(N)-ARRAY OF FILTERED PSD COMPONENTS
C      FLTMAG(N)-ARRAY OF FILTER MAG COEFFICIENTS
C
C      ATTENUATION FACTOR PARAMETERS
C      CTAT-CLUTTER ATTENUATION FACTOR
C
C      CLUTCAN PROGRAM VARIABLES
C      CTEST-INPUT TO CONTROL TEST VARIATION OF CLUTTER
C      CANCELLATION PROBLEM
C      1-NO MORE TESTING
C      2-TEST WITH DIFFERENT CANCELLATION SCHEME

```

```

C      3-TEST WITH DIFFERENT CLUTTER PARAMETERS
C      4-TEST WITH DIFFERENT CLUTTER PARAMETERS AND
C      CANCELLATION SCHEME
C      DATANM-NAME OF FILE RESULTS WRITTEN TO
C
C      THE FOLLOWING CONSTANTS ARE USED BY THE SUBPROGRAMS AND
C      SUBROUTINES CLUTCAN CALLS DIRECTLY OR INDIRECTLY.
C      RE-EARTH RADIUS (KM)
C      GRAV-EARTH GRAVITATIONAL CONSTANT (M/SEC*SEC)
C      CLGHT-VELOCITY OF LIGHT (M/SEC)
C      BK-BOLTZMAN'S CONSTANT
C      DTR-DEGREES TO RADIANS CONVERSION FACTOR
C      RTD-RADIANS TO DEGREES CONVERSION FACTOR
C      PI-PI
C      KMTNM-KILOMETER TO NAUTICAL MILES CONVERSION FACTOR
C      NMTKM-NAUTICAL MILES TO KILOMETERS CONVERSION FACTOR
C
C      *DECLARE AND INITIALIZE VARIABLES*
C      DIMENSION FLCPSD(150),CLTPSD(150),FLMAG(150),CMAG(150),
+      FMAG(150)
C      REAL FREQ,PT,LS,NT,GMAX,GMIN,GCK1,GCK2,GCK3,BEL,BAZ,D,
+      ALPHA,H,ANTAZ,DEPANG,VT,RT,RCS,T,CTAT,KRAD,RE,
+      GRAV,CLGHT,BK,DTR,RTD,PI,KMTNM,NMTKM,FLCPSD,
+      CLTPSD,FLMAG,DELFO,CN,ANGSL,CMB,TAU,PRF,BURST
C      INTEGER CANT,CCLUT,CTER,CSGPDF,CCNSCH,N,CTEST,I,J,
+      K,L,M,BURPRF,TAP
C      CHARACTER DATANM*6
C      COMMON RE,GRAV,CLGHT,BK,DTR,RTD,PI,KMTNM,NMTKM
C      DATA FREQ,PT,LS,NT,GMAX,GMIN,GCK1,GCK2,GCK3,BEL,BAZ,D,
+      ALPHA,H,ANTAZ,DEPANG,VT,RT,RCS,T,CTAT,KRAD,PRF,TAU,
+      DELFO,BURST/26*0.0/,I,J,K,L,M,CANT,CCLUT,CTER,
+      CSGPDF,CCNSCH,N,CTEST,BURPRF,TAP/14*0/
C      DO 10 I=1,150,1
C          FLCPSD(I)=0.0
C          CLTPSD(I)=0.0
C          FLMAG(I)=0.0
10  CONTINUE
C
C      *SET VALUES OF CONSTANTS*
C      PI=3.14159265
C      DTR=PI/180
C      RTD=180/PI
C      CLGHT=2.997925E08
C      RE=6378.388
C      GRAV=9.80665
C      BK=1.38E-23
C      NMTKM=1.853
C      KMTNM=.5396
C
C      *INPUT DATA VALUES*
20  PRINT*,'INPUT RADAR OPERATING FREQUENCY (HZ) '
C      READ*,FREQ
C      PRINT*,'INPUT PULSE REPETITION FREQUENCY (HZ) '
C      READ*,PRF

```


AD-A138 467

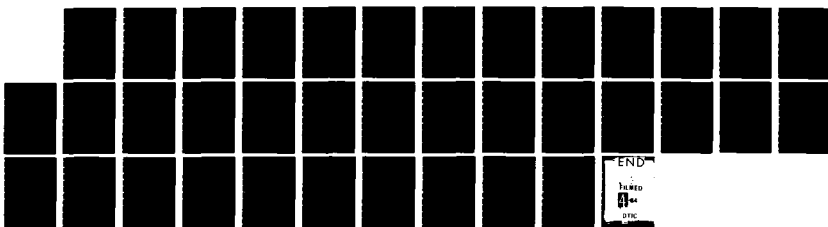
CLUTTER CANCELLATION TECHNIQUES FOR USE IN A
SPACE-BASED RADAR SYSTEM(U) AIR FORCE INST OF TECH
WRIGHT-PATTERSON AFB OH SCHOOL OF ENGINEERING
J DEVENUTO DEC 83 AFIT/GE/EE/83D-18

3/3

UNCLASSIFIED

F/G 77/9

NL





MICROCOPY RESOLUTION TEST CHART
NATIONAL BUREAU OF STANDARDS-1963-A

```

PRINT*, 'INPUT PULSE WIDTH'
READ*, TAU
PRINT*, 'INPUT PEAK BURST TRANSMITTED POWER (WATTS)'
READ*, PT
PRINT*, 'INPUT BURST WIDTH (SEC)'
READ*, BURST
PRINT*, 'INPUT BURST PRF (HZ)'
READ*, BURPRF
PRINT*, 'INPUT SYSTEM LOSSES (DB)'
READ*, LS
PRINT*, 'INPUT SYSTEM NOISE TEMPERATURE (DEGREES KELVIN)'
READ*, NT
PRINT*, 'INPUT ANTENNA CONTROL FUNCTION (1-COMPUTE ANTENNA
+GAIN, 2-FIXED ANTENNA GAIN)'
READ*, CANT
PRINT*, 'INPUT MAX 1-WAY GAIN OF ANTENNA MAINBEAM (DB)'
READ*, GMAX
PRINT*, 'INPUT MIN 1-WAY GAIN OF ANTENNA SIDELOBES (DB)'
READ*, GMIN
PRINT*, 'INPUT CONSTANT TO COMPUTE ANTENNA 1-WAY GAIN
+(RATIO) BETWEEN MBANG AND SLANG'
READ*, GCK1
PRINT*, 'INPUT CONSTANT TO COMPUTE ANTENNA 1-WAY GAIN
+(RATIO) BETWEEN MBANG AND SLANG'
READ*, GCK2
PRINT*, 'INPUT ANGLE SCALE FACTOR TO COMPUTE 1-WAY
+GAIN (DB) BETWEEN MBANG AND SLANG'
READ*, GCK3
PRINT*, 'INPUT ANT.ANGLE SCALE FACTOR TO COMPUTE MB GAIN'
READ*, CMB
PRINT*, 'INPUT EXPONENT TO COMPUTE ANT 1-WAY GAIN BETWEEN
+ANGMB AND ANGSL'
READ*, CN
PRINT*, 'INPUT RADIAL ANGLE BEYOND WHICH MIN SIDELOBE GAIN
+IS COMPUTED'
READ*, ANGSL
PRINT*, 'INPUT ANTENNA ELEVATION BEAMWIDTH (DEG)'
READ*, BEL
PRINT*, 'INPUT ANTENNA AZIMUTH BEAMWIDTH (DEG)'
READ*, BAZ
PRINT*, 'INPUT ANTENNA DIAMETER (M)'
READ*, D
PRINT*, 'INPUT ANTENNA SCAN RATE (DEG/SEC)'
READ*, ALPHA
PRINT*, 'INPUT TARGET VELOCITY (M/SEC)'
READ*, VT
PRINT*, 'INPUT RANGE TO TARGET (KM)'
READ*, RT
PRINT*, 'INPUT TARGET RADAR CROSS SECTION(DB)'
READ*, RCS
PRINT*, 'INPUT SATELLITE ALTITUDE (KM)'
READ*, H
PRINT*, 'INPUT AZ ANGLE OF ANTENNA BORESIGHT (DEG)'
READ*, ANTAN
PRINT*, 'INPUT DEPRESSION ANGLE OF ANTENNA BORESIGHT (DEG)'

```

```

      READ*,DEPANG
      PRINT*, 'INPUT CLUTTER CALCULATION METHOD (1-ASSUME GAUSSIAN
+CLUTTER SPECTRUM, 2-COMPUTE CLUTTER SPECTRUM)'
      READ*,CCLUT
      PRINT*, 'INPUT TERRAIN TYPE (1-LAND, 2-SEA, 3-SNOW & ICE)'
      READ*,CTER
      PRINT*, 'INPUT PDF OF SIGMA-0 (1-CONSTANT, 2-GAUSSIAN,
+3-LOG-NORMAL)'
      READ*,CSGPDF
40  PRINT*, 'INPUT CANCELLATION SCHEME (1-BARTLETT WEIGHTS,
+2-HANNING WEIGHTS, 3-HAMMING WEIGHTS, 4-BLACKMAN
+WEIGHTS, 5-BINOMIAL WEIGHTS, 6-IMPULSE FUNCTION,
+7-UNIFORM WEIGHTS, 8-BUTTERWORTH WEIGHTS)'
      READ*,CCNSCH
      PRINT*, 'INPUT NUMBER OF SAMPLE POINTS'
      READ*,N
      PRINT*, 'INPUT SAMPLING INTERVAL (SEC)'
      READ*,T
      PRINT*, 'INPUT NUMBER OF FILTER TAPS'
      READ*,TAP
      PRINT*, 'INPUT FILE NAME RESULTS ARE WRITTEN TO'
      READ (*,35)DATANM
35  FORMAT(A6)
C
      OPEN(5,FILE=DATANM)
C
C
C      *COMPUTE CLUTTER POWER SPECTRAL DENSITY*
      CALL CLUT(FREQ,PRF,TAU,PT,LS,CANT,GMAX,GMIN,CN,ANGSL,CMB,
+   GCK1,GCK2,GCK3,BEL,BAZ,I,ALPHA,H,ANTAZ,DEPANG,CCLUT,
+   CTER,N,T,CSGPDF,CLTPSD,KRAD,DELFQ,VT,RT,BURST,BURPRF)
C
      CALL CANCEL(CCNSCH,N,T,BURST,CLTPSD,FLCPSD,FLMAG,TAP)
C
C
C
C      *CALCULATE ATTENUATION FACTOR*
      CALL CLTATT(CLTPSD,FLCPSD,N,CTAT)
C
C
C      *OUTPUT STATEMENTS*
48  WRITE(*,100)
      DO 50 I=1,N,1
          WRITE(*,150)CLTPSD(I),FLCPSD(I),FLMAG(I)
50  CONTINUE
      SCL=CLTPSD(1)
      WRITE(*,120)DELFQ,CTAT
      PRINT*, 'INPUT FILTER SCALE FACTOR'
      READ*,FSCL
      PRINT*, 'NORMALIZED VALUES'
      WRITE(*,100)
      DO 60 I=1,N,1
          FLMAG(I)=FLMAG(I)/FSCL
          CLTPSD(I)=CLTPSD(I)/SCL
          FLCPSD(I)=FLCPSD(I)/(SCL*FSCL)
          WRITE(*,150)CLTPSD(I),FLCPSD(I),FLMAG(I)
          WRITE(5,150)CLTPSD(I),FLCPSD(I),FLMAG(I)
60  CONTINUE

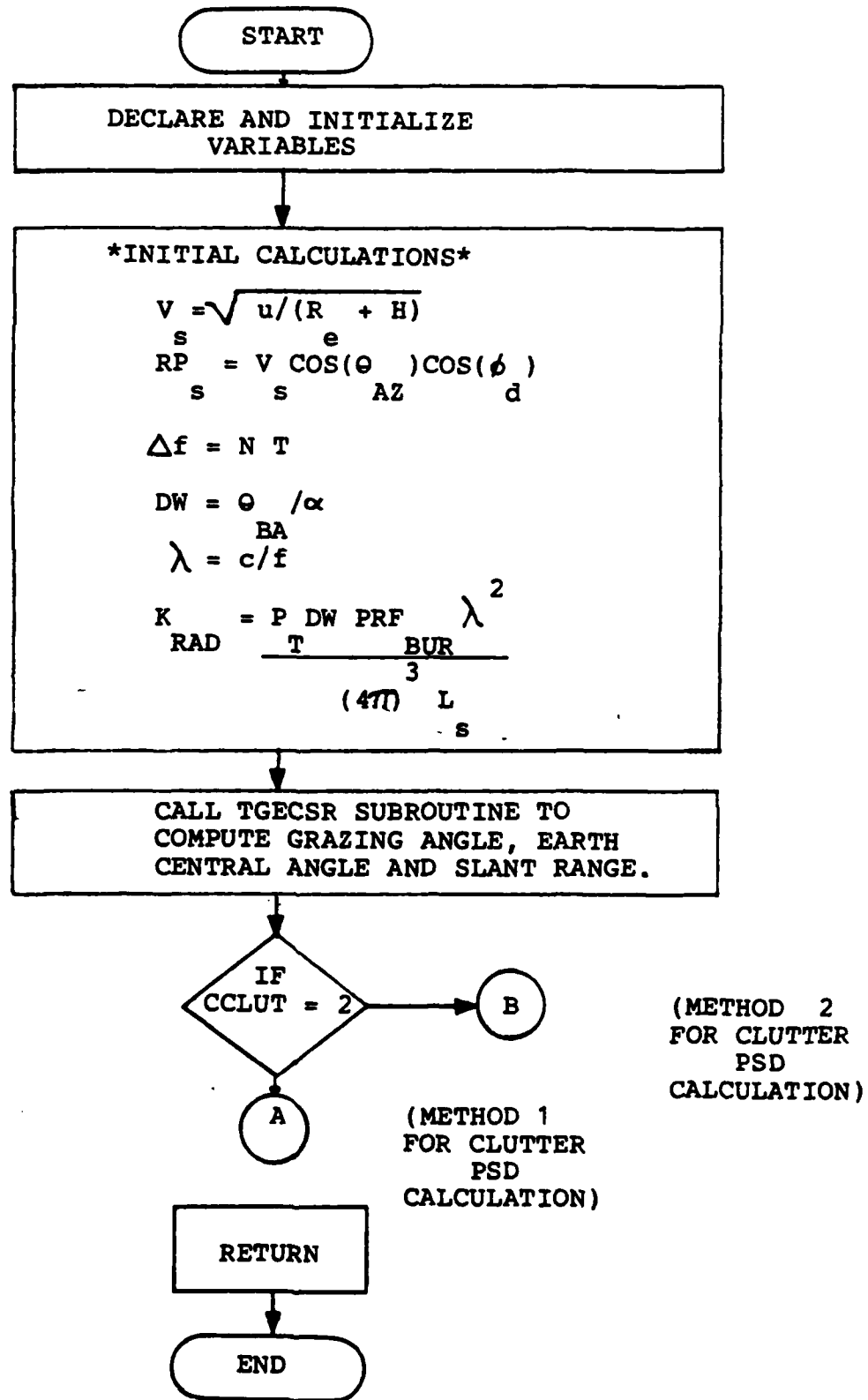
```

```

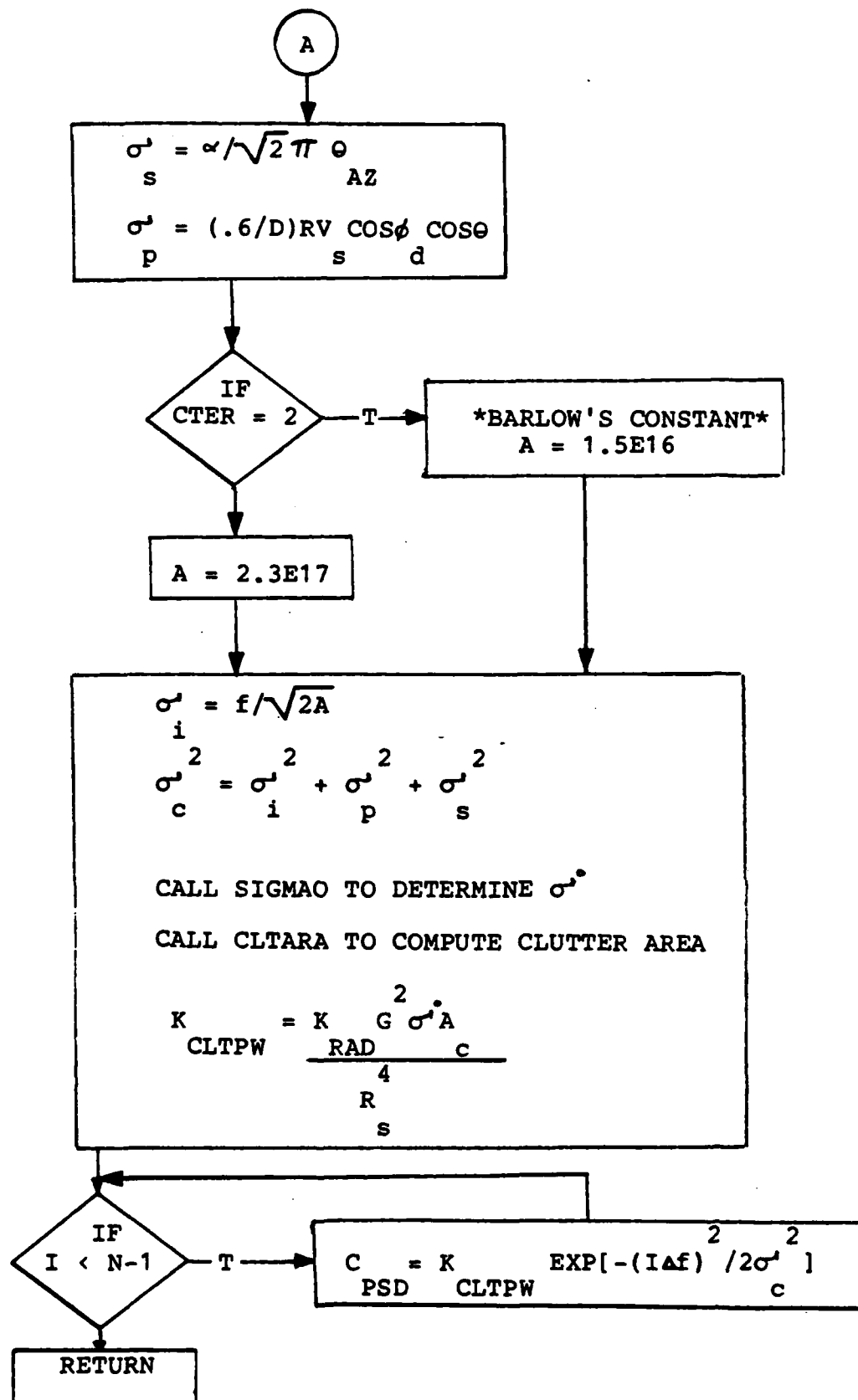
100  FORMAT (5X//11HCLUTTER PSD,10X,20HFILTERED CLUTTER PSD,
+    3X,26HFILTER TRANSFORM MAGNITUDE/)
120  FORMAT (5X//21HFREQUENCY INTERVAL = ,E17.10/
+    26HATTENUATION FACTOR (DB) = ,E17.10)
150  FORMAT (E17.10,4X,E17.10,4X,E17.10)
C
C    *TEST DIFFERENT SENERIO*
PRINT*,('TO TEST A DIFFERENT CASE INPUT'/'1-END TESTING'/
+ '2-TEST DIFFERENT CANCELLATION SCHEME'/'3-TEST
+ DIFFERENT CLUTTER STATISTICS'/'4-TEST DIFFERENT
+ CLUTTER AND CANCELLATION SCHEME')'
READ*,CTEST
IF (CTEST.EQ.1) THEN
    GO TO 200
ELSE
    IF (CTEST.EQ.2) THEN
        GO TO 40
    ELSE
        IF (CTEST.EQ.3) THEN
            GO TO 30
        ELSE
            GO TO 20
        END IF
    END IF
END IF
200  STOP
END
..

```

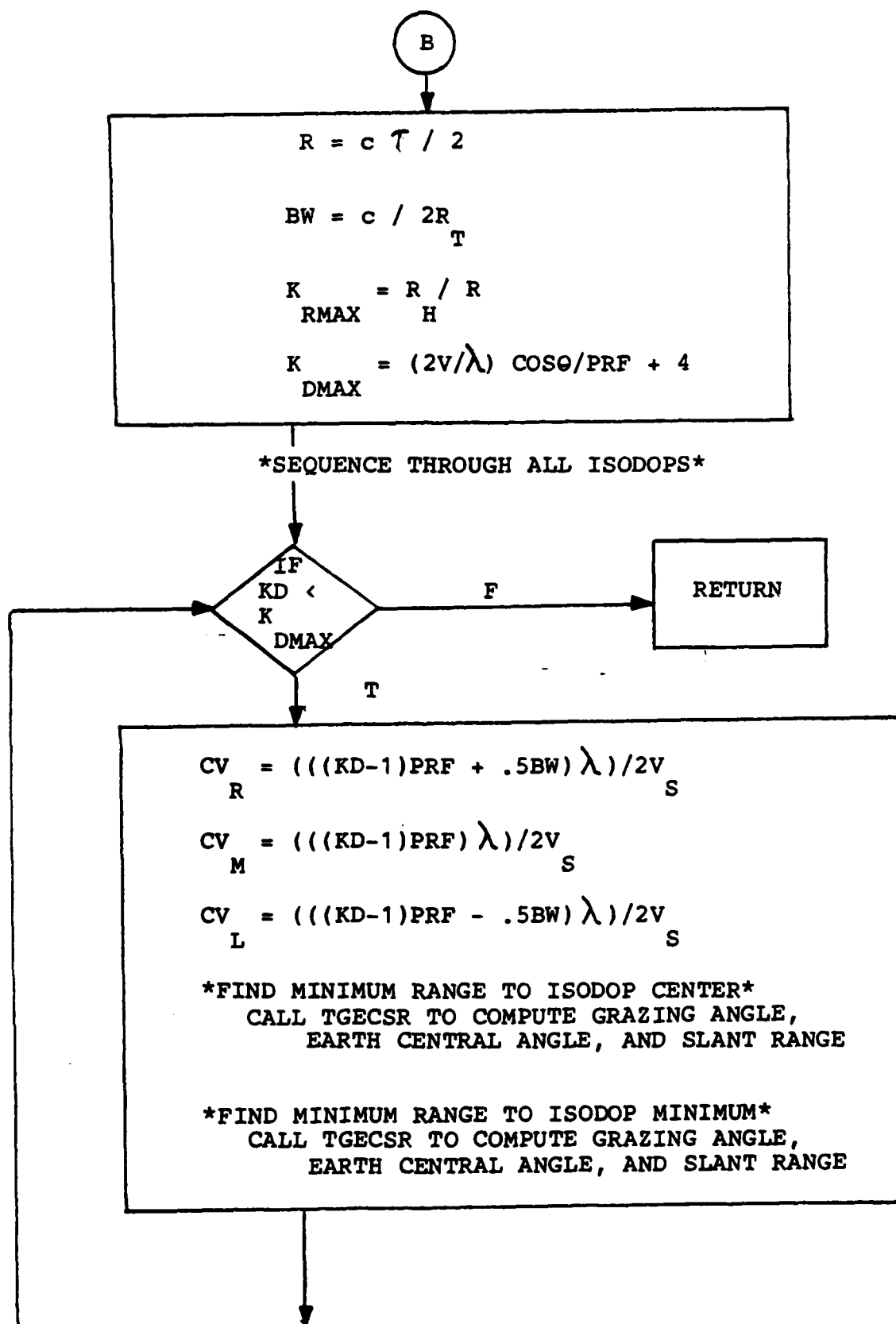
FLOWCHART FOR SUBPROGRAM CLUT



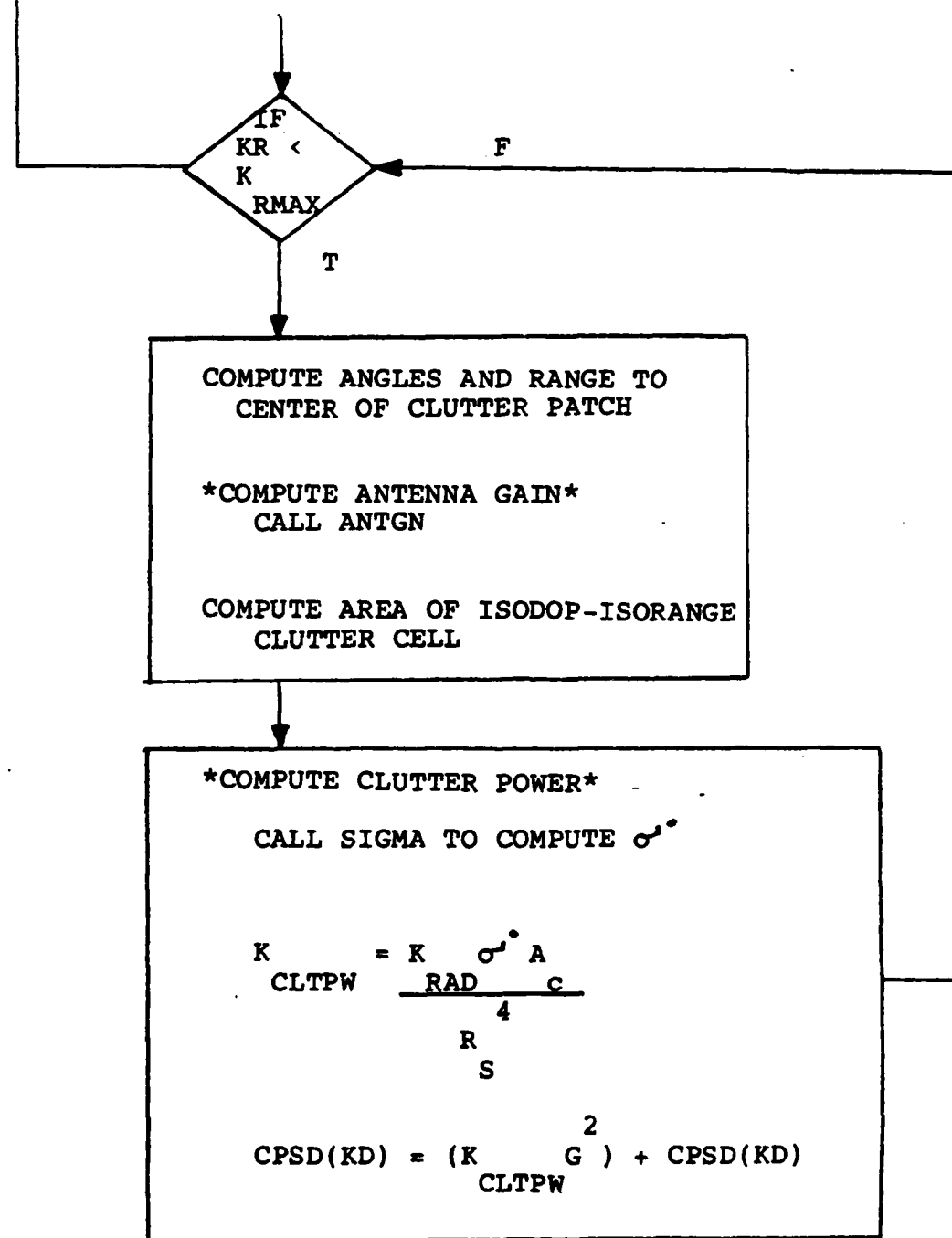
FLOWCHART FOR METHOD 1 CLUTTER PSD CALCULATION



FLOWCHART FOR METHOD 2 CLUTTER PSD CALCULATION



SEQUENCE THROUGH ALL ISORANGE FOR ISODOP



```

SUBROUTINE CLUT(FREQS,PRFS,TAUS,PTS,LSS,CANTS,
+   GMAXS,GMINS,CNS,ANGSLS,CMBS,GCK1S,GCK2S,GCK3S,BELS,BAZS,
+   DS,ALPHAS,HS,ANTAZS,DFANGS,CCLUTS,CTERS,NS,TS,
+   CSGPDS,CLTPSS,KRADS,BELFGS,VTS,RTS,BURSS,BURPRS)

```

```

C *****
C * SUBPROGRAM CLUT *
C * WRITTEN BY:JOE DEVENUTO *
C * 15 SEPTEMBER 1983 *
C *****

```

```

C THE SUBPROGRAM CLUT CALCULATES THE POWER SPEC-
C TRAL DENSITY AS SEEN BY A SPACE-BASED DOPPLER RADAR
C SYSTEM GIVEN THE RADAR SYSTEM PARAMETERS AND THE
C VIEWING GEOMETRY PARAMETERS. THIS SUBPROGRAM
C CALCULATES THE CLUTTER PSD BY EITHER ASSUMING A
C SPECIFIED CLUTTER PSD PDF OR BY SUMMING THE DIS-
C TRIBUTED CLUTTER RETURNS FORM AMBIGUOUS RANGE BINS
C ALONG A GIVEN UNAMBIGUOUS DOPPLER (ISODOP). SUB-
C PROGRAM CLUT RETURNS TO CLTCAN THE CLUTTER POWER
C FOR THE ANALOG FREQUENCY AXIS.

```

```

C CLUT CALLS THE FOLLOWING SUBROUTINES
C CLTARA-CALCULATES THE AREA OF CLUTTER
C ANTGN-CALCULATES THE ANTENNA GAIN
C SIGMA0-CALCULATES THE SIGMA-0 VALUE
C TGECSR-CALCULATES THE GRAZING ANGLE,EARTH
C CENTRAL ANGLE AND SLANT RANGE

```

```

C THE FOLLOWING VARIABLES ARE USED IN "CLUT"
C INPUT VARIABLES

```

```

C FREQS-RADAR OPERATING FREQUENCY (HZ)
C PRFS-PULSE REPETITION FREQUENCY (HZ)
C TAUS-PULSE WIDTH (SEC)
C PTS-PEAK POWER TRANSMITTED PER PULSE (WATTS)
C LSS-SYSTEM LOSSES
C CANTS-INPUT TO CONTROL ANTENNA FUNCTION
C GMAXS-MAX 1-WAY GAIN OF ANTENNA MAINBEAM (DEG)
C GMINS-MIN 1-WAY GAIN OF ANTENNA SIDELOBES (DEG)
C GCK1S,GCK2S,GCK3S-ANTENNA CONSTANTS
C CMBS-ANTENNA ANGLE SCALE FACTOR FOR COMPUTING MAIN
C BEAM GAIN
C CNS-EXPONENT TO COMPUTE ANTENNA 1-WAY GAIN BETWEEN
C ANGMB AND ANGSL
C ANGSLS-RADIAL ANGLE (DEG) BEYOND WHICH MIN SIDE-
C LOBE GAIN IS COMPUTED
C BELS-ANTENNA ELEVATION BEAMWIDTH (DEG)
C BAZS-ANTENNA AZIMUTH BEAMWIDTH (DEG)
C DS-ANTENNA DIAMETER
C ALPHAS-SCAN RATE (DEG/SEC)
C VTS-TARGET VELOCITY (M/SEC)

```

C RTS-RANGE TO TARGET (KM)
 C HS-SATELLITE ALTITUDE (KM)
 C ANTASZ-AZIMUTH ANGLE OF ANTENNA MAINBEAM (DEG)
 C DPANGS-DEPRESSION ANGLE OF MAINBEAM BORESIGHT (DEG)
 C CCLUTS-INPUT TO CONTROL CLUTTER COMPUTATION OPTION
 C CTERS-INPUT TO CONTROL TERRAIN TYPE
 C CSGPDS-INPUT TO CONTROL PDF OF SIGMA-0
 C BURSS-BURST WIDTH (SEC)
 C BURPRS-BURST PRF (HZ)
 C OUTPUT VARIABLES
 C CLTPSS(N)-ARRAY OF CLUTTER PSD VALUES
 C KRAIS-RADAR POWER CONSTANT GIVEN PT,PRF,BAZ,ALPHA(W)
 C DELFQS-FREQUENCY INTERVAL BETWEEN FREQ SPECTRA
 C SUBPROGRAM VARIABLES
 C DW-DWELL TIME
 C VS-VELOCITY OF SATELLITE
 C ARACLT-AREA OF CLUTTER
 C THETAG-GRAZING ANGLE
 C GN1-ANTENNA GAIN WRT CLUTTER PATCH IN 1ST QUAD (DB)
 C GN2-ANTENNA GAIN WRT CLUTTER PATCH IN 2ND QUAD (DB)
 C GN3-ANTENNA GAIN WRT CLUTTER PATCH IN 3RD QUAD (DB)
 C GN4-ANTENNA GAIN WRT CLUTTER PATCH IN 4TH QUAD (DB)
 C RPV-RADIAL PLATFORM VELOCITY
 C LAMDA-WAVELENGTH
 C ECANG-EARTH CENTRAL ANGLE
 C RS-SLANT RANGE
 C LSNDB-SYSTEM LOSSES NOT IN DB
 C RCSNDB-RCS NOT IN DB
 C GMXNDB-1-WAY MAX ANTENNA GAIN NOT IN DB
 C GMNNDB-1-WAY MIN ANTENNA GAIN NOT IN DB
 C STDSCN-CLUTTER SPREAD DUE TO SCANNING
 C STDPTM-CLUTTER SPREAD DUE TO PLATFORM MOTION
 C STDIM-CLUTTER SPREAD DUE TO INTERNAL MOTION
 C KCLTVAR-TOTAL CLUTTER SPREAD
 C KCLTPW-CLUTTER POWER CONSTANT
 C A-BARLOW'S INTERNAL MOTION CONSTANT
 C SIGMA-CLUTTER SIGMA-0 VALUE
 C ANG-ANGLE (DEG)
 C DELR-DELTA RANGE
 C FT-TARGET DOPPLER FREQUENCY (HZ)
 C BWF-FILTER BANDWIDTH (HZ)
 C NAHOR-NADIR ANGLE TO HORIZON (DEG)
 C DEPHOR-DEPRESSION ANGLE TO HORIZON (DEG)
 C ECAHOR-EARTH CENTRAL ANGLE TO HORIZON (DEG)
 C RSHOR-SLANT RANGE TO HORIZON (KM)
 C KI-LOOP VARIABLE FOR ISODOPS
 C KR-LOOP VARIABLE FOR ISORANGE
 C KRMAX-CONTROL FOR MAXIMUM ISORANGES
 C KDMAX-CONTROL FOR MAXIMUM ISODOPS
 C CVR-RIGHT CLUTTER DOPPLER LINE
 C CVM-MIDDLE CLUTTER DOPPLER LINE
 C CVL-LEFT CLUTTER DOPPLER LINE
 C CAANG-CLUTTER AZIMUTH ANGLE TO CENTER OF CLUTTER PATCH
 C CNANG-NADIR ANGLE TO CENTER OF CLUTTER PATCH (DEG)
 C KRMIN-CONTROL FOR MINIMUM ISORANGE

```

C      RMIND-MINIMUM RANGE TO ISODOP (KM)
C      RMINDN-MINIMUM RANGE TO MINIMUM ISODOP (KM)
C      CDEPA-DEPRESSION ANGLE TO CENTER OF CLUTTER PATCH
C      RG-GROUND RANGE OF CLUTTER PATCH (KM)
C      RSF-SLANT RANGE TO FAR EDGE OF CLT PATCH (KM)
C      RSN-SLANT RANGE TO NEAR EDGE OF CLT PATCH (KM)
C      NAF-NADIR ANGLE TO FAR EDGE OF CLT PATCH (DEG)
C      NAN-NADIR ANGLE TO NEAR EDGE OF CLT PATCH (DEG)
C      DEPRF-DEPRESSION ANGLE TO FAR EDGE OF CLT PATCH (DEG)
C      DEPRN-DEPRESSION ANGLE TO NEAR EDGE OF CLT PATCH (DEG)
C      ECANGF-EARTH CENTRAL ANG TO FAR EDGE OF CLT PATCH (DEG)
C      ECANGN-EARTH CENTRAL ANG TO NEAR EDGE OF CLT PATCH (DEG)
C      AANGFL-AZIMUTH ANG OF FAR LEFT EDGE OF CLT PATCH (DEG)
C      AANGFR-AZIMUTH ANG OF FAR RIGHT EDGE OF CLT PATCH (DEG)
C      AANGNL-AZIMUTH ANG OF NEAR LEFT EDGE OF CLT PATCH (DEG)
C      AANGNR-AZIMUTH ANG OF NEAR RIGHT EDGE OF CLT PATCH (DEG)
C      BF-LENGTH OF FAR EDGE OF CLUTTER PATCH (KM)
C      BN-LENGTH OF NEAR EDGE OF CLUTTER PATCH (KM)
C
C      *DECLARE AND INITIALIZE VARIABLES*
C      DIMENSION CLTPSS(150)
C      REAL FREQS,PTS,LSS,GMAXS,GMINS,BELS,BAZS,DS,ALPHAS,
+      HS,ANTAZS,DPANGS,CLTPSS,KRADS,DELFRS,GCK1S,
+      GCK2S,GCK3S,DW,VS,ARACT,THETAG,GN1,GN2,GN3,GN4,
+      RPV,LAMDA,ECANG,RS,GMXNDB,GMNDB,LSNDB,RCSNDB,
+      STDSCN,STDPTH,STDIM,KCLTPW,A,CLTVAR,SIGMA,TAUS,PRFS,
+      BURSS-
C      REAL ANG,DELR,FT,BWF,NAHOR,DEPHOR,ECAHOR,RSHOR,
+      CUR,CVM,CVL,CAANG,CNANG,CDEPA,RMIND,RMINDN,
+      RG,RSF,RSN,NAF,NAN,DEPRF,DEPRN,ECANGF,ECANGN,
+      AANGFL,AANGFR,AANGNL,AANGNR,BF,BN,CNS,ANGSLS,CMBS
C      INTEGER CANTS,CCLUTS,CTERS,CSGPD,S,I,J,L,
+      BURPRS,KD,KR,KRMAX,KDMAX,KRMIN
C      COMMON RE,GRAV,CLGHT,BK,DTR,RTD,PI,KMTNM,NMTKM
C      I=0
C      J=0
C      L=0
C      DO 205 I=1,150,1
C          CLTPSS(I)=0.0
205  CONTINUE
C
C      *INITIAL CALCULATIONS*
C      *COMPUTE PLATFORM RADIAL VELOCITY*
C      VS=SQRT(3.986012E05/(HS+RE))
C      RPV=VS*(COS(ANTAZS*DTR))*(COS(DPANGS*DTR))
C      *COMPUTE FREQ SAMPLING RATE*
C      FRS=PRFS/NS
C      *COMPUTE RADAR POWER CONSTANT*
C      LSNDB=10.**(LSS*.1)
C      DW=BAZS/ALPHAS
C      LAMDA=CLGHT/FREQS
C      KRADS=(PTS*DW*BURPRS*LAMDA*LAMDA)
C      + /(((4*PI)**3)*LSNDB)

```

```

C      *COMPUTE SLANT RANGE*
      CALL TGECSR(HS,DPANGS,THETAG,ECANG,RS)
C
C      *DETERMINE METHOD OF CLUTTER PSD CALCULATION*
      IF (CCLUTS .EQ. 2) GO TO 250
C
C      *COMPUTE CLUTTER PSD VIA GAUSSIAN SPECTRUM*
C      *COMPUTE CLUTTER SPREAD*
      STDSCN=ALPHAS/((2**.5)*PI*BAZS)
      STDPTM=(.6/DS)*VS*DS(DPANGS*DTR)*1000
+      *SIN(ANTAZS*DTR)
      IF (CTERS .EQ. 2) THEN
        A=1.5E16
      ELSE
        A=2.3E17
      END IF
      STDIM=FREQS/((2*A)**.5)
      CLTVAR=(STDSCN**2)+(STDPTM**2)+(STDIM**2)
C
C      *COMPUTE CLUTTER PSD*
      GMXNDB=10.**(GMAXS*.1)
      CALL SIGMAQ(THETAG,CTERS,CSGPIS,SIGMA)
      SIGMA=10.**(SIGMA*.1)
      CALL CLTARA(HS,BAZS,BELS,THETAG,RS,ARACL)
      KCLTPW=(KRADS*GMXNDB*GMXNDB*ARACL*SIGMA*1E06)/
+      ((RS*1000)**4)
      DO 210 I=0,NS-1,1
      ARG=((I*DELFQS)**2)/(2*CLTVAR)
      IF (ARG.GT.250.) THEN
        CLTPSS(I+1) = 0.0
        GO TO 210
      END IF
      CLTPSS(I+1)=KCLTPW*(EXP(-ARG))
210    CONTINUE
      GO TO 290
C
C      *INITIAL CALCULATIONS FOR CLUTTER PSD METHOD 2*
250    DELR=CLGHT*TAUS/(1000*2.)
      BWF=1/(2.*RTS*1000/CLGHT)
C
C      *FIND GEOMETRY AT HORIZON*
      NAHOR=RTD*ASIN(RE/(RE+HS))
      ECAHOR=90.-NAHOR
      RSHOR=(RE+HS)*SIN(DTR*ECAHOR)
      KRMAX=RSHOR/DELR
      KIMAX=((2.*VS*1000/LAMDA)*COS(ECAHOR*DTR))/PRFS + 1
C
      I=1
C
C      *SEQUENCE THRU ALL ISODOPS*
      DO 270 KI=1,KIMAX,1
      CUR=(((KI-1)*PRFS+.5*BWF)*LAMDA)/(2.*VS*1000)
      CUM=(((KI-1)*PRFS)*LAMDA)/(2.*VS*1000)
      CVL=(((KI-1)*PRFS-.5*BWF)*LAMDA)/(2.*VS*1000)
C

```

```

C   *FIND MIN RANGE OF ISODOP CENTER*
C   CDEPA=RTD*ACOS(CVM)
C   CALL TGECSR(HS,CDEPA,THETAG,ECANG,RS)
C   KRMIN=(RS-HS)/DELR + 1
C   RMIND=HS+(KRMIN-1)*DELR
C
C   *FIND MIN RANGE OF ISODOP MIN*
C   CDEPA=RTD*ACOS(CVL)
C   IF (CDEPA.GT.90.) CDEPA=90.0
C   CALL TGECSR(HS,CDEPA,THETAG,ECANG,RMINDN)
C   IF (RMINDN.LT.HS) RMINDN=HS
C
C   SEQUENCE THRU ALL ISORANGES FOR PARTICULAR ISODOP*
C   DO 260 KR=KRMIN,KRMAX,1
C   RS=HS+(KR-1)*DELR+RTS
C   CNANG=RTD*ACOS(((HS+RE)*(HS+RE)+RS*RS-RE*RE)/(2.*(HS+RE)
+   *RS))
C   ECANG=RTD*ACOS(((HS+RE)*(HS+RE)+RE*RE-RS*RS)/(2.*(HS+RE)
+   *RE))
C   THETAG=90.-CNANG-ECANG
C   RG=ECANG*IDTR*RE
C   CDEPA=90.-CNANG
C   CALL ANG0(CVM,CDEPA,CAANG)
C
C   *COMPUTE ANTENNA GAIN*
C   CALL ANTGN(CANTS,CAANG,CDEPA,GMAXS,GMINS,
+   GCK1S,GCK2S,GCK3S,CNS,CMBS,BELS,ANGSLS,ANTAZS,DPANGS,
+   GN1,GN2,GN3,GN4)
C   GN1=10.**(.1*GN1)
C   GN2=10.**(.1*GN2)
C   GN3=10.**(.1*GN3)
C   GN4=10.**(.1*GN4)
C
C   *FIND GEOMETRY OF 4 TRAPEZOID CORNERS*
C   *FIND GEOMETRY OF FURTHER CORNERS*
C   RSF=RS+.5*DELR
C   IF (RSF.GT.RSHOR) RSF=RSHOR
C   CALL ANAD(HS,RSF,NAF)
C   DEPRF=90.-NAF
C   CALL TGECSR(HS,DEPRF,ANG,ECANGF,RSF)
C   CALL ANG0(CVR,DEPRF,AANGFR)
C   CALL ANG0(CVL,DEPRF,AANGFL)
C   IF (AANGFR.GT.90.) AANGFR=90.0
C   IF (AANGFR.LT.0.) AANGFR=0.0
C   IF (AANGFL.GT.90.) AANGFL=90.0
C   IF (AANGFL.LT.0.0) AANGFL=0.0
C
C   *FIND GEOMETRY OF NEAR CORNERS*
C   RSN=RS-.5*DELR
C   IF(RSN.LT.RMINDN) RSN=RMINDN
C   CALL ANAD(HS,RSN,NAN)
C   DEPRN=90.-NAN
C   CALL TGECSR(HS,DEPRN,ANG,ECANGN,RSN)
C   CALL ANG0(CVR,DEPRN,AANGNR)
C   CALL ANG0(CVL,DEPRN,AANGNL)

```

```

IF(AANGNR.GT.90.0) AANGNR=90.0
IF(AANGNR.LT.0.0) AANGNR=0.0
IF(AANGNL.GT.90.0) AANGNL=90.0
IF(AANGNL.LT.0.0) AANGNL=0.0

C
C
*COMPUTE AREA OF CLUTTER PATCH*
BF=(AANGFL-AANGFR)*DTR*RE*SIN(DTR*ECANGF)
BN=(AANGFL-AANGFR)*DTR*RE*SIN(DTR*ECANGN)
ARACLT=(ECANGF-ECANGN)*DTR*RE*.5*(BF+BN)
CALL SIGMAO(THETAG,CTERS,CSGDDS,SIGMA)
SIGMA=10.**(SIGMA*.1)
KCLTPW=(KRADS*SIGMA*ARACLT*1.E06)/((RS*1000)**4)
CLTPSS(I)=CLTPSS(I)+KCLTPW*(GN1*GN1 + GN2*GN2 +
+ GN3*GN3 + GN4*GN4)

```

```

C
260 CONTINUE
    I=I+1
270 CONTINUE
290 RETURN
END
..

```

```

C SUBROUTINE SIGMAO(THETA,CTERSS,CSGPSS,SIGMAO)
C
C *****
C * SUBROUTINE SIGMA-O *
C * WRITTEN BY:JOE DEVENUTO *
C * 7 OCTOBER 1983 *
C *****
C
C THE SUBROUTINE SIGMA-O CALCULATES THE SIGMA-O VALUES
C GIVEN THE TERRAIN TYPE,PDF OF SIGMA-O, AND GRAZING
C ANGLE TO CENTER OF CLUTTER PATCH.
C
C SIGMAO CALLS THE FOLLOWING IMSL SUBROUTINES
C GGNML
C GGNLG
C
C THE FOLLOWING VARIABLES ARE USED IN "SIGMAO"
C INPUT VARIABLES
C CTERSS-INPUT TO CONTROL TERRAIN TYPE
C CSGPSS-INPUT TO CONTROL SIGMA-O'S PDF
C THETA-GRAZING ANGLE TO CENTER OF CLUTTER PATCH
C OUTPUT VARIABLES
C SIGMAS-VALUE OF SIGMA-O (DB)
C SUBROUTINE VARIABLES
C SUBS(N)-SUBROUTINE VALUE OF SIGMA, TERRAIN DEP
C G(N)-ARRAY CONTAINING GROUND SIGMA-O VALUES
C S(N)-ARRAY CONTAINING SEA SIGMA VALUES
C SAI(N)-ARRAY CONTAINING SNOW AND ICE SIGMA VALUES
C ANGG(N)-ARRAY OF GRAZING ANGLES
C NUMPT-NUMBER OF SIGMA-O DATA POINTS
C DSEED-INPUT VARIABLE TO GAUSSIAN DIVIATE GENERATOR
C DSIG(N) DELTA TO SIGMA DUE TO PDF
C NR-NUMBER OF DIVIATES TO BE GENERATED
C STD-STANDARD DEVIATION OF SIGMA
C I-LOOP VARIABLES
C
C *DECLARE AND INITIALIZE VARIABLES*
C DIMENSION G(50),S(50),SAI(50),DSIG(5),ANGG(50),SUBS(50)
C REAL THETA,SIGMAS,G,S,SAI,DSIG,STD,ANGG
C INTEGER CTERSS,CSGPSS,NUMPT,NR,I
C DOUBLE PRECISION DSEED
C
C *SIGMAS VALUES GIVEN THETA*
C DATA G/-22.5,-20.5,-19.5,-18.0,-17.5,-17.5,-17.0,
+ -16.0,-15.0,-14.5,-12.5,-10.0,-8.0,-6.5,
+ -4.5,-2.5,-.5,1.5,2.5,31*0.0/
C DATA S/-45.0,-41.0,-38.0,-35.5,-33.5,-32.0,
+ -30.0,-28.0,-26.0,-23.0,-20.0,
+ -18.0,-15.5,-12.5,-11.0,-3.0,.5,
+ 6.5,13.0,31*0.0/
C DATA SAI/-31.0,-29.0,-28.0,-26.0,-25.5,-23.0,
+ -22.5,-20.0,-18.5,-17.5,-15.0,-14.5,
+ -12.5,-10.5,-8.5,-6.5,-5.0,-4.0,-2.5,31*0.0/
C DATA ANGG/0.0,5.0,10.0,15.0,20.0,25.0,30.0,

```



```

+ 35.0,40.0,45.0,50.0,55.0,60.0,65.0,
+ 70.0,75.0,80.0,85.0,90.0,31*0.0/
NUMPT=19

C
C *CONSTRAIN THETA TO LIMITS OF 0 & 90 DEGREES*
IF (THETA .GT. 90) THEN
    THETA=90.0
END IF
IF (THETA .LT. 0) THEN
    THETA=0.0
END IF

C
C *DETERMINE SIGMAS FOR TERRAIN TYPE*
IF (CTERSS .EQ. 1) THEN
    DO 300 I=1,NUMPT,1
        SUBS(I)=G(I)
300 CONTINUE
    ELSE
        IF (CTERSS .EQ. 2) THEN
            DO 310 I=1,NUMPT,1
                SUBS(I)=S(I)
310 CONTINUE
            ELSE
                DO 320 I=1,NUMPT,1
                    SUBS(I)=SAI(I)
320 CONTINUE
            END IF
        END IF
    END IF

C
C *LOCATE SIGMAS VALUE WITHIN ARRAY OF VALUES*
DO 330 I=2,NUMPT,1
    IF (THETA .LT. ANGG(I)) GO TO 340
330 CONTINUE
340 IF (ANGG(I-1) .EQ. ANGG(I)) THEN
    SIGMAS = SUBS(I)
    GO TO 350
END IF

C
C *DO 2 POINT LINEAR INTERPOLATION OF SIGMAS*
SIGMAS=SUBS(I-1)+(SUBS(I)-SUBS(I-1))*
+ (THETA-ANGG(I-1))/(ANGG(I)-ANGG(I-1))

C
C *COMPUTE SIGMAS-0 DELTA DUE TO PDF*
350 IF (CSGPSS .EQ. 1) THEN
    DSIG(1)=0.0
    GO TO 360
END IF
NR=1
DSEED=123457.0D0
IF (CSGPSS .EQ. 2) THEN
    CALL GGNML(DSEED,NR,DSIG)
ELSE
    STD=1
    XM=SIGMAS
    CALL GGNLG(DSEED,NR,XM,S,DSIG)

```

```
END IF  
360 SIGMAS=SIGMAS+ISIG(1)  
C  
RETURN  
END  
..
```

```

C SUBROUTINE TGECSR(HSS,DEPAG,THETAS,ECANGS,RSS)
C *****
C * SUBROUTINE TGECSR *
C * WRITTEN BY: JOE DEVENUTO *
C * 7 OCTOBER 1983 *
C *****
C
C THE SUBROUTINE TGECSR COMPUTES THE GRAZING ANGLE
C AND THE CORRESPONDING EARTH CENTRAL ANGLE AND THE
C SLANT RANGE GIVEN THE ALTITUDE (KM) AND THE DEPRESSION
C ANGLE.
C
C THE FOLLOWING VARIABLES ARE USED IN "TGECSR"
C INPUT VARIABLES
C HSS-ALTITUDE OF PLATFORM (KM)
C DEPAG-DEPRESSION ANGLE (DEG)
C OUTPUT VARIABLES
C ECANGS-EARTH CENTRAL ANGLE (DEG)
C THETAS-GRAZING ANGLE (DEG)
C RSS-SLANT RANGE (KM)
C SUBROUTINE VARIABLES
C NANG-NADIR ANGLE
C ARG-ARGUMENT
C DECLARE AND INITIALIZE VARIABLES
C REAL HSS,DEPAG,ECANGS,THETAS,RSS,NANG
C COMMON RE,GRAV,CLGHT,BK,DTR,RTD,PI,KMTNM,NMTKM
C
C *COMPUTE THETAG*
C NANG=90.0-DEPAG
C ARG=(SIN(DTR*NANG)*(RE+HSS)/RE)
C IF (ABS(ARG).GT.1.0) THEN
C ARG= ARG-1.0
C THETAS=ASIN(ARG)*RTD
C GO TO 396
C END IF
C THETAS= 90.0 - ASIN(ARG)*RTD
C
C *COMPUTE EARTH CENTRAL ANGLE*
C 396 ECANGS=90.0-NANG-THETAS
C
C *COMPUTE SLANT RANGE*
C IF (NANG.EQ.0.) THEN
C RSS=HSS
C GO TO 399
C END IF
C RSS=RE*SIN(ECANGS*DTR)/SIN(NANG*DTR)
C
C 399 RETURN
C END
C

```

```

SUBROUTINE ANTGN(CANTSS,AZCTS,DEPCTS,GMXSS,GMINSS,
+ GCK1SS,GCK2SS,GCK3SS,CNSS,CMBSS,BELSS,ANGSL,
+ ANAZS,DEPAS,GN1S,GN2S,GN3S,GN4S)

```

```

*****
* SUBROUTINE ANTGN *
* WRITTEN BY: C.R.RISER *
* MODIFIED BY: JOE DEVENUTO *
* 10 SEPTEMBER 1983 *
*****

```

THE SUBROUTINE ANTGN COMPUTES THE 1-WAY ANTENNA GAIN TO THE CENTER OF CLUTTER PATCHES IN 4 QUADRANTS ON THE EARTH LOOKING DOWNWARD FROM A SBR SYSTEM. CLUTTER PATCHES ARE ASSUMED TO BE SYMMETRICAL WITH THOSE IN THE 1ST QUADRANT. THE ANTENNA GAIN IS ASSUMED TO BE CIRCULAR, BEING FORMED BY A FUNCTION OF REVOLUTION. THE ANTENNA GAIN IS COMPUTED FROM 1 OF 4 DIFFERENT FUNCTIONS DEPENDING ON THE RADIAL ANGLE FROM THE MAIN BEAM BORESIGHT.

THE FOLLOWING VARIABLES ARE USED IN "ANTGN"

INPUT VARIABLES

CANTSS-INPUT TO CONTROL ANTENNA FUNCTION
 AZCTS-AZIMUTH ANGLE TO CENTER OF CLUTTER PATCH (DEG)
 DEPCTS-DEPRESSION ANGLE TO CENTER OF CLUTTER PATCH
 GMXSS-MAX 1-WAY GAIN OF ANTENNA MAINBEAM (DB)
 GMINSS-MIN 1-WAY GAIN OF ANTENNA SIDELOBES (DB)
 GCK1SS-
 GCK2SS-CONSTANT TO COMPUTE 1-WAY GAIN BETWEEN MB & SL
 GCK3SS-ANGLE SCALE FACTOR TO COMPUTE 1-WAY GAIN
 BETWEEN MB AND SL
 BELSS-ANTENNA ELEVATION BEAMWIDTH (DEG)
 CNSS-EXPONENT TO COMPUTE ANTENNA 1-WAY GAIN BETWEEN
 ANGMB AND ANGSL
 CMBSS-ANTENNA ANGLE SCALE FACTOR FOR COMPUTING
 MAINBEAM GAIN
 ANGSL-ANGSL-RADIAL ANGLE FROM BORESIGHT BEYOND WHICH
 SIDELORE MAIN IS COMPUTED
 ANAZS-AZIMUTH ANGLE OF ANT. MAINBEAM BORESIGHT (DEG)
 DEPAS-DEPRESSION ANGLE OF MAINBEAM BORESIGHT (DEG)

OUTPUT VARIABLES

GN1S-1-WAY GAIN OF ANTENNA IN 1ST QUADRANT
 GN2S-1-WAY GAIN OF ANTENNA IN 2ND QUADRANT
 GN3S-1-WAY GAIN OF ANTENNA IN 3RD QUADRANT
 GN4S-1-WAY GAIN OF ANTENNA IN 4TH QUADRANT

PROGRAM VARIABLES

ARG1-ARGUMENT IN 1ST QUADRANT
 ARG2-ARGUMENT IN 2ND QUADRANT
 ARG3-ARGUMENT IN 3RD QUADRANT
 ARG4-ARGUMENT IN 4TH QUADRANT
 ANG-ANGLE

DECLARE VARIABLES

REAL AZCTS,DEPCTS,GMXSS,GMINSS,GCK1SS,GCK2SS,GCK3SS,

```

+   BELSS,CNSS,CMBSS,ANGSL5,ANAZS,DEPAS,GN1S,GN2S,
+   GN3S,GN4S,ARG1,ARG2,ARG3,ARG4,ANG
INTEGER CANTSS
COMMON RE,GRAV,CLGHT,BK,DTR,RTD,PI,NMTNM,NMTNF
C
C   *CHECK GAIN CALCULATION METHOD*
IF (CANTSS.EQ.2) THEN
    GN1S=GMINSS
    GN2S=GMINSS
    GN3S=GMINSS
    GN4S=GMINSS
    GO TO 495
END IF
C
C   *COMPUTE ANTENNA GAIN*
C   *COMPUTE ANGLE BETWEEN MAINBEAM BORESIGHT AND 1ST QUADRANT
C   CLUTTER PATCH CENTER*
ARG1=SIN(DTR*DEPCTS)*SIN(DTR*DEPAS)+COS(DTR*DEPCTS)*
+   COS(DTR*DEPAS)*COS(DTR*(AZCTS-ANAZS))
IF (ABS(ARG1).GT.1.0) THEN
    ANG=90.0
    GO TO 405
END IF
ANG=RTD*ACOS(ARG1)
C
C   *FIND ANGLE SECTOR FOR FIRST RADIAL ANGLE AND COMPUTE
C   ANTENNA GAIN*
405 IF (ANG.LT.1.0E-5) GO TO 410
    IF (ANG.LT.BELSS) GO TO 415
    IF (ANG.LT.ANGSL5) THEN
        GO TO 420
    ELSE
        GO TO 425
    END IF
410 GN1S=GMAXSS
    GO TO 430
415 GN1S=(COS(DTR*CMBSS*ANG))**2.5
    GN1S=10.*ALOG10(GN1S)
    GN1S=GN1S+GMAXSS
    GO TO 430
420 GN1S=GCK1SS+GCK2SS/((SIN(DTR*GCK3SS*ANG))**CNSS)
    GN1S=10.*ALOG10(GN1S)
    GO TO 430
425 GN1S=GMINSS
C
C   *COMPUTE ANGE BETWEEN MAINBEAM BORESIGHT AND
C   CLUTTER PATCH CENTER IN 2ND QUADRANT*
430 ARG2=SIN(DTR*DEPCTS)*SIN(DTR*DEPAS)+COS(DTR*DEPCTS)*
+   COS(DTR*DEPAS)*COS(DTR*(180.-AZCTS-ANAZS))
IF (ABS(ARG2).GT.1.0) THEN
    ANG=180.
    GO TO 435
END IF
ANG=RTD*ACOS(ARG2)
C

```

```

C      *FIND ANGLE SECTOR FOR 2ND RADIAL ANGLE AND COMPUTE
C      ANTENNA GAIN*
435  IF (ANG.LT.1.E-5) GO TO 440
      IF (ANG.LT.BELSS) GO TO 445
      IF (ANG.LT.ANGSLG) THEN
          GO TO 450
      ELSE
          GO TO 455
      END IF
440  GN2S=GMAXSS
      GO TO 460
445  GN2S=(COS(DTR*CMBSS*ANG))**2.5
      GN2S=10.*ALOG10(GN2S)
      GN2S=GN2S+GMAXSS
      GO TO 460
450  GN2S=GCK1SS+GCK2SS/((SIN(DTR*GCK3SS*ANG))**CNSS)
      GN2S=10.*ALOG10(GN2S)
      GO TO 460
455  GN2S=GMINSS
C
C      *COMPUTE ANGLE BETWEEN MAINBEAM BORESIGHT AND
C      CLUTTER PATCH CENTER IN 3RD QUADRANT*
460  ARG3=SIN(DTR*DEPCTS)*SIN(DTR*DEPAS)+COS(DTR*DEPCTS)*
+      COS(DTR*DEPAS)*COS(DTR*(180.+AZCTS-ANAZS))
      IF (ABS(ARG3).GT.1.0) THEN
          ANG=90.0
          GO TO 465
      END IF
      ANG=RTD*ACOS(ARG3)
C
C      *FIND ANGLE SECTOR FOR 3RD RADIAL ANTENNA ANGLE AND
C      COMPUTE GAIN*
465  IF (ANG.LT.1.E-5) GO TO 470
      IF (ANG.LT.BELSS) GO TO 475
      IF (ANG.LT.ANGSLG) THEN
          GO TO 480
      ELSE
          GO TO 482
      END IF
470  GN3S=GMAXSS
      GO TO 485
475  GN3S=(COS(DTR*CMBSS*ANG))**2.5
      GN3S=10.*ALOG10(GN3S)
      GN3S=GN3S+GMAXSS
      GO TO 485
480  GN3S=GCK1SS+GCK2SS/((SIN(DTR*GCK3SS*ANG))**CNSS)
      GN3S=10.*ALOG10(GN3S)
      GO TO 485
482  GN3S=GMINSS
C
C      *COMPUTE ANGLE BETWEEN MAINBEAM BORESIGHT AND CLUTTER
C      PATCH CENTER IN 4TH QUADRANT*
485  ARG4=SIN(DTR*DEPCTS)*SIN(DTR*DEPAS)+COS(DTR*DEPCTS)*
+      COS(DTR*DEPAS)*COS(DTR*(360.-AZCTS-ANAZS))
      IF (ABS(ARG4).GT.1.0) THEN

```

```

      ANG=90.0
      GO TO 486
      END IF
      ANG=RTD*ACOS(ARG4)
C
C      *FIND ANGLE SECTOR FOR 4TH RADIAL ANTENNA AND
C      COMPUTE GAIN*
486  IF (ANG.LT.1.E-5) GO TO 488
      IF (ANG.LT.BELSS) GO TO 490
      IF (ANG.LT.ANGSL5) THEN
        GO TO 492
      ELSE
        GO TO 494
      END IF
488  GN4S=GMAXSS
      GO TO 495
490  GN4S=(COS(DTR*CMBS5*ANG))**2.5
      GN4S=10.*ALOG10(GN4S)
      GN4S=GMAXSS+GN4S
      GO TO 495
492  GN4S=GCK1SS+GCK2SS/((SIN(DTR*GCK3SS*ANG))**CNSS)
      GN4S=10.*ALOG10(GN4S)
      GO TO 495
494  GN4S=GMINSS
C
495  RETURN
      END

```

```

SUBROUTINE SIGNAL(NSS,TSS,SGCOES)
C
REAL TSS
INTEGER NSS,I,J
COMPLEX SGCOES(200)
C
DO 460 I=1,30,2
    SGCOES(I)=(1.0,0.0)
    SGCOES(I+1)=CMPLX(0.,0.)
460 CONTINUE
J=NSS-30
DO 465 I=31,J,1
    SGCOES(I)=CMPLX(0.,0.)
465 CONTINUE
RETURN
END
..

```



```

C SUBROUTINE CLTARA(HSS,BAZSS,BELSS,THETSS,RSS,ARCLS)
C *****
C * SUBROUTINE CLTARA *
C * WRITTEN BY: JOE DEVENUTO *
C * 5 SEPTEMBER 1983 *
C *****
C
C THE SUBROUTINE CLTARA CALCULATES THE AREA OF
C CLUTTER SEEN BY A SPACE-BASED RADAR SYSTEM GIVEN THE
C PLATFORM ALTITUDE, RADAR AZIMUTH AND ELEVATION BEAM-
C WIDTHS, THE GRAZING ANGLE AND THE SLANT RANGE.
C
C THE FOLLOWING VARIABLES ARE USED IN "CLTARA"
C INPUT VARIABLES
C HSS-SATELLITE ALTITUDE(KM)
C BAZSS-ANTENNA AZIMUTH BEAMWIDTH (DEG)
C BELSS-ANTENNA ELEVATION BEAMWIDTH (DEG)
C THETSS-GRAZING ANGLE (DEG)
C RSS-SLANT RANGE (KM)
C OUTPUT VARIABLES
C ARCLS-CLUTTER AREA (KM*KM)
C PROGRAM VARIABLES
C ANG-ANGLE (DEG)
C
C *DECLARE VARIABLES*
C REAL HSS,BAZSS,BELSS,THETSS,RSS,ARCLS,ANG
C COMMON RE,GRAV,CLGHT,BK,DTR,RTD,PI,KMTNM,NMTKM
C
C *COMPUTE CLUTTER AREA*
C ANG=ASIN((RE/(RE+HSS))*COS(DTR*THETSS)) - (BELSS*DTR)
C ARG=((HSS+RE)/RE)*SIN(ANG)
C IF (ABS(ARG).GT.1.0) THEN
C ARG=2.0-ARG
C END IF
C ARCLS=(ACOS(ARG)-(THETSS+BELSS)*DTR)*
+ BAZSS*DTR*RE*RSS
C
C RETURN
C END

```

```

C      SUBROUTINE ANAD(HSS,RSS,NAS)
C
C      *****
C      *      SUBROUTINE ANAD
C      *      WRITTEN BY: JOE DEVENUTO      *
C      *      1 OCTOBER 1983                *
C      *****
C
C      THE SUBROUTINE ANAD COMPUTES THE RADAR ANGLE USING
C      THE LAW OF COSINES GIVEN THE SLANT RANGE AND SATELLITE
C      ALTITUDE.
C
C      THE FOLLOWING VARIABLES ARE USED IN "ANAD"
C      INPUT VARIABLES
C      HSS-SATELLITE ALTITUDE
C      RSS-SLANT RANGE
C      OUTPUT VARIABLES
C      NAS-NADIR ANGLE
C      ARG-ARGUMENT
C
C      *DECLARE VARIABLES*
C      REAL HSS,RSS,NAS,ARG
C      COMMON RE,GRAV,CLGHT,BK,DTR,RTD,PI,KMTNM,NHTKM
C
C      *COMPUTE NADIR ANGLE*
C      ARG=(((HSS+RE)**2)+(RSS**2)-(RE**2))/
C      + (2*(HSS+RE)*RSS)
C      IF (ABS(ARG).GT.1.0) THEN
C      ARG=2.0-ARG
C      END IF
C      NAS=RTD*ACOS(ARG)
C
C      RETURN
C      END
C
C      ..

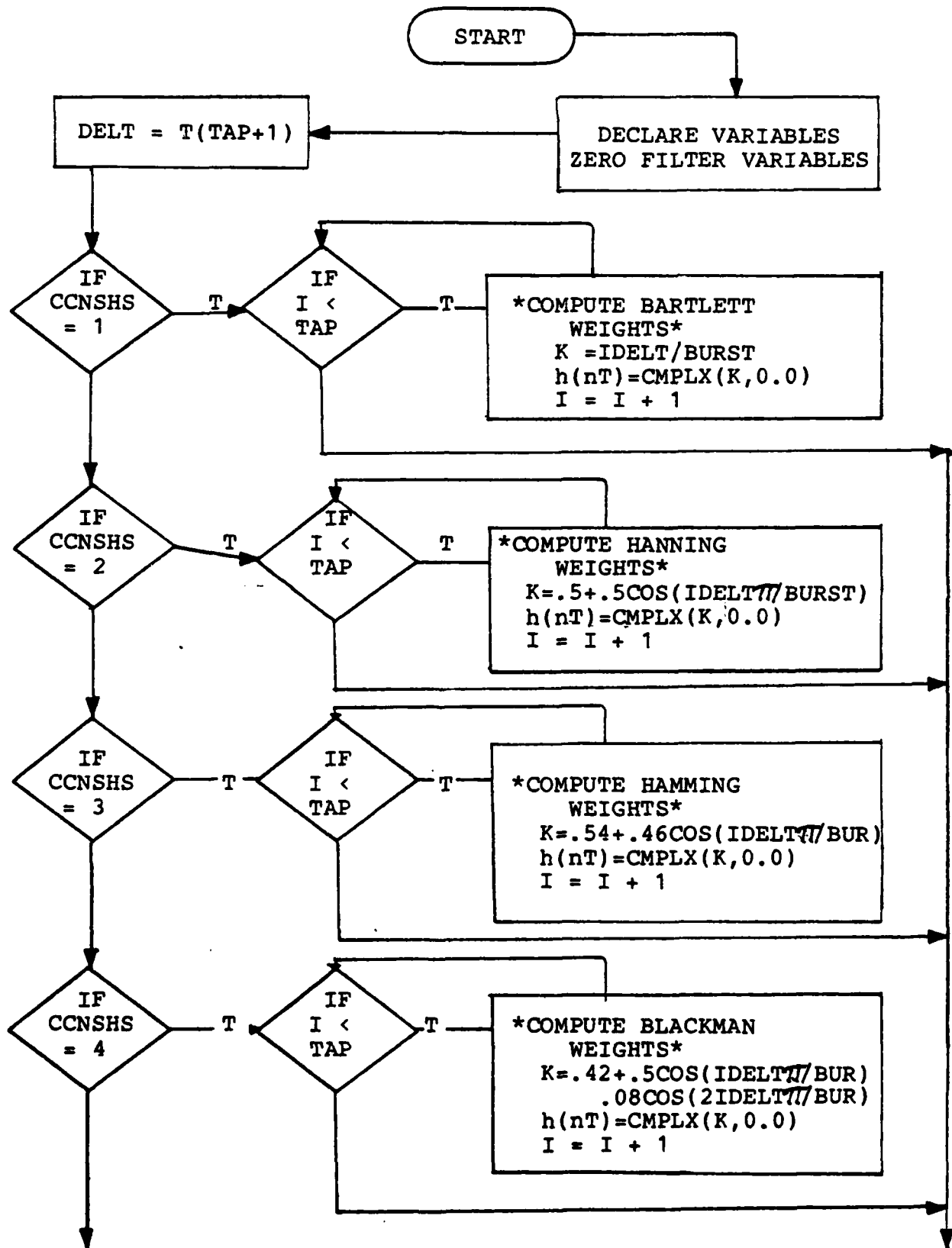
```

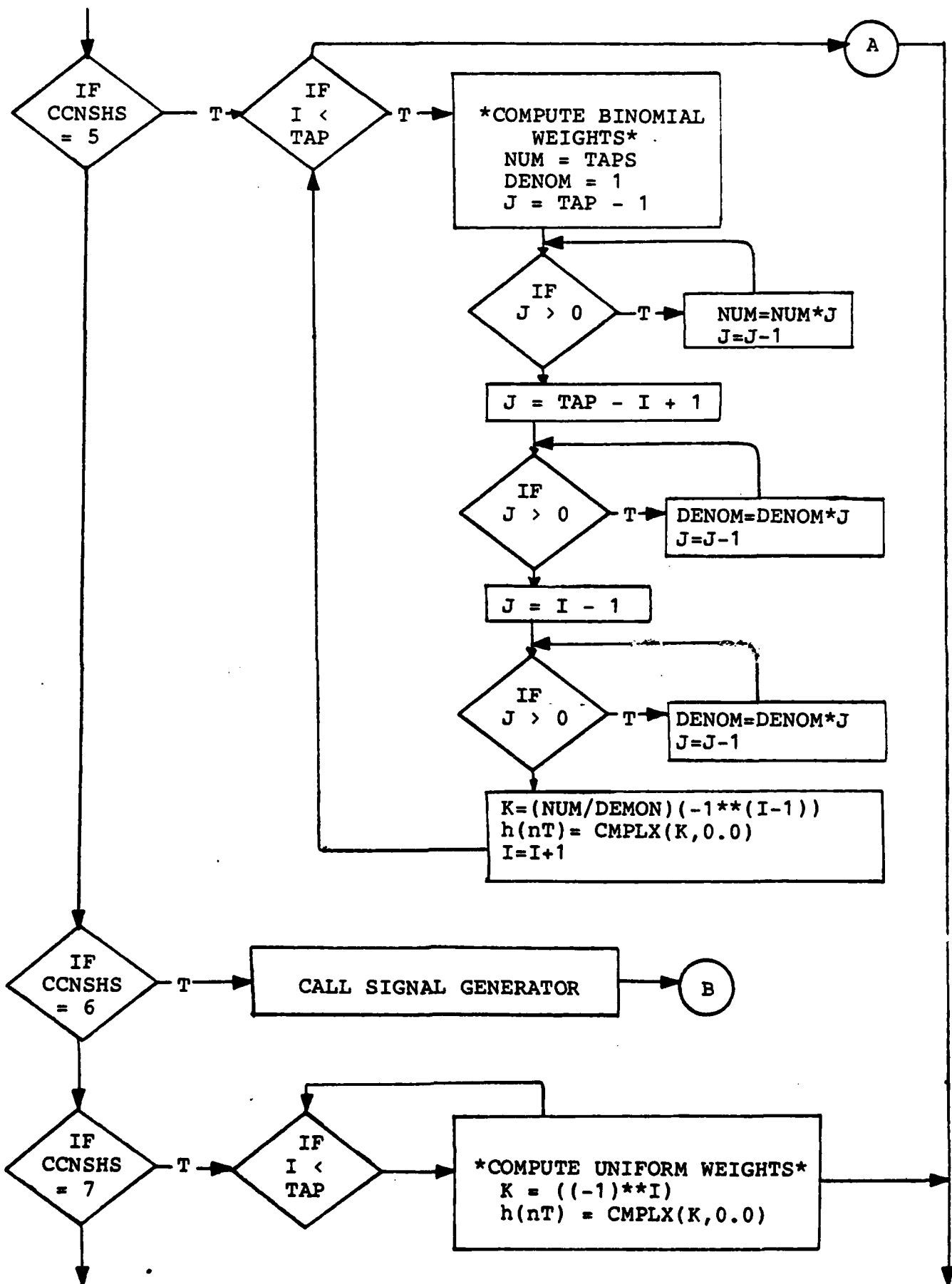
```

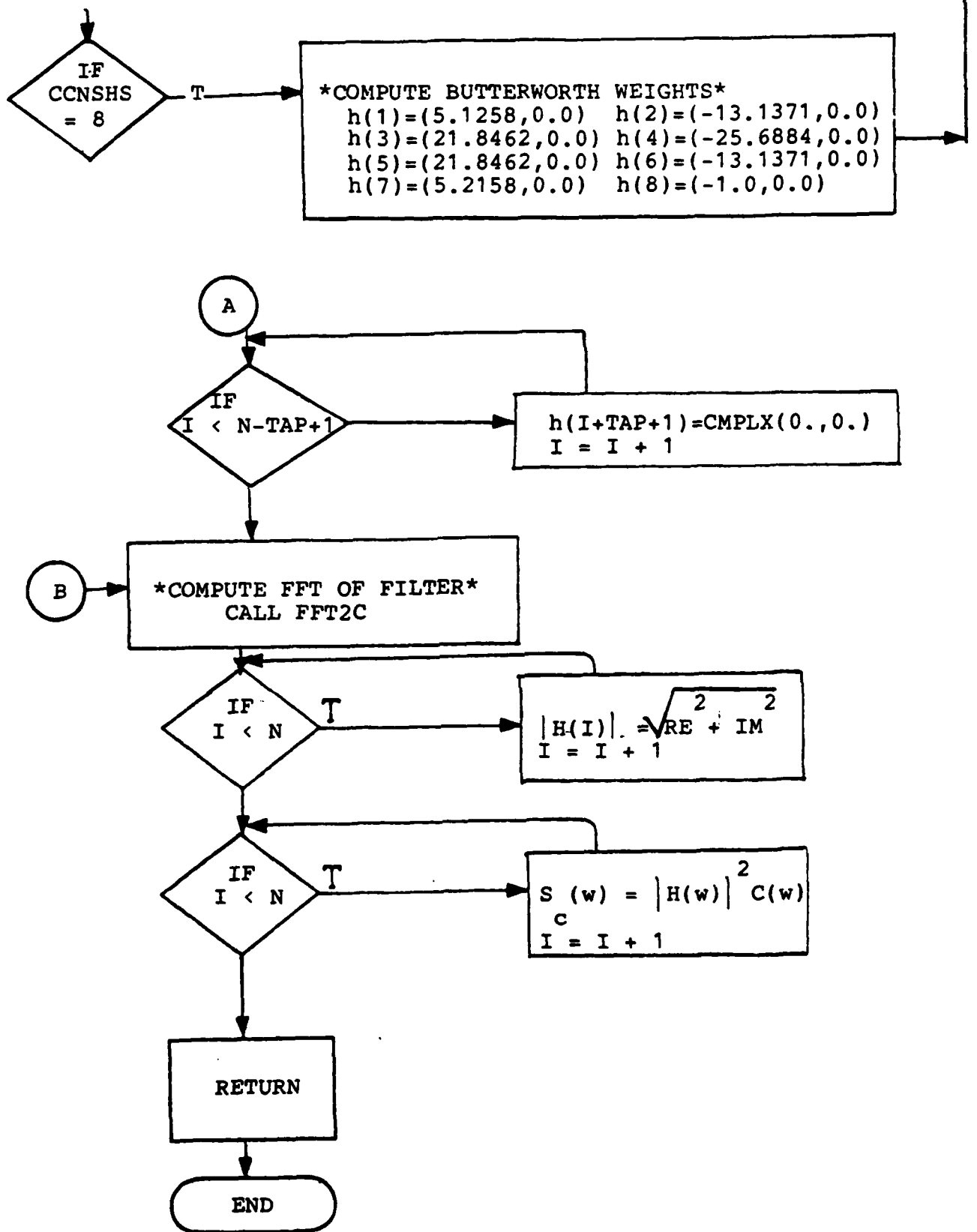
C      SUBROUTINE ANGC(CVX,DEPAS,AZANG)
C
C      *****
C      *      SUBROUTINE ANGC
C      *      WRITTEN BY: C.R. RISER
C      *      MODIFIED BY: JOE DEVENUTO
C      *      10 OCTOBER 1983
C      *****
C
C      THE SUBROUTINE ANGC COMPUTES THE AZIMUTH ANGLE
C      BETWEEN THE DEPRESSION ANGLE VECTOR AND THE CVX VECTOR.
C
C      THE FOLLOWING VARIABLES ARE USED IN "ANGC"
C      INPUT VARIABLES
C      CVX=(FT+(KD-1)*PRF+N*RWF)*LAMDA)/(2.*US)
C      DEPAS-DEPRESSION ANGLE
C      OUTPUT VARIABLE
C      AZANG-AZIMUTH ANGLE
C      PROGRAM VARIABLES
C      DENOM-DENOMINATOR
C      ARG-ARGUMENT
C
C      *DECLARE VARIABLES
C      REAL CVX,DEPAS,AZANG
C      COMMON RE,GRAV,CLGHT,BK,DTR,RTD,PI,KMTNM,NMTKM
C
C      DENOM=COS(DTR*DEPAS)
C      IF(ABS(DENOM).LT.1E-148) THEN
C      DENOM=SIGN(1E-148,DENOM)
C      END IF
C      ARG=CVX/DENOM
C      IF(ABS(ARG).GT.1.0) THEN
C      ARG=2.-ARG
C      END IF
520  AZANG=RTD*ACOS(ARG)
C
C      RETURN
C      END

```

FLOWCHART FOR SUBPROGRAM CANCEL







```

SUBROUTINE CANCEL(CCNSHS,NS,TS,BURSS,CLTPSS,FLCPSS,
+   FLMAGS,TAPS)
C   *****
C   *   SUBPROGRAM CANCEL   *
C   *   WRITTEN BY: JOE DEVENUTO   *
C   *   10 SEPTEMBER 1983   *
C   *****
C
C   THE SUBPROGRAM CANCEL SIMULATES A GIVEN
C   CLUTTER FILTER AND THEN PERFORMS THE FILTERING
C   ON THE CLUTTER PSD CALCULATED IN SUBPROGRAM
C   CLUT.
C
C   CANCEL CALLS THE FOLLOWING SUBROUTINES
C   FFT2C
C   SIGNAL
C
C   THE FOLLOWING VARIABLES ARE USED IN "CANCEL"
C   INPUT VARIABLES
C   CCNSHS-INPUT TO CONTROL CANCELLATION SCHEME
C   NS-NUMBER OF POINTS
C   TS-SAMPLING INTERVAL
C   CLTPSS(N)-ARRAY OF CLUTTER PSD VALUES
C   BURSS-BURST TIME (SEC)
C   TAPS-NUMBER OF FILTER TAPS
C   OUTPUT VARIABLES
C   FLCPSS(N)-ARRAY OF FILTERED CLUTTER PSD VALUES
C   FLMAGS(N)-ARRAY OF FILTER MAGNITUDE COEF
C   SUBPROGRAM VARIABLES
C   FLCOEF(N)-ARRAY OF COMPLEX FILTER COEFFICIENTS
C   REVAL-REAL PART OF COMPLEX VARIABLE
C   IMVAL-IMAJINARY PART OF COMPLEX VARIABLE
C   I,J,K,L-LOOP VARIABLES
C   IWK(N)-WORK ARRAY FOR FFT2C SUBROUTINE
C   FLTAMG(N)-ARRAY OF H(W) FILTER COEF.
C   SGCDEF(N)-ARRAY OF COMPLEX SIGNAL COEF.
C   DELT-DELTA TIME
C   DENOM-DENOMINATOR
C
C   *DECLARE AND INITIALIZE VALUES*
C   DIMENSION CLTPSS(200),FLCPSS(200),IWK(200),
+   FLMAGS(200),FLTAMG(200)
C   REAL TS,CLTPSS,FLCPSS,REVAL,IMVAL,FLMAGS,
+   FLTAMG,K,BURSS,DELT,NUM,DENOM
C   INTEGER CCNSHS,NS,I,L,J,IWK,TAPS
C   COMPLEX FLCOEF(200),SGCDEF(200)
C   COMMON RE,GRAV,CLGHT,BK,DTR,RTD,PI,KMTNM,NMTKM
C   DO 605 I=1,150,1
C       FLTAMG(I)=0.0
605  CONTINUE
C
C   *CHOOSE WEIGHTING SCHEME AND DETERMINE TAP WEIGHTS*

```

```

      DELT=TS/(TAPS+1)
      PRINT*, 'DELT= ', DELT, ' CCNSHS= ', CCNSHS
      *BARTLETT WEIGHTS*
      IF (CCNSHS.EQ.1) THEN
        DO 600 I=0, TAPS, 1
          K=(1-I*DELT/BURSS)*((-1)**I)
          FLCDEF(I+1)=CMPLX(K,0.0)
600    CONTINUE
        GO TO 650
        END IF
C      *HANNING WEIGHTS*
        IF (CCNSHS.EQ.2) THEN
          DO 610 I=0, TAPS, 1
            K=(.5+.5*(COS(I*DELT*PI/BURSS)))*((-1)**I)
            FLCDEF(I+1)=CMPLX(K,0.0)
610    CONTINUE
          GO TO 650
          END IF
C      *HAMMING WEIGHTS*
        IF (CCNSHS.EQ.3) THEN
          DO 620 I=0, TAPS, 1
            K=(.54+.46*(COS(I*DELT*PI/BURSS)))*((-1)**I)
            FLCDEF(I+1)=CMPLX(K,0.0)
620    CONTINUE
          GO TO 650
          END IF
C      *BLACKMAN WEIGHTS*
        IF (CCNSHS.EQ.4) THEN
          DO 630 I=0, TAPS, 1
            K=(.42+.5*(COS(I*DELT*PI/BURSS)) +
+          .08*(COS(2*I*DELT*PI/BURSS)))*((-1)**I)
            FLCDEF(I+1)=CMPLX(K,0.0)
630    CONTINUE
          GO TO 650
          END IF
C      *BINOMIAL WEIGHTS*
        IF (CCNSHS.EQ.5) THEN
          DO 635 I=1, TAPS+1, 1
            NUM=TAPS
            DENOM=1
            J=TAPS-1
636          IF (J.GT.0) THEN
            NUM=NUM*J
            J=J-1
            GO TO 636
          END IF
          J=TAPS-I+1
637          IF (J.GT.0) THEN
            DENOM=DENOM*J
            J=J-1
            GO TO 637
          END IF
          J=I-1
638          IF (J.GT.0) THEN
            DENOM=DENOM*J

```

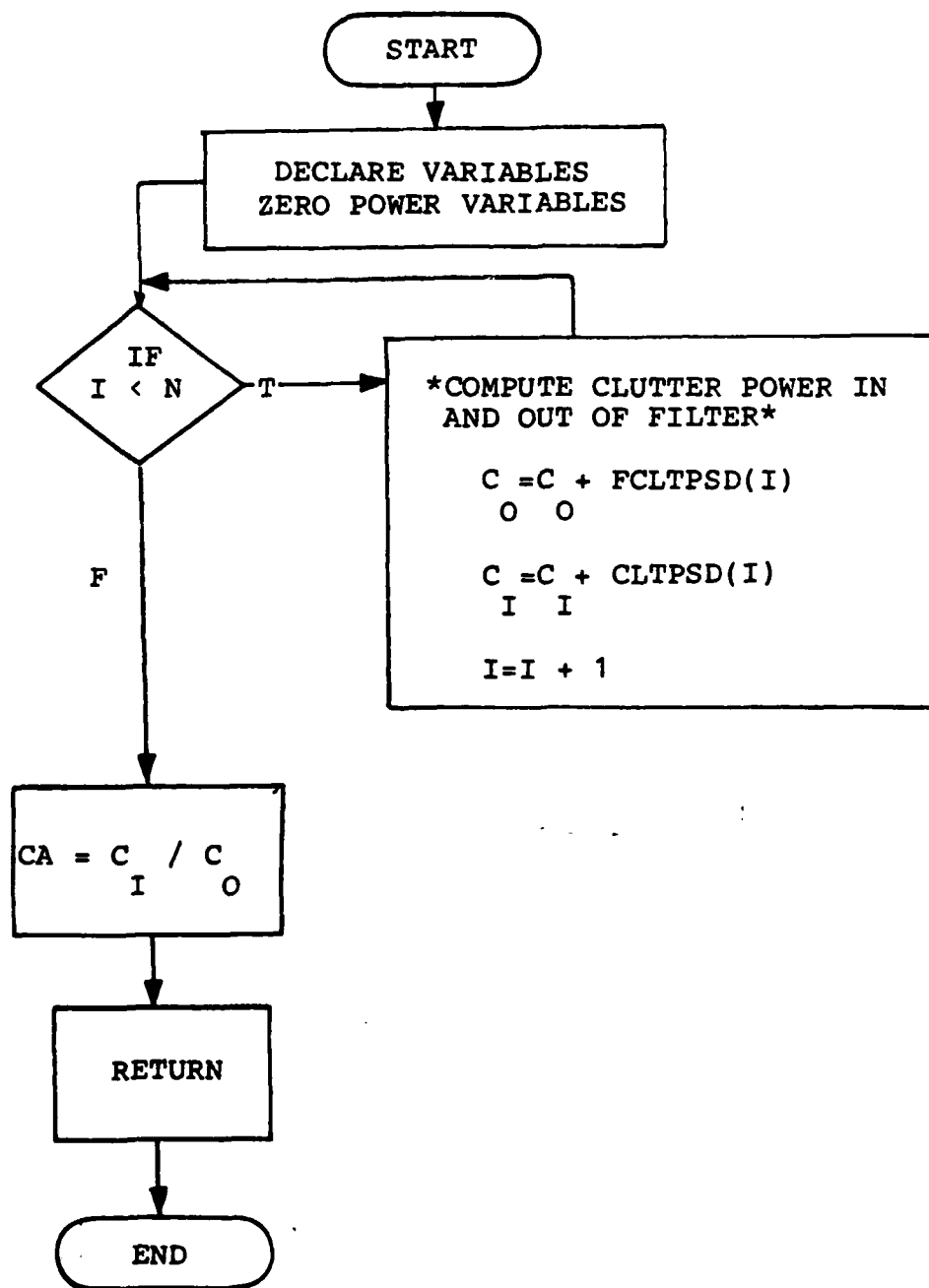


```

        J=J-1
        GO TO 638
    END IF
        K=(NUM/DENOM)*((-1)**(I-1))
        FLCOEF(I)= CMPLX(K,0.)
635  CONTINUE
    GO TO 650
    END IF
C    *IMPULSE RESPONSE*
    IF (CCNSHS.EQ.6) THEN
        CALL SIGNAL(NS,TS,SGCOEF)
        DO 640 I=1,NS,1
            FLCOEF(I)=(SGCOEF(I))
640  CONTINUE
    GO TO 660
    END IF
C    *UNIFORM WEIGHTS*
    IF (CCNSHS.EQ.7) THEN
        DO 645 I=0,TAPS,1
            K=(-1)**I
            FLCOEF(I+1) = CMPLX(K,0.0)
645  CONTINUE
    END IF
C    *BUTTERWORTH WEIGHTS*
    IF (CCNSHS.EQ.8) THEN
        FLCOEF(1)=(5.1258,0.)
        FLCOEF(2)=(-13.1371,0.)
        FLCOEF(3)=(21.8462,0.)
        FLCOEF(4)=(-25.6884,0.)
        FLCOEF(5)=(21.8462,0.)
        FLCOEF(6)=(-13.1371,0.)
        FLCOEF(7)=(5.1258,0.)
        FLCOEF(8)=(-1.,0.)
    END IF
C    *ZERO FILL FILTER*
650  L=NS-(TAPS+1)
    DO 655 I=1,L,1
        FLCOEF(I+(TAPS+1))=CMPLX(0.0,0.0)
655  CONTINUE
    J=(ALOG10(REAL(NS)))/(ALOG10(2.))
660  CALL FFT2C(FLCOEF,J,IWK)
    DO 670 I=1,NS,1
        REVAL=REAL(FLCOEF(I))
        IMVAL=AIMAG(FLCOEF(I))
        FLMAGS(I)=((REVAL**2) + (IMVAL**2))**.5
670  CONTINUE
C
C    *COMPUTE FILTER CLUTTER PSD VALUES*
    DO 690 I=1,NS,1
        FLCPSS(I) = FLMAGS(I)*FLMAGS(I)*CLTPSS(I)
690  CONTINUE
    RETURN
    END

```

FLOWCHART FOR CLTATT SUBPROGRAM



```

C      SUBROUTINE CLTATT (CLTPSS,FLCPSS,NS,CTATS)
C      *****
C      *      SUBPROGRAM CLTATT      *
C      *      WRITTEN BY: JOE DEVENUTO      *
C      *      1 OCTOBER 1983      *
C      *****
C
C      THE SUBPROGRAM CLTATT COMPUTES THE CLUTTER ATTENUATION
C      FACTOR GIVEN THE CLUTTER PSD AS SEEN BY A SPACE-BASED RAD-
C      AR AND THE CLUTTER CANCELLATION SCHEME.
C
C      THE FOLLOWING VARIABLES ARE USED IN "CLTATT"
C      INPUT VARIABLES
C      CLTPSS(N)-ARRAY OF CLUTTER PSD VALUES
C      FLCPSS(N)-ARRAY OF FILTERED CLUTTER PSD
C      FCOFMG(N)-ARRAY OF FILTER COEFFICIENTS
C      NS-NUMBER OF DATA POINTS
C      OUTPUT VARIABLES
C      CTATS-CLUTTER ATTENUATION FACTOR
C      SUBPROGRAM VARIABLES
C      FCLTPW-FILTERED CLUTTER POWER
C      CLTPW-RECEIVED CLUTTER POWER
C      I,J,L-LOOP CONTROL
C
C      DIMENSION CLTPSS(200),FLCPSS(200),FSGPSD(200)
C      DIMENSION IWK(200),FFTSIG(200),FCOFMG(200)
C      REAL VTS,RTS,RCSS,KRADS,CLTPSS,FLCPSS,FCLTPW,CLTPW,
C      +   FSGPW,SIGPW,GAIN,GMAXS,CTATS,FSGPSD,
C      +   RCSNDB,REVAL,INVAL,FFTSIG,FCOFMG
C      COMPLEX SGCOES(200)
C      INTEGER NS,I,K,J,L,IWK
C
C      *ZERO POWER VARIABLES*
C      FCLTPW=0.0
C      CLTPW=0.0
C
C      *COMPUTE CLUTTER POWER IN & OUT OF FILTER*
C      DO 800 I=1,NS,1
C          FCLTPW=FCLTPW + FLCPSS(I)
C          CLTPW=CLTPW + CLTPSS(I)
C      800 CONTINUE
C
C      *COMPUTE ATTENUATION FACTOR*
C      CTATS=10*ALOG10(CLTPW/FCLTPW)
C
C      RETURN
C      END

```

VITA

Joseph DeVenuto was born on 25 January 1958 in Louisville, Kentucky. He graduated validictorian from Casa Grande High School in Petaluma, California in 1976. From June 1976 to May 1980 he attended the United States Air Force Academy in Colorado Springs, Colorado. There he received the degree of Bachelor of Science in Astronautical Engineering and Electrical Engineering and a commission in the United States Air Force. He then was assigned to Air Force Space Division, Space Defense Program Office. While assigned to Space Division he served as System Integration Officer for the Space-based IR Space Surveillance System, as System Integration Officer for the USAF Space Surveillance Architecture Program, as Project Engineer for the Space-based Radar System and as System Engineer for Space Defense Development Programs. In June 1982 he entered the School of Engineering at the Air Force Institute of Technology in Dayton, Ohio. Upon graduation from the Air Force Institute of Technolgy in December 1983, he is scheduled for assignment to Squadron Officer School in Alabama and then to Air Force Space Division in California.

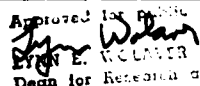
While serving at Space Division he earned the Air Force Commendation Medal and the Air Force Association Citation of Honor.

He is happily married to the former Denise Hunt and has two daughters. His permanent address is 1320 Ponderosa Drive, Petaluma, California 94952.

UNCLASSIFIED

SECURITY CLASSIFICATION OF THIS PAGE

REPORT DOCUMENTATION PAGE

1a. REPORT SECURITY CLASSIFICATION Unclassified		1b. RESTRICTIVE MARKINGS	
2a. SECURITY CLASSIFICATION AUTHORITY		3. DISTRIBUTION/AVAILABILITY OF REPORT Approved for public release; distribution unlimited	
2b. DECLASSIFICATION/DOWNGRADING SCHEDULE			
4. PERFORMING ORGANIZATION REPORT NUMBER(S) AFIT/GE/EE/83D-18		5. MONITORING ORGANIZATION REPORT NUMBER(S)	
6a. NAME OF PERFORMING ORGANIZATION Air Force Institute of Technology	6b. OFFICE SYMBOL (If applicable) AFIT-EN	7a. NAME OF MONITORING ORGANIZATION Space Defense SPO	
6c. ADDRESS (City, State and ZIP Code) Wright-Patterson AFB, Ohio 45433		7b. ADDRESS (City, State and ZIP Code) Space Division El Segundo, Ca. 90009	
8a. NAME OF FUNDING/SPONSORING ORGANIZATION Space Defense SPO	8b. OFFICE SYMBOL (If applicable) YNR	9. PROCUREMENT INSTRUMENT IDENTIFICATION NUMBER	
8c. ADDRESS (City, State and ZIP Code) Space Division El Segundo, Ca. 90009		10. SOURCE OF FUNDING NOS.	
		PROGRAM ELEMENT NO.	PROJECT NO.
		TASK NO.	WORK UNIT NO.
11. TITLE (Include Security Classification) CLUTTER CANCELLATION FOR USE IN A SPACE-BASED RADAR SYSTEM			
12. PERSONAL TECHNIQUES DeVenuto, Joseph			
13a. TYPE OF REPORT MS Thesis	13b. TIME COVERED FROM TO	14. DATE OF REPORT (Yr., Mo., Day) December, 1983	15. PAGE COUNT 214
16. SUPPLEMENTARY NOTATION			
<p style="text-align: right;">Approved for public release: RTR RTR 100-10  John E. KOUNTER Dean for Research and Professional Development Air Force Institute of Technology (AFIT) Wright-Patterson AFB, Ohio 45433</p>			
17. COSATI CODES		18. SUBJECT TERMS (Continue on reverse if necessary)	
FIELD	GROUP	SUB. GR.	
		Clutter, Clutter processing, Space-borne clutter Clutter Cancellation Techniques, Radar signal processing	
19. ABSTRACT (Continue on reverse if necessary and identify by block number)			
<p>The ability of a space-based radar surveillance system to obtain target information from a clutter corrupted radar echo signal is dependent upon the clutter cancellation technique employed. To thoroughly understand the nature of clutter so as to efficiently and effectively design and develop clutter cancellation techniques, fundamental mathematical relationships dealing with radar signal representation, probability theory, detection and estimation theory and signal comparison techniques were established and defined. Since the implementation of the mathematical expressions which describe clutter and clutter cancellation techniques are accomplished digitally, digital signal representation and digital filter characterization via FFT's were also established and defined. Drawing upon the established mathematical principals, as well as temporal probability models, spectral models and average backscatter coefficient models, clutter was described.</p>			
20. DISTRIBUTION/AVAILABILITY OF ABSTRACT		21. ABSTRACT SECURITY CLASSIFICATION	
UNCLASSIFIED/UNLIMITED <input checked="" type="checkbox"/> SAME AS RPT. <input type="checkbox"/> DTIC USERS <input type="checkbox"/>		Unclassified	
22a. NAME OF RESPONSIBLE INDIVIDUAL 1 st Lt. Joseph DeVenuto		22b. TELEPHONE NUMBER (Include Area Code) 513 255-5533	22c. OFFICE SYMBOL AFIT/EN

UNCLASSIFIED

SECURITY CLASSIFICATION OF THIS PAGE

Capitalizing on the different spectral characteristics between clutter and targets, three representative doppler cancellation schemes were developed. The three schemes were delay line cancelers, doppler filter banks and multiple look systems. ✓

Using the models developed for clutter and clutter cancellation schemes an interactive simulation was developed, and used to analyze the clutter cancellation ability of various cancellation methods against different backgrounds.

UNCLASSIFIED

SECURITY CLASSIFICATION OF THIS PAGE

FILM
4-8